MODULATION OF PHYSIOLOGIC RESPONSES OF INSULIN SECRETING CELLS USING ELECTRICAL AND PHOTOSTIMULATION

By

Caleb Nathaniel Liebman

DISSERTATION

Submitted in partial fulfillment of the requirements for the degree of

Doctor of Philosophy at

The University of Texas at Arlington

August 2020

Arlington, Texas

Supervising Committee:

Michael Cho, Ph.D. (Supervising Professor),

George Alexandrakis, Ph.D., Alan Bowling, Ph.D., Hanli Liu, Ph.D., Zui Pan, Ph.D.

ABSTRACT

MODULATION OF PHYSIOLOGIC RESPONSES OF INSULIN SECRETING CELLS USING ELECTRICAL AND PHOTOSTIMULATION

Caleb Nathaniel Liebman

The University of Texas at Arlington

Supervising Professor: Michael Cho

Islet transplantation is a surgical procedure aimed at providing insulin independence to those suffering with Type I diabetes. Prior to implantation, a therapeutic window exists *ex vivo* where the cells can be treated in order to improve the procedure's efficacy. It is well established that physical stimuli are able to affect cellular functionality. Thus the work herein is designed to elucidate the effects and mechanisms by which the insulin secreting β-cells respond to non-invasive electric field stimulation and photobiomodulation.

Insulin secreting β-cells are an electrically active cell type and utilize their calcium dynamics to control insulin secretion. The calcium dynamics is driven by the metabolic state of the cell, and thus are stimulated under an elevated glucose environment. Electric field stimulation has been shown to modulate the calcium dynamics in various cell types, but its effects on β-cells has not been fully explored. By adjusting the field strength, membrane depolarization events can be altered, yielding control over the cell's calcium dynamics and thereby its insulin secretion. Through this control of calcium dynamics, various cellular signaling pathways could be affected for therapeutic benefit.

Given the important role the metabolic state plays in the functionality of these cells, near-infrared photobiomodulation could prove an effective therapeutic modality. Similar to electric

field stimulation, this modality of external physical stimulation to modulate the β-cell phenotype is its early stage of development. The primary coupling mechanism by which photobiomodulation exerts its effects is through the stimulation of cytochrome c oxidase that leads to an increase in cellular respiration. Given its ability to stimulate the metabolic state of a cell, photobiomodulation could also be used to augment the calcium and insulin dynamics of insulin secreting cells.

To further understand the effects of these modalities, we have integrated and modified previously published models to predict the functional effects of these stimuli on β-cells. In so doing, various mechanisms of action could be tested and compared to experimental results. In addition, any synergistic or additive effects could be predicted, thus providing a means of estimating optimal stimulation parameters. By elucidating these mechanisms and cellular responses, this research may open new therapeutic avenues to treating diabetes alongside a better understanding of how β-cells respond to their physical environment.

COPYRIGHT

Copyright by

Caleb Nathaniel Liebman

2020

ACKNOWLEDGEMENTS

I would like to acknowledge the following people and organizations for supporting this research:

My advisor, Dr. Michael Cho for his wisdom, guidance, and patience throughout all of my work and life experiences while pursuing the completion of this research.

My committee members, Drs. George Alexandrakis, Alan Bowling, Hanli Liu, and Zui Pan for their knowledge, experience, and their consultation.

Drs. Alfred and Janet Potvin alongside The University of Texas at Arlington's Dissertation Fellowship for their financial support that made this research possible.

My lab members and co-authors, Dr. Edidiong Inyang, Dr. Andrew McColloch, Dr. Bo Chen, Ms. Thao-Mi Vu, and Ms. Ann Phillips for their camaraderie and help during the completion of this work.

DEDICATION

I dedicate this work firstly to God and his providence. To my wonderful wife Kimberly Liebman for her love, patience, and unwavering support during the completion of this work. To all of my family for their love, guidance, and support. And to my friends for their support and fellowship that kept me going.

TABLE OF CONTENTS

TABLE OF FIGURES

CHAPTER 1:
DIABETES AND B-CELL PHYSIOLOGY

Diabetes Classification and Pathogenesis:

Diabetes mellitus is on metabolic pathology characterized by an inability to regulate blood glucose levels. It is generally classified as either Type I or II, depending on the pathogenesis of the disease.[1] The first type (T1), is due to the loss of β-cell mass via their autoimmune destruction.[2] This is generally caught early in life, and thus has been referred to as juvenile diabetes. However, maturity onset diabetes of the young (MODY) is another form of autoimmune diabetes that can occur later in life, likely as a young adult.[3] The mechanisms leading to T1 diabetes are still incompletely understood, but both genetic and environmental factors have been attributed to its formation.[4] T1 commonly progresses as killer T-cells begin to infiltrate islets and diminishing β-cell mass to the point that glucose homeostasis cannot be achieved.[5]

Unlike T1, the second type (T2) usually occurs later in life and is caused by either dysfunctional β-cells or via the insulin resistance of insulin responsive tissues.[6] Insulin resistance is the most common form of T2, and is commonly developed by a high caloric diet leading to chronic glucose loads. The β-cells respond to this chronic glucose load by exhaustively secreting insulin in an effort to stimulate liver, fat, and muscle cells to remove glucose from the blood.[7] Under chronic stimulation, these cells eventually develop a resistance to insulin leading to an imbalance of glucose homeostasis. In an effort to offset this resistance, β-cells increase their insulin production and secretion which in turn results in cellular stress and the eventual loss of functionality, which has been termed glucose toxicity.[8] The pathology of this β-cell dysfunction is different than the initial insulin resistance, and thus must be treated accordingly.[9]

Other mechanism leading to diabetes have been seen and do not cleanly fall into either category. Most notably, gestational diabetes mellitus (GDM) with insulin resistance being observed and likely due to the hormonal changes during the pregnancy alongside inflammatory processes stemming from mother child interactions. These effects can eventually lead to β-cell dysfunction with GDM being a precursor to T2 Diabetes.[10] Another classification, latent autoimmune diabetes in adults (LADA), is commonly misdiagnosed as T2 diabetes since it commonly presents itself in adults past the age of 30.[11] In the case of LADA, it is more similar to T1 diabetes since autoantibodies are present, but the destruction of β-cell mass slowly progresses. This results in symptoms more similar to T2 diabetes as the β-cell attempt to compensate for the slowly diminishing islet mass.[12] Aside from these variants, other insults leading to diabetes have included auxiliary mutations, pancreatitis caused by virus and/or bacterial infections, and various chemical toxins.[13]

Canonical Insulin Secretion:

Insulin producing β-cells respond to elevated glucose loads via a metabolic sensing mechanism. While most cells of the body use hexokinase during the initial step in glycolysis, β-cells use the isoform glucokinase which has a lower binding affinity and is not inhibited by its product glucose-6-phosphate.[14] These alterations allow the cell to sense and respond appropriately to elevated levels of blood glucose. Mutational dysfunctions of glucokinase can lead to hyperglycemia or hyperinsulism depending on how the mutation affects the sensitivity of this enzyme.[15]

Following glycolysis, an increase in mitochondrial respiration results in elevations in cytosolic ATP. This is then sensed by ATP-sensitive potassium (K_{ATP}) channels located on the

plasma membrane. These K_{ATP} channels close in response to the stimulus leading to the depolarization of the cellular membrane. As depolarization occurs, voltage dependent potassium channels (VDKCs) activate to repolarization the cellular membrane completing an action potential.[16] During each action potential, voltage gated calcium channels (VGCCs) open leading to an influx of calcium.[17] This repetition of depolarization events builds up intracellular calcium until the calcium affects the membrane potential leading to the cessation of depolarization events and the closure of VGCCs, thus resulting in the completion of a calcium spike.[18] These transient calcium spikes are important in inducing insulin secretion, as calcium directly stimulates the fusion of primed insulin vesicle near the plasma membrane's surface.[19] As the tissues of the body reduce the blood glucose in response to the elevations of insulin brought about by the aforementioned process, the glucose consumption and thus ATP production reduces in the β-cells. This reduction in the cell's metabolic state leads to the cessation of calcium dynamics and thus the reduction in insulin secretion.[20]

Given the dependence of insulin secretion by calcium and ATP, any stimulation that can elevate these factors should lead to insulin release. A commonly used technique to demonstrate this is the complete depolarization of the cellular membrane. This is commonly done by elevating extracellular potassium beyond physiological conditions causing the depolarization of the cell and elevating intracellular calcium via VGCCs, thus inducing insulin secretion.[21] Sulfonylureas, used in the treatment of T2 diabetes, act by increasing the closed state of K_{ATP} channels resulting in more frequent depolarization events thus increasing in insulin secretion and sensitivity.[22] Juxtapose to Sulfonylureas, the drug Diazoxide acts to keep K_{ATP} channels open, thereby inhibiting depolarization events and thus reducing insulin secretion.[23] Overall, it is clear that the electrophysiological state of these cells greatly affect their functional role in insulin secretion.

Calcium Dynamics and β-cell Electrophysiology:

Calcium is a ubiquitous secondary messenger that is capable of amplifying a great number of biological signals.[24] Given its importance in cellular processes, intracellular calcium is tightly maintained by a large family of calcium channels located in the plasma membrane, endoplasmic reticulum, mitochondria, and other organelles.[25] The plasma membrane contains various isoforms of VGCCs such as L-/N-/T- type channels with different opening responses to the membrane potential to allow for calcium influx from the extracellular medium.[26] Calcium can also be transported from the cytosol to the extracellular space via various active transport pumps.[27] A large player in intracellular calcium is the endoplasmic reticulum (ER), which can store or release calcium during particular signaling events.[28] SERCA pumps are the dominant mechanism by which the ER transports calcium from the cytosols into its lumen, and increases its activity when cytosolic calcium is high.[29] Other channels such as the IP3- and Ryanodine- receptors can release calcium from the ER into the cytosol when stimulation by either elevations in IP3 or intracellular calcium in the process of calcium induced calcium release (CICR) respectively.[30] When calcium levels in the ER are low, STIM signaling mechanisms can induce calcium entry into the cytosol from the extracellular space to allow restoration of ER calcium stores in a process known as store operated calcium entry (SOCE).

Calcium dynamics are found in almost every cell type but very greatly by the rate of calcium spiking frequency.[31] While calcium dynamics have been studied for over half a century, the interpretation of the information that they provide is still not fully understood.[32] Many groups have suggested that calcium dynamics are interpreted via their frequency and/or their amplitude,

but some recent studies using optogenetics have demonstrated that the duty cycle may be another important factor.[33]

While calcium spiking is a transient process, its effects can last for longer periods of time by affecting various transcription factors via calcium dependent protein kinases alongside the family of calcium modulated proteins (Calmodulin).[34] Through these interactions calcium dynamics have been shown to affect cellular proliferation, survivability, stem cell differentiation, and protein expression.[35] Some of the primary transcription factors effected by the calcium dynamics are NFAT, NF-kB, and CREB which play roles in cellular stress responses, proliferation and apoptosis, and various areas of functionality.[36]

Metabolic Physiology of β-cells:

While the primary driver for insulin secretion is calcium, other signaling pathways have been seen to modulate insulin dynamics. In particular, mitochondrial reactive oxygen species (ROS) have been shown to alter insulin secretion.[37] ROS plays a complex role in cellular physiology by interacting with various signaling pathways and ion channels.[38] While chronic elevations in ROS can lead to DNA damage and apoptosis, transient ROS elevations have been shown to have therapeutic potential by increasing the expression levels of antioxidant enzymes such as superoxide dismutase-2 (SOD2).[39,40] In regards to ionic interactions, ROS have been shown to increase intracellular calcium, which is known to cause calcium induced apoptosis.[41]

During the normal operation of the electron transport chain (ETC), electrons will commonly leak via complexes I and III forming the ROS superoxide (SO).[42] The amount of SO produced is proportional to the electron flux through the ETC.[43] Aside from the superoxide byproduct of ETC flux, nitric oxide (NO) can be formed via nitric oxide synthase (NOS).[44] NO

plays important roles in various signaling mechanisms, most notably the process of vasodilation by acting on vascular smooth muscle cells contractibility.[45] Through cysteine interactions, ROS and NO can affect ionic currents along with intracellular calcium concentrations by activating or inhibiting various cation channels.[46] These species have been shown to modulate the open fraction of various cation channels such as IP3- and Ryanodine- receptors on the surface of the endoplasmic reticulum.[47]

Mitochondrial production of ATP is also dependent on intracellular calcium levels.[48] The mitochondria can act as a calcium buffer by absorbing elevated cytosolic calcium. The primary channels that provide calcium currents between the mitochondria and the cytosol are the mitochondrial calcium uniporters (MCU) and the mitochondrial sodium calcium exchangers (mNCX).[49] Elevations in intra-mitochondrial calcium lead to an increase in ATP production alongside an increase in SO production, providing a feedback loop between calcium and ROS.[50] When the calcium concentration becomes too high, it can lead to a condition known as calcium cytotoxicity that is initiated by the release of cytochrome c from the mitochondria and eventually results in cellular apoptosis.[51] Thus calcium not only plays a critical role in a vast array of cellular processes, but it also modulated the survivability of the cell.

Conclusions and Research Aims:

Diabetes results from either a loss of β-cell mass or functionality. While the former requires exogenous insulin or islet transplantation, the latter can be treated by altering the environmental factors, commonly through drugs and/or diet. The functionality of β-cells depends on their electrophysiological and metabolic states, given the direct roles they play in calcium dynamics and insulin secretion. Thus by altering these states, the insulin functionality of the β-cell can be

manipulated. The work outlined herein, is aimed at investigating potential methods by which this cell type could be manipulated via physical means. To this end, three aims are presented with appropriate sub-aims:

Aim 1: To determine the effects of electric field stimulation on the calcium dynamics in β-cells.

1(A): Measure the viability of cells following treatment with various electrical field strengths to establish the safety of the stimulation.

1(B): To demonstrate the ability for EFS to increase the intracellular calcium concentration and how it alters the calcium dynamics. In addition, to elucidate the likely mechanisms by which EFS exerts ifs effects on this cell type.

1(C): Given the alterations in intracellular calcium brought on by EFS, demonstrate its ability to induce insulin secretion via these mechanisms.

Aim 2: Determine the calcium and secretory responses to photobiomodulation (810 nm) and to investigate potential mechanisms by which PBM could be exerting its effects.

2(A): Record observations in calcium dynamics and ROS production following exposure to PBM.

2(B): Using various channel inhibitors, demonstrate the origin of cytosolic calcium influx and which calcium channels likely play a role.

2(C): To demonstrate the ability of PBM to induce insulin secretion under a differential glucose load.

Aim 3: To integrate β-cell models with new models for the effects of PBM in order to predict cellular responses to the individual or combinatory effects of these modalities.

3(A): To develop a model to predict the response of β-cells to EFS and PBM.

3(B): Compare and contrast the resulting predictions of the model to experimentally derived results for EFS and PBM independently.

3(C): To investigate the involvement of various PBM mechanisms and how they cumulate in the cellular response and predict optimal parameters for combinatory PBM and EFS stimulation.

References:

1. Tuomi, T., 2005. Type 1 and Type 2 Diabetes: What Do They Have in Common?. *Diabetes*, 54(Supplement 2), pp.S40-S45.

2. Paschou, S., Papadopoulou-Marketou, N., Chrousos, G. and Kanaka-Gantenbein, C., 2018. On type 1 diabetes mellitus pathogenesis. *Endocrine Connections*, 7(1), pp.R38-R46.

3. Bishay, R. and Greenfield, J., 2016. A review of maturity onset diabetes of the young (MODY) and challenges in the management of glucokinase-MODY. *Medical Journal of Australia*, 205(10), pp.480-485.

4. Bluestone, J., Herold, K. and Eisenbarth, G., 2010. Genetics, pathogenesis and clinical interventions in type 1 diabetes. *Nature*, 464(7293), pp.1293-1300.

5. Rodriguez-Calvo, T., Ekwall, O., Amirian, N., Zapardiel-Gonzalo, J. and von Herrath, M., 2014. Increased Immune Cell Infiltration of the Exocrine Pancreas: A Possible Contribution to the Pathogenesis of Type 1 Diabetes. *Diabetes*, 63(11), pp.3880-3890.

6. Kahn, S., Cooper, M. and Del Prato, S., 2014. Pathophysiology and treatment of type 2 diabetes: perspectives on the past, present, and future. *The Lancet*, 383(9922), pp.1068-1083.

7. Weir, G. and Bonner-Weir, S., 2004. Five Stages of Evolving Beta-Cell Dysfunction During Progression to Diabetes. *Diabetes*, 53(Supplement 3), pp.S16-S21.

8. Robertson, R., Harmon, J., Tran, P., Tanaka, Y. and Takahashi, H., 2003. Glucose Toxicity in β-Cells: Type 2 Diabetes, Good Radicals Gone Bad, and the Glutathione Connection. *Diabetes*, 52(3), pp.581-587.

9. Cerf, M., 2013. Beta Cell Dysfunction and Insulin Resistance. *Frontiers in Endocrinology*, 4.

10. Baz, B., Riveline, J. and Gautier, J., 2016. ENDOCRINOLOGY OF PREGNANCY: Gestational diabetes mellitus: definition, aetiological and clinical aspects. *European Journal of Endocrinology*, 174(2), pp.R43-R51.

11. Pieralice, S. and Pozzilli, P., 2018. Latent Autoimmune Diabetes in Adults: A Review on Clinical Implications and Management. *Diabetes & Metabolism Journal*, 42(6), p.451.

12. Pozzilli, P. and Pieralice, S., 2018. Latent Autoimmune Diabetes in Adults: Current Status and New Horizons. *Endocrinology and Metabolism*, 33(2), p.147.

13. Murphy, R., Ellard, S. and Hattersley, A., 2008. Clinical implications of a molecular genetic classification of monogenic β-cell diabetes. *Nature Clinical Practice Endocrinology & Metabolism*, 4(4), pp.200-213.

14. Matschinsky, F., 2002. Regulation of Pancreatic-Cell Glucokinase: From Basics to Therapeutics. *Diabetes*, 51(Supplement 3), pp.S394-S404.

15. Gloyn, A., 2003. Glucokinase (GCK) mutations in hyper- and hypoglycemia: Maturity-onset diabetes of the young, permanent neonatal diabetes, and hyperinsulinemia of infancy. *Human Mutation*, 22(5), pp.353-362.

16. Rorsman, P. and Ashcroft, F., 2018. Pancreatic β-Cell Electrical Activity and Insulin Secretion: Of Mice and Men. *Physiological Reviews*, 98(1), pp.117-214.

17. Chay, T., 1997. Effects of extracellular calcium on electrical bursting and intracellular and luminal calcium oscillations in insulin secreting pancreatic beta-cells. *Biophysical Journal*, 73(3), pp.1673-1688.

18. Fridlyand, L., Tamarina, N. and Philipson, L., 2003. Modeling of Ca2+ flux in pancreatic β-cells: role of the plasma membrane and intracellular stores. *American Journal of Physiology-Endocrinology and Metabolism*, 285(1), pp.E138-E154.

19. Draznin, B., 1988. Intracellular calcium, insulin secretion, and action. *The American Journal of Medicine*, 85(5), pp.44-58.

20. Rorsman, P., Braun, M. and Zhang, Q., 2012. Regulation of calcium in pancreatic α- and β-cells in health and disease. *Cell Calcium*, 51(3-4), pp.300-308.

21. Brüning, D., Reckers, K., Drain, P. and Rustenbeck, I., 2017. Glucose but not KCl diminishes submembrane granule turnover in mouse beta-cells. *Journal of Molecular Endocrinology*, 59(3), pp.311-324.

22. Thulé, P. and Umpierrez, G., 2014. Sulfonylureas: A New Look at Old Therapy. *Current Diabetes Reports*, 14(4).

23. Henquin, J., Nenquin, M., Sempoux, C., Guiot, Y., Bellanné-Chantelot, C., Otonkoski, T., de Lonlay, P., Nihoul-Fékété, C. and Rahier, J., 2011. In vitro insulin secretion by pancreatic tissue from infants with diazoxide-resistant congenital hyperinsulinism deviates from model predictions. *Journal of Clinical Investigation*, 121(10), pp.3932-3942.

24. Clapham, D., 2007. Calcium Signaling. *Cell*, 131(6), pp.1047-1058.

25. Enomoto, M., Nishikawa, T., Siddiqui, N., Chung, S., Ikura, M. and Stathopulos, P., 2017. From Stores to Sinks: Structural Mechanisms of Cytosolic Calcium Regulation. *Advances in Experimental Medicine and Biology*, pp.215-251.

26. Catterall, W., 2011. Voltage-Gated Calcium Channels. *Cold Spring Harbor Perspectives in Biology*, 3(8), pp.a003947-a003947.

27. Brini, M. and Carafoli, E., 2010. The Plasma Membrane Ca2+ ATPase and the Plasma Membrane Sodium Calcium Exchanger Cooperate in the Regulation of Cell Calcium. *Cold Spring Harbor Perspectives in Biology*, 3(2), pp.a004168-a004168.

28. Stutzmann, G. and Mattson, M., 2011. Endoplasmic Reticulum Ca2+ Handling in Excitable Cells in Health and Disease. *Pharmacological Reviews*, 63(3), pp.700-727.

29. Zhang, I., Raghavan, M. and Satin, L., 2019. The Endoplasmic Reticulum and Calcium Homeostasis in Pancreatic Beta Cells. *Endocrinology*, 161(2).

30. Santulli, G., Nakashima, R., Yuan, Q. and Marks, A., 2017. Intracellular calcium release channels: an update. *The Journal of Physiology*, 595(10), pp.3041-3051.

31. Dolmetsch, R., Xu, K. and Lewis, R., 1998. Calcium oscillations increase the efficiency and specificity of gene expression. *Nature*, 392(6679), pp.933-936.

32. Smedler, E. and Uhlén, P., 2014. Frequency decoding of calcium oscillations. *Biochimica et Biophysica Acta (BBA) - General Subjects*, 1840(3), pp.964-969.

33. Hannanta-anan, P. and Chow, B., 2016. Optogenetic Control of Calcium Oscillation Waveform Defines NFAT as an Integrator of Calcium Load. *Cell Systems*, 2(4), pp.283-288.

34. Giorgi, C., Danese, A., Missiroli, S., Patergnani, S. and Pinton, P., 2018. Calcium Dynamics as a Machine for Decoding Signals. *Trends in Cell Biology*, 28(4), pp.258-273.

35. Tonelli, F., Santos, A., Gomes, D., da Silva, S., Gomes, K., Ladeira, L. and Resende, R., 2012. Stem Cells and Calcium Signaling. *Advances in Experimental Medicine and Biology*, pp.891-916.

36. Sabatini, P., Speckmann, T. and Lynn, F., 2019. Friend and foe: β-cell Ca2+ signaling and the development of diabetes. *Molecular Metabolism*, 21, pp.1-12.

37. Leloup, C., Tourrel-Cuzin, C., Magnan, C., Karaca, M., Castel, J., Carneiro, L., Colombani, A., Ktorza, A., Casteilla, L. and Penicaud, L., 2008. Mitochondrial Reactive Oxygen Species Are Obligatory Signals for Glucose-Induced Insulin Secretion. *Diabetes*, 58(3), pp.673-681.

38. Ray, P., Huang, B. and Tsuji, Y., 2012. Reactive oxygen species (ROS) homeostasis and redox regulation in cellular signaling. *Cellular Signalling*, 24(5), pp.981-990.

39. Cox, C., McKay, S., Holmbeck, M., Christian, B., Scortea, A., Tsay, A., Newman, L. and Shadel, G., 2018. Mitohormesis in Mice via Sustained Basal Activation of Mitochondrial and Antioxidant Signaling. *Cell Metabolism*, 28(5), pp.776-786.e5.

40. Li, Z., Shi, K., Guan, L., Cao, T., Jiang, Q., Yang, Y. and Xu, C., 2010. ROS leads to MnSOD upregulation through ERK2 translocation and p53 activation in selenite-induced apoptosis of NB4 cells. *FEBS Letters*, 584(11), pp.2291-2297.

41. Görlach, A., Bertram, K., Hudecova, S. and Krizanova, O., 2015. Calcium and ROS: A mutual interplay. *Redox Biology*, 6, pp.260-271.

42. Dröse, S. and Brandt, U., 2012. Molecular Mechanisms of Superoxide Production by the Mitochondrial Respiratory Chain. *Advances in Experimental Medicine and Biology*, pp.145-169.

43. Murphy, M., 2008. How mitochondria produce reactive oxygen species. *Biochemical Journal*, 417(1), pp.1-13.

44. GHAFOURIFAR, P. and CADENAS, E., 2005. Mitochondrial nitric oxide synthase. *Trends in Pharmacological Sciences*, 26(4), pp.190-195.

45. Chen, K., Pittman, R. and Popel, A., 2008. Nitric Oxide in the Vasculature: Where Does It Come From and Where Does It Go? A Quantitative Perspective. *Antioxidants & Redox Signaling*, 10(7), pp.1185-1198.

46. Trebak, M., Ginnan, R., Singer, H. and Jourd'heuil, D., 2010. Interplay Between Calcium and Reactive Oxygen/Nitrogen Species: An Essential Paradigm for Vascular Smooth Muscle Signaling. *Antioxidants & Redox Signaling*, 12(5), pp.657-674.

47. Song, M., Makino, A. and Yuan, J., Role of Reactive Oxygen Species and Redox in Regulating the Function of Transient Receptor Potential Channels. Antioxidants & Redox Signaling, 2011; 15(6), pp.1549-1565.

48. Tarasov, A., Griffiths, E. and Rutter, G., 2012. Regulation of ATP production by mitochondrial Ca2+. *Cell Calcium*, 52(1), pp.28-35.

49. Pathak, T. and Trebak, M., 2018. Mitochondrial Ca2+ signaling. *Pharmacology & Therapeutics*, 192, pp.112-123.

50. Adam-Vizi, V. and Starkov, A., 2010. Calcium and Mitochondrial Reactive Oxygen Species Generation: How to Read the Facts. *Journal of Alzheimer's Disease*, 20(s2), pp.S413-S426.

51. Kass, G. and Orrenius, S., 1999. Calcium signaling and cytotoxicity. *Environmental Health Perspectives*, 107(suppl 1), pp.25-35.

CHAPTER 2:

ALTERED B-CELL CALCIUM DYNAMICS VIA ELECTRIC FIELD EXPOSURE

Caleb Liebman, Thao-Mi Vu, Ann Phillips, Bo Chen, and Michael Cho

Material From:

Caleb Liebman, Thao-Mi Vu, Ann Phillips, Bo Chen, and Michael Cho (2020)

Altered β-Cell Calcium Dynamics *via* Electric Field Exposure. *Annals of Biomedical Engineering*. https://doi.org/10.1007/s10439-020-02517-w

Abstract:

Electric field stimulation has long been investigated with results supporting its therapeutic potential; however, its effects on insulin secreting cells has yet to be fully elucidated. Herein we explored the effects of physiological direct current (DC) electric field stimulation on the intracellular calcium dynamics of mouse derived βTC-6insulinoma cells. This electrical stimulation resulted in an elevation in intracellular calcium along with a rise in calcium spiking activity. Further investigation indicated that the rise in intracellular calcium was mediated by an influx of calcium via L-type voltage gated calcium channels. Additionally, the effects of the electric field stimulation were able to induce insulin secretion in the absence of glucose stimulation. Given these results, DC electric field stimulation could be used as a non-invasive tool to modulate intracellular calcium dynamics and insulin secretion of b-cells for therapeutic application.

Introduction:

In insulin producing β-cells, their calcium dynamics play a critical role in the signaling mechanisms affecting their functionality. It affects the secretion and production of insulin, the expression of transcription factors, and the cell's viability.[20] In healthy β-cells, insulin secretion is normally initiated by an elevation in glucose uptake, resulting in an increase of glucokinase activity, ultimately leading to an increase in glucose catabolism.[28] The resulting rise in ATP closes ATP sensitive potassium channels leading to membrane depolarization. The resulting depolarizing events activate voltage gated calcium channels (VGCCs) leading to an increase in intracellular calcium. This rise in cytosolic calcium directly activates insulin granule exocytosis leading to insulin secretion.[40] Unfortunately, this process along with insulin production can be hindered by several disease states or by chronic cellular stress resulting in β-cell dysfunction.

The most common disease state affecting β-cell function is type II Diabetes Mellitus (DM).[31] In type II diabetes, β-cells will eventually become dysfunctional due to glucotoxicity brought about by a chronic hyperglycemic environment.[36] Hyperglycemia can usually be managed with diet, exercise, and drugs such as metformin, leading to some recovery of β-cell function.[32] However, in some cases chronic hyperglycemia can lead to irreversible glucotoxicity, and thus a more direct intervention would be required.[34] Drugs such as Sulfonylurea's and GLP-1 agonists exert direct effects on β-cells to improve insulin secretion and manage type II DM. While these drugs act via differing mechanisms, both influence the calcium dynamics and thus insulin release dynamics within these cells.[39]

Exogenous electric fields (EFs) have demonstrated the capacity to affect a multitude of cellular processes.[2] Its therapeutic potential has been well demonstrated in wound healing by effecting cell migration, proliferation, and protein expression in various cell types.[24] Some of these responses have been attributed to the ability of various modes of EFs to modify intracellular calcium dynamics. For instance, there has been success in controlling intracellular calcium dynamics and thus their biological effects via pulsed electric fields.[5,22,42] While pulsed fields have some advantages over continuous DCEFs, the naturally occurring DC endogenous fields are commonly found at strengths between 1 and 5 V/cm.[18] In addition, by using a constant DCEFs we can limit the effects of electrical stimulation to the cell membrane surface, as pulsed fields are able to effect intracellular dynamics.[38] Of particular interest here, DCEFs have also been shown to alter intracellular calcium dynamics in several cell types.[4,16] While these cell types have been investigated, very little knowledge exists about the effects of EFs on the calcium dynamics of β-cells. By elucidating the effects of electric field stimulation (EFS) on the calcium dynamics of a

β-cell model, new modes of therapies could be adapted for in vivo stimulation and islet transplantation for type II and type I diabetes, respectively.

Methods:

Device Design: The electric field exposure chamber was designed to minimize temperature rise (< 0.1 °C) and unwanted byproducts, as described in detail elsewhere.[14] Briefly, a direct current from an amplifier (BOP100, KEPCO, Flushing, NY) was applied to the chamber using two platinum electrodes. The cross-sectional area of the chamber has been designed with specific dimensions (16 mm x 0.8 mm) to minimize the input electrical current (< 4 mA) and yet produce an electric field strength of up to 3 ± 0.1 V/cm. This range of electric field strengths was intentionally chosen to represent the physiological electric field of ~ 2 V/cm.[44] A feedback control mechanism was applied to maintain a constant current during the 15 min exposure. The electric field was calculated using Ohm's law, J = r E, when J is the current density and r is the conductivity of the buffer (1 S/m at room temperature) and monitored using an oscilloscope (Model 2205, Tektronix, Beaverton, OR). It should be noted that the device was designed for a short time EF exposure (< 1 h) to living cells and to be mounted onto a microscope stage for real-time observation. All experiments were performed at room temperature.

Cell Culture: Insulinoma (βTC-6) mouse b-cells were purchased from ATCC (CRL-11506) and used as a model to study the effect of EFS on b-cells. The cells were cultured in a high glucose (4.5 g/L) DMEM (Sigma) with 15% FBS (Gibco) and 1% Penicillin–Streptomycin according to the prescribed protocol.[25] Cells were passaged using 0.25% Trypsin–EDTA and seeded on glass coverslips immersed in a low glucose (1.0 g/L) DMEM media. These samples

were allowed to grow for 2 to 5 days at 37°C and in a humidified 5% CO2 environment before being imaged.

Calcium Fluorescent Microscopy: Fluo-8, a calcium specific AM ester dye, was used to determine any changes in intracellular calcium. Samples were washed and stained with 0.8 lM Fluo-8 and 1 drop/mL Nucblue in Hanks Balanced Salt Solution (HBSS) for 30 min at 37 °C. Samples were then loaded onto the EF chamber and imaged for calcium rise and spiking. Measurements for calcium rise recorded a single static image before and after EF exposure, while calcium spiking was recorded over 2 min before and after EFS with a 5 second sampling interval.[11]

Calcium Image Analysis: For calcium rise, the mean intensity of clusters in the sample were measured at 0 min (Pre) and 15 min (Post) time points using Nikon Elements. Background subtraction was then performed and the percent change was determined by comparing the post-exposure to the pre-exposure mean intensities. For calcium spiking, regions of interest (ROIs) were generated over the nuclei of individual cells. The mean intensity over time was measured for both the pre and post imaging sessions. A moving average (n = 10) was used as a baseline with a 10% (F/Fo) threshold for spiking determination. This was done account for the background rise in calcium along with filtering out noise. For spatial analysis, each cluster's ROI centroid coordinates (x, y) were determined along with the centroid coordinates for each cell's ROI. The radial distance for each cell from the center of the cluster was determined using the equation:

$$r = \sqrt{(x_{cell} - x_{cluster})^2 + (y_{cell} - y_{cluster})^2}$$

Each cells change in Fluo-8 intensity was determined and compared to its radial distance from its respective cluster's center.

Blocking Experimentation: Samples were imaged before and after EF stimulation for average calcium rise under differing buffer conditions. HBSS with calcium was used as the control,

while calcium-free HBSS (supplemented with 0.8 mM magnesium) was used to demonstrate the calcium influx from the extracellular space. Verapamil (100 μM) was added to the HBSS staining solution and incubated for 30 minutes prior to imaging for testing the role of a calcium influx through L-type VGCCs.

Immunofluorecent Microscopy: Samples were washed and fixed in 4% paraformaldehyde for 15 min, followed by permeabilization using 0.25% Triton-X100 solution for 10 min. Blocking was performed using 1% BSA solution for 30 min and then 1:100 primary staining for CaV1.3 (Abcam ab85491) overnight at 4 °C. Secondary staining was carried out for 90 min at room temperature with 1:200 anti-mouse Alexa 555. Samples were then washed and mounted for imaging.

Insulin Secretion: Samples for insulin secretion were seeded at 50,000 cell/cm^2 3 days prior to experimentation. Kreb's Ringer buffer (KRB) with 0.1% BSA was used for all steps in secretion (118.5 mM NaCl, 2.54 mM CaCl2, 1.9 mM KH2PO4, 4.74 mM KCL, 25 mM NaHCO3, 1.19 mM MgSO4, 10 mM HEPES, pH 7.4).[19] Samples were first washed and incubated for 30 min in (KRB) without glucose at 37 °C, and then KRB was replaced and samples were incubated another 30 min. Samples were then washed and mounted to the EF device and exposed to either no EF (control) or 3 V/cm EF for a total of 15 min. Following exposure, approximately 600 μL of solution was taken from the chamber at the area were the cells were exposed and was frozen. A mouse insulin ELISA kit from Thermofisher (EMINS) was used. All samples were diluted 1:10 for the assay reading.

CyQuant for Secretion: To normalize the insulin secretion, CyQuant (Thermo), a nucleic acid assay, was used to estimate the number of cells in each sample used for insulin secretion. Samples were first frozen at -20°C and then lysed with 2 mL of CyQuant 1X lysing solution. A cell scrapper was used to suspend the cells and then 200 μL (1:10 dilution for assay) of the sample

lysate were added to three wells for each sample in a black sided 96 well plate. CyQuant stain was then added to each well for a 2x concentration in accordance with the manufactures protocol for cell counts up to 100,000 cells.

Viability Experimentation: Samples were stained using Nucblue for all nuclei and Nucgreen for the nuclei of dead cells. All samples were mounted to the device and exposed to either no EF (sham) or EF at 1, 2, and 3 V/cm. Samples were then placed into new dishes, re-immersed in media, and placed inside the incubator overnight. The following day cells were stained and imaged. Nikon Elements auto generation for ROI was used to determine the total area of Nucblue (viable cells) or Nucgreen (dead cells). The percent viability was determined by the following equation:

$$Viability(\%) = \frac{(N - D)}{N} \times 100\%$$

Where N is the total area of all nuclei in the image and D is the total area of all the NucGreen stained nuclei in the image.

Statistical Analysis: A two-tailed paired t test was used to determine significance between the pre and post conditions for all calcium experiments. For insulin secretion, a simple unpaired t test was performed, while the viability testing used a one factor ANOVA with post hoc multiple unpaired t-tests with bonferroni correction. An Iglewicz and Hoaglin's multiple outlier test (modified Z score of 3.5) was used for to detect outliers for spatial calcium results and insulin secretion. Analysis was performed using Microsoft Excel, Contchart software for outlier tests, and the plugin from Real Statistics Resource Pack.[43]

Results:

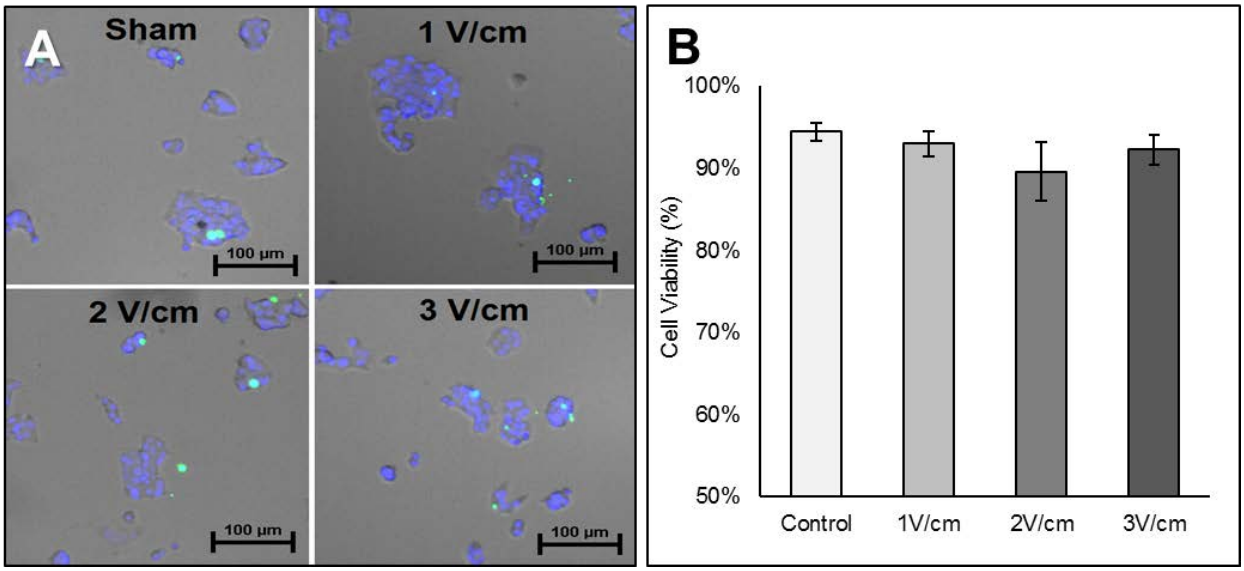

Figure 2-1: (A) Representative images for cell viability in response to EF. Blue stained for all nuclei while green stained for nuclei of dead cells. (B) Quantification of changes in cell viability by various EF strengths. Data represent mean ± SEM from 3 independent experiments.

Cell Viability: To determine if an external electric field caused any cytotoxic effects, βTC-6 insulinoma cells were exposed to 1, 2, and 3 V/cm electric fields for 15 min, and the cell viability was assessed as described above. A composite image (Fig. 2-1a) was constructed to illustrate representative cell viability tests using the three different EF strengths. Quantitative results demonstrated cell viability of approximately 90% or greater for all exposure conditions with no significant differencewhen compared to the sham experiments (Fig. 2-1b). Application of electric fields in range of 1 to 3 V/cm for 15 min exposure did not adversely affect the cell viability.

Intracellular Calcium Dynamics: Imaging for Fluo-8 intensity, βTC-6 insulinoma cells demonstrated an elevation in intracellular calcium that appeared to depend on the strength of the EF exposure (Fig. 2-2a). Following the 15 min of exposure, the percent change in Fluo-8 intensity was measured to quantify the rise in intracellular calcium. The application of the three different electric field strengths induced a 9, 11, and 18% response to 1, 2, and 3 V/cm, respectively (Fig. 2-2b). As anticipated, application of a 1 V/cm EF did not induce a statistically significant elevation

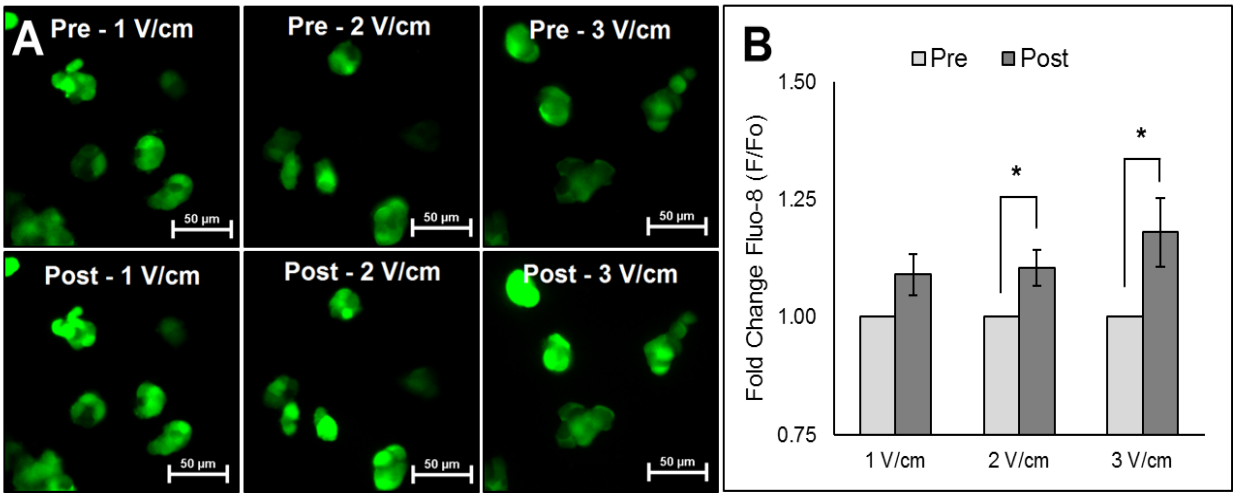

Figure 2-2: (A) Representative images of intracellular calcium increase after 15 minutes of exposure to various EF strengths. (B) Average increase in intracellular calcium after the 15 minutes of exposure. Data represent 14, 11, and 10 independent samples for 1, 2, and 3 V/cm respectively. All error bars represent standard error of the mean. * $p < 0.05$.

in the intracellular calcium level. This is consistent with our previously reported results that a weak EF (e.g., 1 V/cm) would require ~ 52 min exposure to illicit maximum changes, whereas only a 20 min exposure of a 3 V/cm EF should be sufficient to raise the intracellular calcium level.[23] Because we have limited the exposure time to 15 min (see Discussion below) to determine short-term effects, a 1 V/cm EF may not be sufficient in strength to elevate the intracellular calcium level.

Potential calcium pathways that might mediate the EF-induced increase in the intracellular calcium level were probed. First, the presence of L-type VGCCs on the cells was confirmed using immunofluorescence. An abundant expression of L-type calcium channels stained with anti-CaV1.3 antibodies was clearly visible on the βTC-6 cells (Fig. 2-3a). Next, we depleted the calcium ions in the extracellular buffer. The removal of calcium from the buffer inhibited any rise in intracellular calcium in response to a 3 V/cm EF (Fig. 2-3b). This suggests that an influx across the cell membrane was responsible for the EF-mediated calcium rise. Based on previously reported

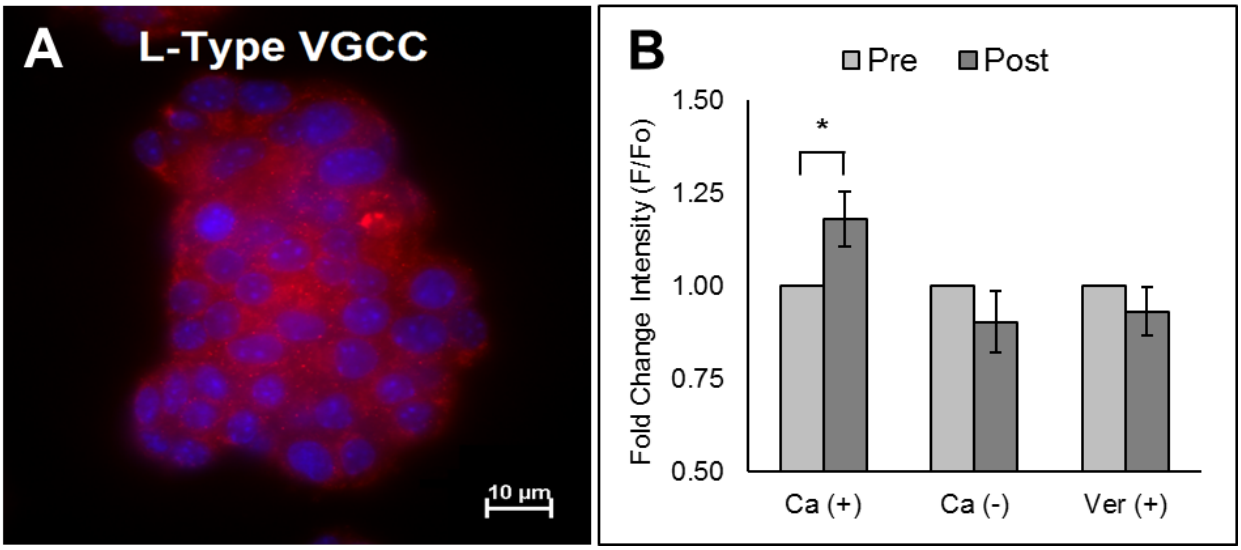

Figure 2-3: (A) Anti-CaV1.3 fluorescent imaging demonstrating expression of L-type VGCCs in β-TC6 cells with counterstained nuclei. (B) Intracellular calcium increase after 15 minutes of exposure to 3 V/cm in Hanks solution, Hanks without calcium, and Hanks with a L-type VGCC inhibitor (verapamil). Data represens 10, 9, and 9 independent samples for the conditions respectively. The control data (e.g., normal Hanks solution) were repeated from Fig. 2-2. All error bars represent standard error of the mean. * $p < 0.05$.

findings,[16] and the immunofluorescent images we recorded (see Fig. 2-3a), it is plausible that L-type VGCCs were likely one of the dominant pathways for the calcium influx. To demonstrate the role of L-type VGCCs, cells were incubated with a specific L-type channel inhibitor (verapamil) prior to EF exposure. Verapamil effectively blocked the increase in intracellular calcium level (Fig. 2-3b), providing evidence that the L-type channels may have been activated.

Since these βTC-6 cells grow in clusters and VGCCs are affected by the local field strength, we hypothesized that the location of each individual cell within a cluster may alter its intracellular calcium response to the electrical stimulation. This is because cells at the periphery of a cluster are likely to experience the full impact of an EF, but cells near the center would be shielded. While we determined the average response of the clusters, variation within a given cluster may be explained by the shielding effect. We first determined the centroid of each cell based on the

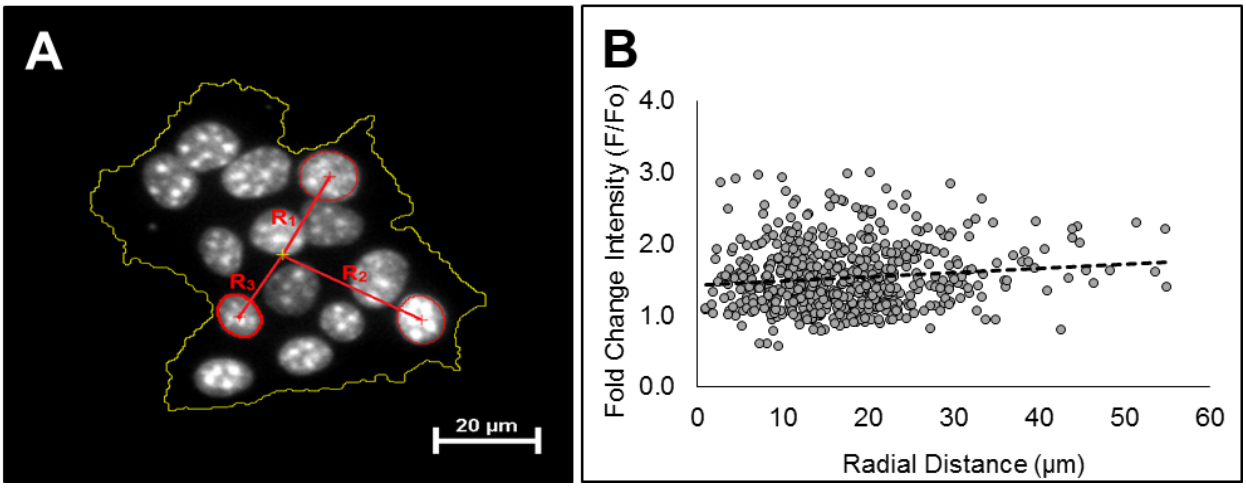

Figure 2-4: (A) Illustrative image of positional ROI's and how distance from cluster center was determined. (B) Fold change in individual cell's Fluo-8 intensity in response to a EFS (3 V/cm) with respect to distance from its cluster's center. Data represent 547 cells exposed to the EF.

location of its nucleus, and then determined the centroid of its respective cluster. The radial distance from the centroid of each cell to the centroid of its cluster was calculated. As an illustration, in Fig. 2-4a, three cells within a cluster were randomly selected, and the distance from each cell to the center of the cluster was denoted by R1, R2 and R3. Such a strategy of data analysis led to establishing a correlation between the Fluo-8 intensity of each cell and its location relative to the cluster's center (Fig. 2-4b). Using a linear regression, we observed a 5.8% increase for every 10 µm the cell was located away from the cluster's center. Not surprisingly, a Pearson coefficient of 0.12 was calculated indicating that other factors are also likely affecting the cellular response to the EF in addition to the shielding effect.

Insulin secreting cells have been shown to depend critically on intracellular calcium levels[30] as well as the calcium dynamics (e.g., calcium spiking).[17] In an effort to understand the effects of EFs on calcium spiking, we recorded the Fluo-8 intensity over a 2 min imaging window before and after the EF was applied. It is interesting to note here that the baseline calcium level did not remain stable but varied during the calcium spiking recording (Fig. 2-5a). This presented

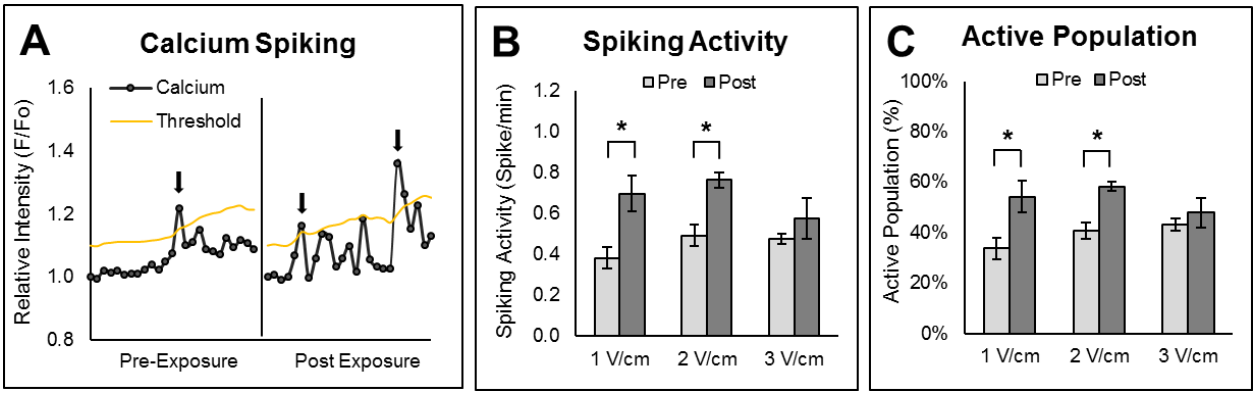

Figure 2-5: (A) Calcium tracing of a cell before and after EFS at 3 V/cm (black line) alongside the moving average threshold (gold line). A moving average was used to account for background calcium increase and to reduce noise. (B) Mean spiking frequency of all measured cells before and after exposure, against all EF strengths. (C) The average percentage of the population found to spike at least once during the observation time period before and after EF exposure. Both spiking activity and active population represent 10, 10, and 9 independent samples for 1, 2, and 3 V/cm respectively. All error bars represent standard error of the mean. * $p < 0.05$.

a challenge in defining a calcium spike. For example, using a constant baseline might lead to an excessive estimate of calcium spikes due to the changing baseline. We therefore applied a moving 10 data point average threshold and scored as a calcium spike if the Fluo-8 intensity was at least 10% above the moving average baseline (Fig. 2-5a). Mean activity was defined as the total number of spikes recorded over time divided by the number of cells being measured. The mean calcium spiking activity following the EF stimulation was found to increase in response to a 1 or 2 V/cm but not 3 V/cm EF (Fig. 2-5b). Interestingly, there was also a change in the number of cells showing active spiking. The percentage of cells that spiked at least once during the observation time period was compared between pre- and post-exposure (Fig. 2-5c). Again, both 1 and 2 V/cm but not 3 V/cm EF were found to significantly increase the percentage of actively spiking cells.

Given that calcium directly activates insulin granule exocytosis, we aimed to determine if the EF could stimulate insulin secretion even in the absence of glucose in response to a 3 V/cm EF, since this EF strength demonstrated the greatest rise in intracellular calcium level. All samples

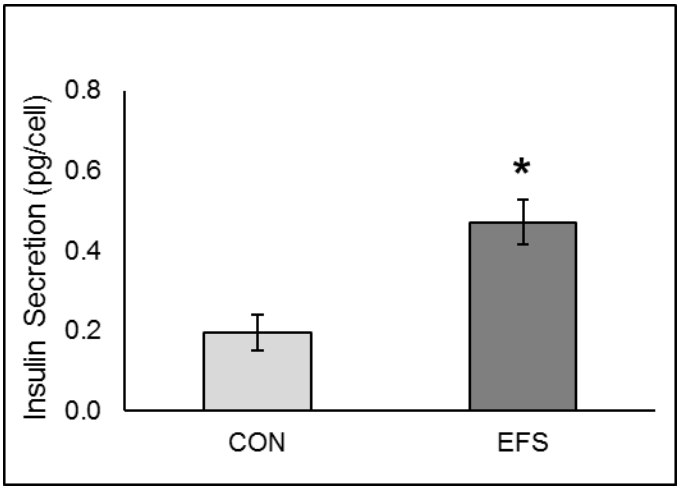

Figure 2-6: Average insulin secretion per cell for 0 mM glucose (CON) and 0 mM glucose and 3 V/cm EF exposure after 15 minutes. Data represent 7 and 8 independent samples over 3 separate experiment sets for CON and EFS, respectively. Error bars represent standard error of the mean. * $p < 0.05$.

were mounted on the device and immersed in glucose free Kreb's Ringer buffer. By sampling the buffer after stimulation, we were able to determine the total insulin secretion. Using a nucleic acid assay (CyQuant) we were then able to determine average insulin secretion per cell. In response to a 3 V/cm EF for a 15 min exposure, the insulin secretion per cell demonstrated a > 2-fold increase (Fig. 2-6). This is to be expected as a significant rise in intracellular calcium produces more total insulin secretion than small transient rises derived from calcium spiking.[21]

Discussion:

The aim of the study was to apply physiologically relevant electric fields (e.g., 1–3 V/cm DC electric field; DCEF) while limiting the exposure time to focus on the short term effects (e.g., 15 min exposure). Under these exposure conditions, direct activation of the L-type VGCCs by the DCEF is unlikely since a 3 V/cm EF strength would only induce a small membrane voltage differential. For example, considering a typical β-cell cluster ~ 50 lm in size, it can be considered as an electrical insulator in response to a direct current EF.[38] The expected membrane potential

change would be ~15 mV, not sufficient to depolarize the membrane potential. Instead, many laboratories including ours have repeatedly demonstrated that the charged cell surface receptors may be redistributed on the cell surface in response to an external electrical stimulation.[1,13]

The diffusion and electromigration coefficients of cell surface receptors have been measured using various experimental techniques including fluorescence recovery after photobleaching (FRAP).[15] The lateral diffusion coefficients (D) in the membrane plane are in the range of 10^{-9} and 10^{-11} cm^2/s, and the electromigration coefficients (μ) in the range of 10^{-6} (cm/s)/(V/cm).[12] The distance traversed by random movement is described by $X_D = (4D\ t)^{1/2}$, and that by electromigration should be $X_E = \mu\ E\ t$. The characteristic time after which the electromigration becomes dominant may be estimated by assuming the ratio of $[(4Dt)^{1/2}/(\mu Et)]$ to be 0.05, e.g., 5% of the distance traversed by electromigtation. Assuming $D = 10^{-10}$ cm^2/s, the characteristic time is calculated 15 min. It has been predicted and shown that the charged surface receptors do indeed redistribute,[27] and that selection of the exposure time of 15 min was carefully chosen based on this prediction in order to mitigate the effects of redistribution. As seen in fibroblast cells, an EF of 10 V/cm for an hour was required for an 80% asymmetrical redistribution of charged surface receptors.[41] For comparative purposes, one can also estimate the time that would be required to induce a similar cell surface receptor redistribution if a 1 V/cm EF was applied (~ 45 min). This time estimate is consistent with our previous results[23] that a weak 1 V/cm EF should be applied for > 50 min to induce maximal changes in the intracellular calcium level.

Although the estimated change in membrane potential is small and would be insufficient to induce membrane depolarization, it could nonetheless increase calcium influx through several potential mechanisms. During EF exposure, the shift in membrane potential could lead to the redistribution of charged cell surface receptors along with alterations in other ionic currents.[27,29]

For example, the sodium channels may be more sensitive and respond to the 15 mV change attributed to exposure to a 3 V/cm EF. These events could further influence the membrane potential yielding a direct effect on the magnitude of the calcium current.[8] This rise in the electromotive force for calcium could increase the rate of calcium entry across open VGCCs, thus elevating the cytosolic calcium concentration. Once the applied EF is removed, an increased activity in calcium dynamics is expected to gradually decrease. Within a 60 min observation time period post-field, the calcium spiking activity appeared to be abated but remained above the baseline.

These β-cells typically grown in clusters. Since cellular membranes acts as electrical insulators, we hypothesized that cells at the periphery of the cluster would experience a stronger local EF than those at the cluster's center. If so, cells near the cluster's edge should demonstrate a greater response to the EFS than those near the center.[38] We addressed this question by first determining the centroid of each cell's nucleus along with its respective cluster's centroid. One can then calculate each cell's radial distance from the center of its cluster. As shown in Fig. 2-4, we observed a suppressed calcium elevation in cells near the cluster's center, while cells near the perimeter had greater calcium elevations. Such data analysis supports our hypothesis that the EF would differentially affect a given cell's intracellular calcium level depending on its spatial location within a cluster. Optimization of electrical stimulation for therapeutic purposes would likely need to overcome this type of shielding effect. Alternative modes such as pulsed or AC fields should be further investigated.

Since calcium spiking is thought to be an integral part of β-cell physiology, we aimed to determine the effects of EF exposure on calcium spiking activity.[7] It has been seen in neuronal cell types that weak electrical stimulation can modulate the spike timing and frequency of depolarization events.[35] Since depolarization spiking trains are responsible for the calcium spiking

events, it should follow that an increase in electrical activity would lead to an increase in calcium activity.[26] From our results, it was clear that EF exposure did influence calcium spiking activity along with increasing the number of active cells. Interestingly, our observations demonstrated an inverse relationship between calcium accumulation and calcium spiking activity. Since L-type VGCCs are known to be sensitive to calcium dependent inactivation (CDI), it may be that the significant rise in intracellular calcium brought about by a stronger EF (e.g., 3 V/cm) interferes with the calcium spiking machinery thus reducing calcium spiking frequency.[10] This response could be a protective mechanism to prevent the cytotoxic effects of calcium overload.[37]

Since insulin secretion directly depends on a rise in intracellular calcium, we aimed to determine the capacity of EFS to induce insulin secretion in the absence of glucose.[3] Following our initial observations on calcium accumulation, the EF strength of 3 V/cm was chosen since it had the greatest effect on intracellular calcium. Our results demonstrated the ability of EFS to induce insulin secretion even in the absence of glucose. Since calcium is the direct trigger for insulin secretion, it makes sense that the significant rise in calcium due to EFS would correspond with insulin secretion.[33] A commonly used method to induce insulinsecretion is exposure to high concentrations of potassium chloride (KCl). This depolarizes the cellular membrane resulting in a dramatic and sustained elevation in intracellular calcium via L-type VGCCs.[6] Calcium elevation via KCl exposure can induce a stronger initial insulin release than glucose and appear to differentially affect granule turnover rate.[9] The mechanisms by which EFS stimulates insulin secretion may be similar to those of KCl-induced insulin secretion.

Overall, we have shown that a DCEF is able to modulate both the intracellular calcium concentration and the spiking activity, which appears to be inversely related with the strength of the EF. Although a longer exposure of EFS may result in a greater insulin secretion, we

demonstrated that even a 15 min exposure was sufficient to induce insulin secretion despite an absence of glucose. While the electric field parameters have yet to be optimized for applications in modulating the calcium and insulin dynamics of β-cells, it is feasible to contemplate the development of non-pharmaceutical therapies to modulate intracellular calcium and potentially stimulate dysfunctional β-cells.

Acknowledgments:

This work was supported in part by the generous donations from Drs. Alfred and Janet Potvin.

References:

1. Allen, G., A. Mogilner, and J. Theriot. Electrophoresis of cellular membrane components creates the directional cue guiding keratocyte galvanotaxis. Curr. Biol. 23:560–568, 2013.

2. Balint, R., N. Cassidy, and S. Cartmell. Electrical stimulation: a novel tool for tissue engineering. Tissue Eng. B 19:48–57, 2013.

3. Bardy, G., A. Virsolvy, J. Quignard, M. Ravier, G. Bertrand, S. Dalle, G. Cros, R. Magous, S. Richard, and C. Oiry. Quercetin induces insulin secretion by direct activation of l-type calcium channels in pancreatic beta cells. Br. J. Pharmacol. 169:1102–1113, 2013.

4. Bedlack, R., M. Wei, and L. Loew. Localized membrane depolarizations and localized calcium influx during electric field-guided neurite growth. Neuron 9:393–403, 1992.

5. Beebe, S., P. Blackmore, J. White, R. Joshi, and K. Schoenbach. Nanosecond pulsed electric fields modulate cell function through intracellular signal transduction mechanisms. Physiol. Meas. 25(4):1077–1093, 2004.

6. Berdan, C., K. Erion, N. Burritt, B. Corkey, and J. Deeney. Inhibition of monoacylglycerol lipase activity decreases glucose-stimulated insulin secretion in INS-1 (832/13) cells and rat islets. PLoS ONE 11:e0149008, 2016.

7. Bertram, R., A. Sherman, and L. S. Satin. Electrical bursting, calcium oscillations, and synchronization of pancreatic islets. In: The Islets of Langerhans. Advances in Experimental Medicine and Biology, Vol. 654, edited by M. Islam. Dordrecht: Springer, 2010.

8. Borys, P. On the biophysics of cathodal galvanotaxis in rat prostate cancer cells: Poisson–Nernst–Planck equation approach. Eur. Biophys. J. 41:527–534, 2012.

9. Bru¨ ning, D., K. Reckers, P. Drain, and I. Rustenbeck. Glucose but not KCl diminishes submembrane granule turnover in mouse beta-cells. J. Mol. Endocrinol. 59:311–324, 2017.

10. Budde, T., S. Meuth, and H. Pape. Calcium-dependent inactivation of neuronal calcium channels. Nat. Rev. Neurosci. 3:873–883, 2002.

11. Chen, B., J. Tjahja, S. Malla, C. Liebman, and M. Cho. Astrocyte viability and functionality in spatially confined microcavitation zone. ACS Appl. Mater. Interfaces. 11:4889–4899, 2019.

12. Cho, M. A review of electrocoupling mechanisms mediating facilitated wound healing. IEEE Trans. Plasma Sci. 30:1504–1515, 2002.

13. Cho, M., H. Thatte, R. Lee, and D. Golan. Induced redistribution of cell surface receptors by alternating current electric fields. FASEB J. 8:771–776, 1994.

14. Cho, M. R., H. S. Thatte, M. T. Silvia, and D. E. Golan. Transmembrane calcium influx induced by ac electric fields. FASEB J. 13:677–683, 1999.

15. Cho, M., et al. Membrane dynamics of the water transport protein Aquaporin-1 in intact human red cells. Biophys. J .76:1136–1144, 1999.

16. Dube´, J., et al. Human keratinocytes respond to direct current stimulation by increasing intracellular calcium: preferential response of poorly differentiated cells. J. Cell. Physiol. 227:2660–2667, 2012.

17. Fridlyand, L., N. Tamarina, and L. Philipson. Bursting and calcium oscillations in pancreatic b-cells: specific pacemakers for specific mechanisms. Am. J. Physiol. 299:E517–E532, 2010.

18. Funk, R. Endogenous electric fields as guiding cue for cell migration. Front. Physiol. 2015. https://doi.org/10.3389/fphys.2015.00143/full.

19. Garcı´a-Montalvo, E., H. Reyes-Pe´ rez, and L. Del Razo. Fluoride exposure impairs glucose tolerance via decreased insulin expression and oxidative stress. Toxicology 263:75–83, 2009.

20. Gilon, P., H. Chae, G. Rutter, and M. Ravier. Calcium signaling in pancreatic b-cells in health and in type 2 diabetes. Cell Calcium 56:340–361, 2014.

21. Henquin, J., N. Ishiyama, M. Nenquin, M. Ravier, and J. Jonas. Signals and pools underlying biphasic insulin secretion. Diabetes 51:S60–S67, 2002.

22. Joshi, R., A. Nguyen, V. Sridhara, Q. Hu, R. Nuccitelli, S. Beebe, J. Kolb, and K. Schoenbach. Simulations of intracellular calcium release dynamics in response to a highintensity, ultrashort electric pulse. Phys. Rev. E 75(4):041920, 2007.

23. Khatib, L., D. Golan, and M. Cho. Physiologic electrical stimulation provokes intracellular calcium increase mediated by phospholipase C activation in human osteoblasts. FASEB J. 18:1903–1905, 2004.

24. Kloth, L. Electrical stimulation for wound healing: a review of evidence from in vitro studies, animal experiments, and clinical trials. Int. J. Low. Extrem. Wounds 4:23–44, 2005.

25. Kwon, K., R. Nityanandam, J. New, and H. Daniell. Oral delivery of bioencapsulated exendin-4 expressed in chloroplasts lowers blood glucose level in mice and stimulates insulin secretion in beta-TC6 cells. Plant Biotechnol. J. 11:77–86, 2012.

26. Ladewig, T., and B. Keller. Simultaneous patch-clamp recording and calcium imaging in a rhythmically active neuronal network in the brainstem slice preparation from mouse. Pflu¨g. Arch. 440:322, 2000.

27. Lee, R., T. Gowrishankar, R. Basch, P. Patel, and D. Golan. Cell shape-dependent rectification of surface receptor transport in a sinusoidal electric field. Biophys. J. 64:44–57, 1993.

28. Matschinsky, F. Regulation of pancreatic β-cell glucokinase: from basics to therapeutics. Diabetes 51:S394–S404, 2002.

29. Mycielska, M., and M. Djamgoz. Cellular mechanisms of direct-current electric field effects: galvanotaxis and metastatic disease. J. Cell Sci. 117:1631–1639, 2004.

30. Navarro-Tableros, V., T. Fiordelisio, A. Herna´ ndez-Cruz, and M. Hiriart. Physiological development of insulin secretion, calcium channels, and GLUT2 expression of pancreatic rat β-cells. Am. J. Physiol. 292:E1018–E1029, 2007.

31. NCD Risk Factor Collaboration. Worldwide trends in diabetes since 1980: a pooled analysis of 751 populationbased studies with 4Æ4 million participants. Lancet 387:1513–1530, 2016.

32. Page, K., and T. Reisman. Interventions to preserve beta cell function in the management and prevention of type 2 diabetes. Curr. Diab. Rep. 13:252–260, 2013.

33. Pedersen, M., and A. Sherman. Newcomer insulin secretory granules as a highly calcium-sensitive pool. Proc. Natl. Acad. Sci. USA 106:7432–7436, 2009.

34. Poitout, V. Minireview: secondary-cell failure in type 2 diabetes–a convergence of glucotoxicity and lipotoxicity. Endocrinology 143:339–342, 2002.

35. Radman, T., Y. Su, J. An, L. Parra, and M. Bikson. Spike timing amplifies the effect of electric fields on neurons: implications for endogenous field effects. J. Neurosci. 27:3030–3036, 2007.

36. Robertson, R. Chronic oxidative stress as a central mechanism for glucose toxicity in pancreatic islet beta cells in diabetes. J. Biol. Chem. 279:42351–42354, 2004.

37. Rosenmund, C., A. Feltz, and G. Westbrook. Calciumdependent inactivation of synaptic NMDA receptors in hippocampal neurons. J. Neurophysiol. 73:427–430, 1995.

38. Schoenbach, K., et al. Ultrashort electrical pulses open a new gateway into biological cells. Proc. IEEE 92:1122–1137, 2004.

39. Seino, S. Cell signalling in insulin secretion: the molecular targets of ATP, cAMP and sulfonylurea. Diabetologia 55:2096–2108, 2012.

40. Seino, S., T. Shibasaki, and K. Minami. Dynamics of insulin secretion and the clinical implications for obesity and diabetes. J. Clin. Investig. 121:2118–2125, 2011.

41. Tank, D., W. Fredericks, L. Barak, and W. Webb. Electric field-induced redistribution and postfield relaxation of low density lipoprotein receptors on cultured human fibroblasts. J Cell Biol. 101(1):148–157, 1985.

42. Vernier, P., Y. Sun, L. Marcu, S. Salemi, C. Craft, and M. Gundersen. Calcium bursts induced by nanosecond electric pulses. Biochem. Biophys. Res. Commun. 310(2):286–295, 2003.

43. Zaiontz, C., The data analysis for this paper was generated using the Real Statistics Resource Pack software (Release 6.2). Copyright, 2013–2019.

44. Zhang, J., R. Ren, X. Luo, P. Fan, X. Liu, S. Liang, L. Ma, P. Yu, and H. Bai. A small physiological electric field mediated responses of extravillous trophoblasts derived from HTR8/SVneo cells: involvement of activation of focal adhesion kinase signaling. PLoS ONE 2014. https://doi.org/10.1371/journal.pone.0092252.

CHAPTER 3:

STIMULATORY EFFECTS OF NEAR-INFRARED (810 nm) PHOTOBIOMODULATION ON CALCIUM DYNAMICS AND INSULIN SECRETION IN β-CELLS

Caleb Liebman and Michael Cho

Submitted and awaiting decision

Abstract

Background and Objective: Near-infrared (810 nm) photobiomodulation has been shown to have therapeutic applications on various cell types. However, only a small amount of work has investigated its effects on β-cell functionality. Herein, studies are designed to demonstrate the ability for 810 nm light to stimulate intracellular calcium dynamics that can lead to an increase in insulin secretion. The main focus is to elucidate the calcium-dependent mechanisms in real time, and therefore the cellular responses are monitored and record for a 15-minute observation time.

Materials and Methods: To quantitatively determine the effects of 810 nm laser at the fluence of 9 J/cm^2, mouse βTC-6 insulinoma cells were exposed to laser light for 1 minute and specific fluorophores were used to record in real time the calcium spiking patterns and ROS levels, with ELISA for the measurement of insulin secretion.

Results: Using various pharmacological agents, 810 nm laser light appears to activate transient receptor potential (TRP) channels expressed on the cell surface and mediate an influx of extracellular calcium via voltage-operated calcium channels to initiate the calcium spiking. In addition, intracellular calcium stores were also involved in the regulation of calcium dynamics via reactive oxygen species produced by the photo-stimulatory effects on Cytochrome C Oxidase. The stimulated and enhanced intracellular calcium dynamics were capable of increasing insulin secretion under glucose loading.

Conclusion: We demonstrated the use of 810 nm laser light to stimulate calcium dynamics in βTC-6 cells, thereby promoting an increase in insulin secretion. Taken together, we present a model by which 810 nm light may be able to affect the β-cell calcium dynamics and insulin secretion. This working model could potentially be clinically applied to pre-treatment, for example, isolated islets prior to transplantation.

Introduction

Over the last 50 years, low level laser therapy (LLLT) has been investigated for use in various medical applications.[1] However, the cellular mechanisms by which this method provides its therapeutic effects has not been rigorously explored until recently. Now more commonly known as photobiomodulation (PBM), it has been shown to effect Cytochrome C Oxidase (CCO) activity, mitochondrial reactive oxygen species (mROS), and intracellular calcium levels.[2] By influencing these physiological functions, PBM has been shown to modulate stem cell differentiation and impart an increased resistance to oxidative stress.[3]

Given these effects, PBM could be used to modulate β-cell physiology and thus insulin secretion in response to glucose load. Some research has investigated this possibility, yet very little has been shown on how PBM drives its effects in this cell type.[4, 5] Insulin secretion is canonically initiated by elevations in ATP, leading to depolarization and calcium influx and driven by the resulting rise of intracellular calcium.[6] The effects of PBM on calcium dynamics mediated by the pathways other than ATP elevation may also lead to insulin secretion.

β-cells are an electrically active cell type displaying spontaneous calcium spiking behavior.[7] These patterns of calcium spiking influence a wide array of cellular functions including transcription factor expression, apoptosis and survival, and in particular exocytosis of insulin granules.[8] Calcium spiking frequency directly affects pulsatile insulin secretion.[9] When challenged by a glucose load, the β-cell spiking frequency and activity increase that spurs insulin secretion.[10] Thus we hypothesized that PBM could emulate or alter β-cell calcium dynamics and subsequently regulate their insulin functionality.

The current mechanistic theory suggests that near-infrared light (NIR) can be absorbed by CCO and disassociates nitric oxide (NO) binding. This disassociation allows for an increase in

oxygen binding, thus increasing the rate oxidative phosphorylation.[11] The rise in oxidative phosphorylation increases ATP production and is accompanied by an increase in mROS generation.[12] While signaling by mROS and NO have been shown to be involved in insulin secretion, the primary driver of insulin secretion is intracellular calcium and thus remained the focus of our investigation.[13, 14]

While a shift in the ATP/ADP ratio causes depolarization with activation of voltage gated calcium channels (VGCCs), it has been shown that transient receptor potential calcium channels (e.g., TRPV1) are also activated by NIR light.[15] Blocking these channels inhibit the effects of NIR PBM on intracellular calcium thus supporting the involvement of TRPV channels.[16] However, other groups have shown that calcium spikes can be initiated by NIR-PBM and inhibited by various intracellular calcium channel blockers.[17, 18] Since these photons transmit through the entire cell, it would be anticipated that absorption by various chromophores is likely to result in a complex and multifaceted response.

Methods:

Cell Culture: Mouse insulinoma cells (βTC-6) were obtained from ATCC (CRL-11506, Manassas, VA) and cultured in high glucose DMEM (D6429, Sigma, St. Louis, MO) with 15% FBS (16000044, Gibco) and 1% Penicillin-Streptomyzin. Cell passage was performed weekly with 0.25% Trypsin-EDTA. Samples were prepared by seeding βTC-6 cells on glass coverslips in low glucose media. These samples were used for experimentation between days 2 through 5. All cells were incubated at 37 °C in a 5% CO2 environment.

PBM Parameters: A Cytonsys (Austin, TX) 810 nm near-infrared laser was used to perform all experimentation. Previous reports have demonstrated therapeutic effects of this

wavelength on various cell types.[19] The energy density of 9 J/cm^2 was previously shown to have therapeutic effects on hepatic tissue in a diabetic state.[20] In addition, 810 nm PBM stimulation at the fluence of 10.2 J/cm^2 was shown to have therapeutic potential as a diabetic therapy on mice.[21] Densities higher than 10 J/cm^2 have been shown to exhibit inhibitory effects.[22] Herein, we exposed all βTC-6 samples to 810 nm for 1 minute with an irradiance of 150 mW/cm^2, resulting in a fluence of 9 J/cm^2. To measure the bulk temperature rise due to laser exposure, an Omega HH42A thermistor was used before and after irradiation.

Live Cell Imaging: For calcium and mitochondrial superoxide (mROS) detection, the cells were stained with Fluo-8 (0.8 μM, Abcam, Cambridge, UK), Mitosox (5 μM, Thermo-Fisher, Waltham, MA) and 1 drop/mL of Nucblue (Thermo-Fisher, Waltham, MA) for detection of intracellular calcium, mROS, and nucleic acid, respectively. The fluorescent dye DAF-FM (5 μM, Thermo-Fisher) was used to detect and measure cytosolic nitric oxide (NO). Hanks balanced salt solution (HBSS) was used (H8264, Sigma, St. Louis, MO) unless stated otherwise. Samples were stained at 37 °C for 30 minutes before being washed and mounted onto the imaging chamber.

*Calcium Activity Analysis:*Regions of interest (ROIs) were placed on individual cells using the nucleic acid staining and transferred to perform and calculate mean fluorescent intensity over time with background subtraction. Approximately 100 to 200 cells were monitored for each data point, and the results were averaged. A conservative moving average threshold (10 data points) with a 10% cutoff was used to determine a calcium spike.[23] (see Fig. 3-1A) Any cell that displayed at least one spike above the moving threshold during each imaging window was defined to be active. The active population was defined by the total number of active cells divided by the number of cells analyzed. The average spiking frequency of these active cells was then determined at each time point. Measurements were taken using Nikon Elements software and data analysis was carried

out using Microsoft Excel. Heat mapping of calcium activity was produced using ImageJ by taking the absolute difference between 2 frames and summing the differences together. A Gaussian smoothing was performed in ImageJ to remove background noise.[24]

Pharmacologic Studies: All drugs were added to the staining buffer. Samples were treated with each drug for 30 minutes before imaging. For L-type VGCC blocking, Verapamil (100 μM, V4629, Sigma) was applied. Capsazepine (10 μM, C191, Sigma) was added as a TRPV1 antagonist. Dantrolene (50 μM, 251680, Sigma) and 2-APB (10 μM, 100065, Sigma) were used to inhibit the Ryanodine- or IP_3-receptors respectively. Ascorbic Acid (2.5 mM, A0278, Sigma) was used as an antioxidant to diminish the effects of ROS.

Insulin Secretion Assay: Krebs Ringer Buffer (KRB) was made (118.5 mM NaCl, 2.54 mM CaCl2,1.19mM KH2PO4, 4.74 mM KCL, 25 mM NaHCO3, 1.19 mM MgSO4, 10 mM HEPES, pH 7.4), followed by 0.1% bovine serum albumin being added before insulin secretion experiment.[25] Either 0.5 mM or 3.0 mM glucose was added to simulate a low or high glucose loading.[26] Samples were seeded at 40,000 cells/cm^2 three days before experimentation. Samples were then washed with 0 mM KRB and incubated for 1 hour without glucose. Following an additional wash, samples were mounted to the chamber with the appropriate glucose concentration and with or without laser irradiation. After 15 minutes, samples were removed and frozen. A mouse insulin ELISA (EMINS, Thermo-Fisher) was used to measure insulin content with a 1:10 dilution. Cyquant (C7026, Thermo-Fisher), a nucleic acid assay, was used to estimate the number of cells for each sample and normalize the total insulin by the estimated number of cells.

Immunostaining: Cell samples were first washed and fixed for 15 minutes in 4% paraformaldehyde and permeabilized using 0.25% Triton-X100 for 10 minutes. BSA (1%) blocking was then performed for 30 minutes. Primary staining for L-type VGCC utilized 1:100

primary anti-CaV1.3 (Abcam AB85491) while staining for TRPV1 used 1:1000 anti-VR1 (Abcam, AB31895) with overnight staining at 4 °C. Secondary staining was performed at room temperature for 90 minutes with 1:200 anti-mouse Alexa 555 for CaV1.3 and 1:200 anti-rabbit Alexa 488 for TRPV1. Samples were then washed and imaged.

Statistical Analysis: For calcium spiking frequency, each group was screened for outliers using Iglewicz and Hoaglin's test with a modified Z score of 3.5.[27] To determine significance for the effects of PBM, a one-way repeated measures ANOVA was performed followed by pairwise t-tests between each time point and the baseline with Holms-Bonferonni correction.[28] Significance between PBM time points and all pharmacological runs was determined using pairwise t-tests also utilizing Holms-Bonferonni correction. Unpaired t-tests were used to test between the 0.5 mM and 3.0 mM glucose insulin secretion groups. All data was processed using Microsoft Excel with the Real Statistics Resource Pack.[29] Outlier tests were performed using Contchart software.

Results:

Bulk Temperature Rise: Laser irradiation can induce heating. Before proceeding with quantitative determination of PBM effects, it is important to delineate potential temperature rise due to laser exposure. A thermistor was used to measure the temperature in the media. After 1 minute of 810 nm exposure at 150 mW/cm^2, the average bulk temperature rise was 0.08 ± 0.02 °C. This is well below the suggested threshold of 1 °C that might induce non-negligible thermal effects.[3]

Calcium Spiking Response: We aimed to determine how PBM could affect the intracellular calcium dynamics in the β-cell phenotype. Using the fluorescent probe Fluo-8, we were able to record calcium spiking activity in βTC-6 cells. Using a 10-point moving average with 10%

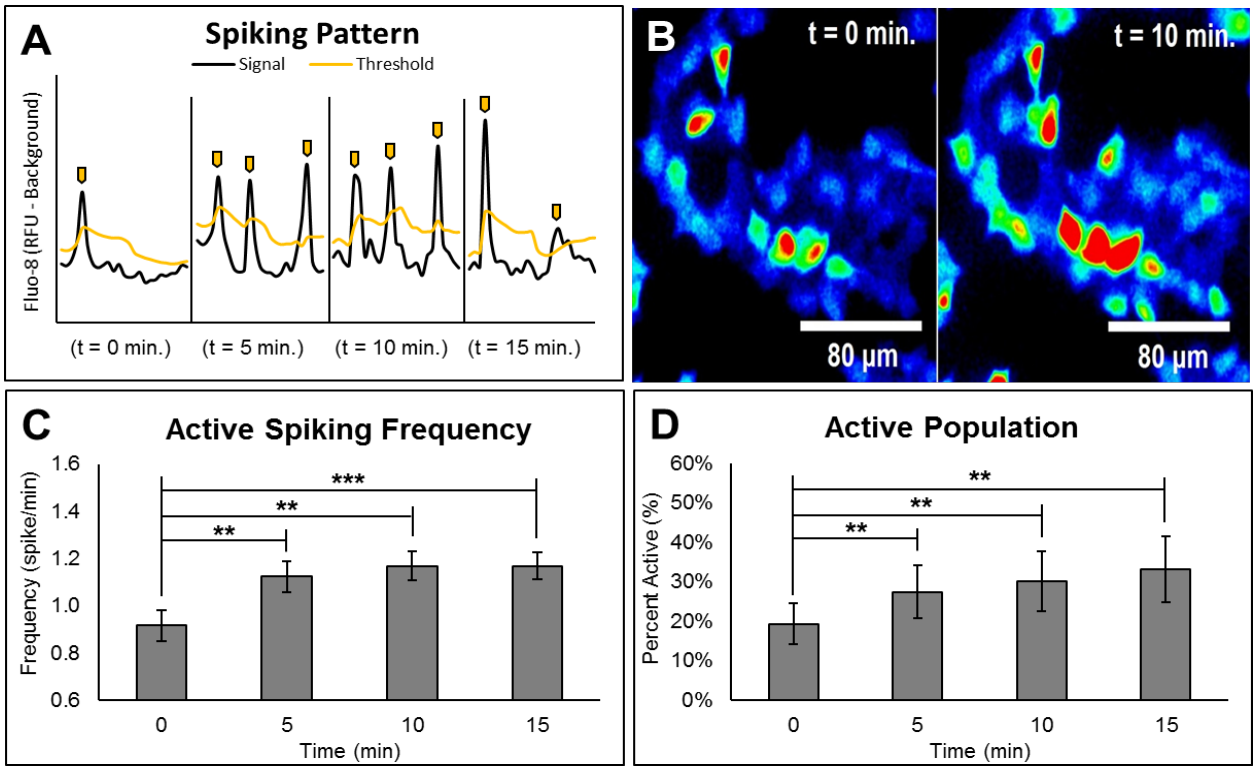

Figure 3-1: (A) Representative graph of Fluo-8 signal alongside moving average threshold with indicators for counted spikes. (B) Heat map images of the summed absolute difference between frames yielding a visual representation of calcium activity. Blue to red indicates low to high spiking activity. **(C)** Mean spiking frequency for active cells (1 or more spikes) over 18 independent samples involving ~1,200 cells. **(D)** Percentage of the population that was counted as active. All data represents mean +/- standard error mean. ***** $p<0.05$, ** $p<0.01$, *** $p<0.001$

threshold for quantifying calcium spikes, we observed a significant increase in calcium activity following PBM exposure. (Fig. 3-1A and 3-1B) Active cells were defined as any cell with at least one spike during an imaging window. Of these cells, we observed a significant increase in frequency from 0.92 ± 0.07 to 1.17 ± 0.06 spikes per minute. (Fig. 3-1C) In addition to elevating the spiking frequency, the number of active cells increased following the irradiation. The average proportion of active cells was found to increase from 19.3 ± 5.2% to 33.2 ± 8.3% after PBM. (Fig. 3-1D) These results demonstrated that 810 nm PBM is capable of stimulating the calcium activity in β-cells.

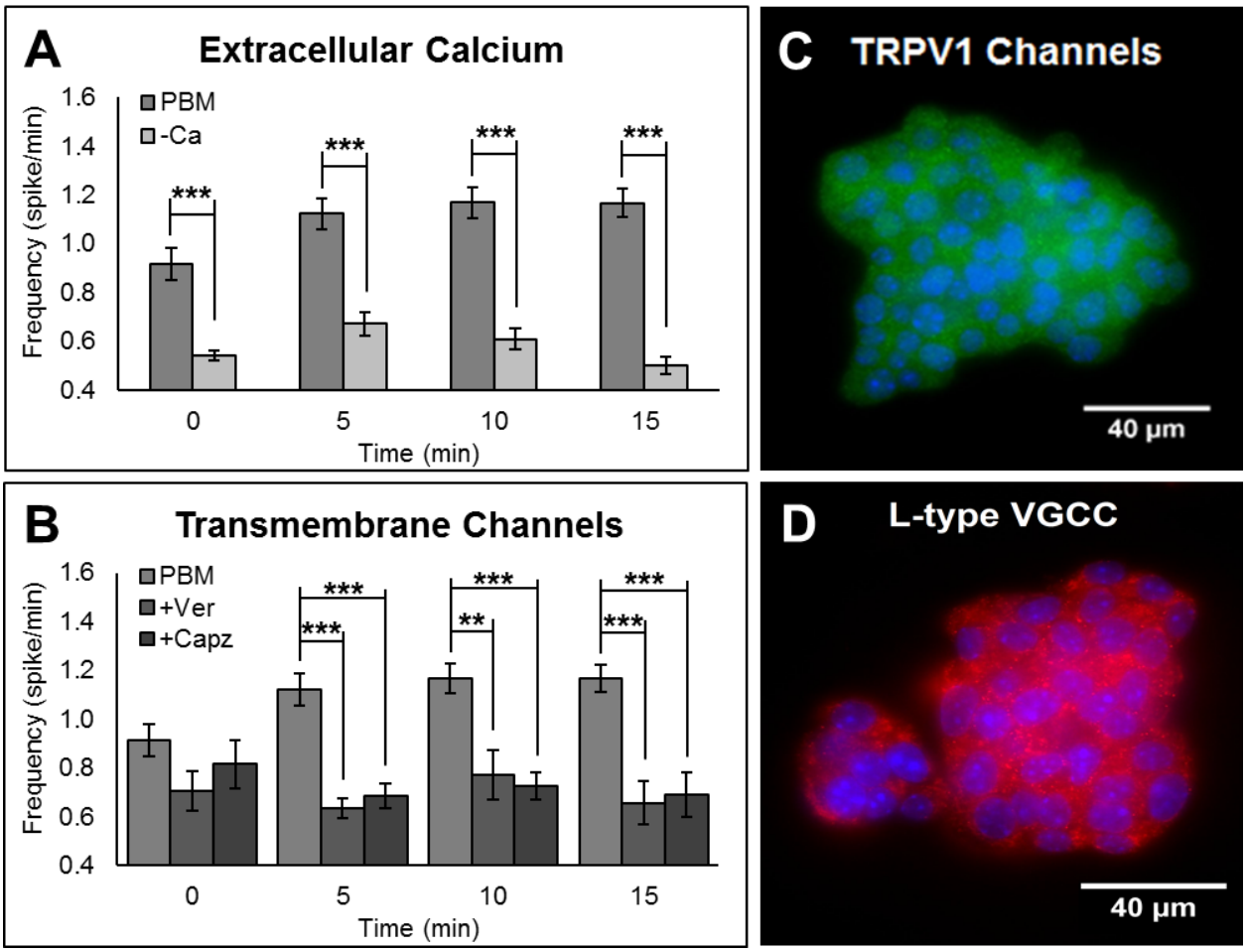

Figure 3-2: (A) Calcium spiking frequency following PBM exposure with and without extracellular calcium. (B) Calcium spiking frequency following PBM after treatment with Verapamil (100 µM) and Capsazepine (10 µM). Data includes 10, 9, and 10 independent samples involving ~130, 60, and 60 active cells for –Ca, +Ver, and +Capz respectively. (C-D) Immunostained images for TRPV1 and L-type VGCCs respectively with nuclei counterstaining. All data represents mean +/- standard error mean. * $p<0.05$, ** $p<0.01$, *** $p<0.001$.

Extracellular Calcium and Entry Pathways: In an effort to understand the mechanism(s) by which PBM exerts these effects, we first determined the dominant source of calcium rise by depleting the extracellular calcium ions. This significantly impeded the spiking frequency following PBM exposure. This indicates that the primary source of calcium influx was across the cell membrane and into the cytosol. (Fig. 3-2A) Since the cell membrane has several pathways to mediate calcium influx, we blocked both L-type VGCCs and cell membrane TRPV1 channels

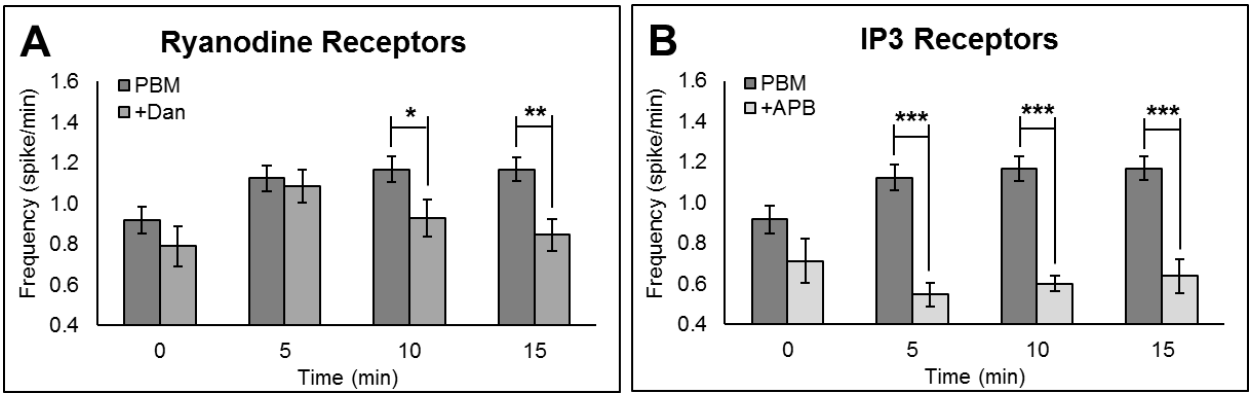

Figure 3-3: (A) Calcium spiking frequency after exposure to PBM following treatment with Dantrolene (50 μM) demonstrating the role of the endoplasmic Ryanodine receptor channels. Data includes 8 independent samples involving ~170 active cells. (B) Calcium spiking frequency after exposure with 2-APB (10 μM) demonstrating the role of IP3 receptor channels. Data includes 8 independent samples involving ~40 active cells. All data represents mean +/- standard error mean. * $p<0.05$, ** $p<0.01$, *** $p<0.001$.

using Verapamil and Capsazepine, respectively. Calcium spiking frequency between the PBM-treated group and those treated with PBM and channel blockers was significantly different, suggesting both L-type VGCCs and TRPV1 channels are involved in the rise of calcium spiking activity by PBM. (Fig. 3-2B) Capsazepine was intentionally selected because it is membrane-impermeant (Millipore-Sigma, https://www.sigmaaldrich.com/catalog/product/mm/211280?lang=en&region=US). This suggests that the TRPV1 channels expressed on the cell surface were preferentially blocked. However, immunolabeling experiments showed both of these two channels are abundantly expressed in βTC-6 cells (Fig. 3-2C and 3-2D). Thus these pharmacological studies alone may not be able to directly delineate the role of the two channel types in response to PBM stimulation.

Intracellular Calcium: Despite the dominant influx of calcium from the extracellular space, one cannot readily rule out the contribution of PBM-induced activation of intracellular stores.[30] Thus, we treated the cells with either dantrolene or 2-APB to inhibit the Ryanodine- and IP_3-

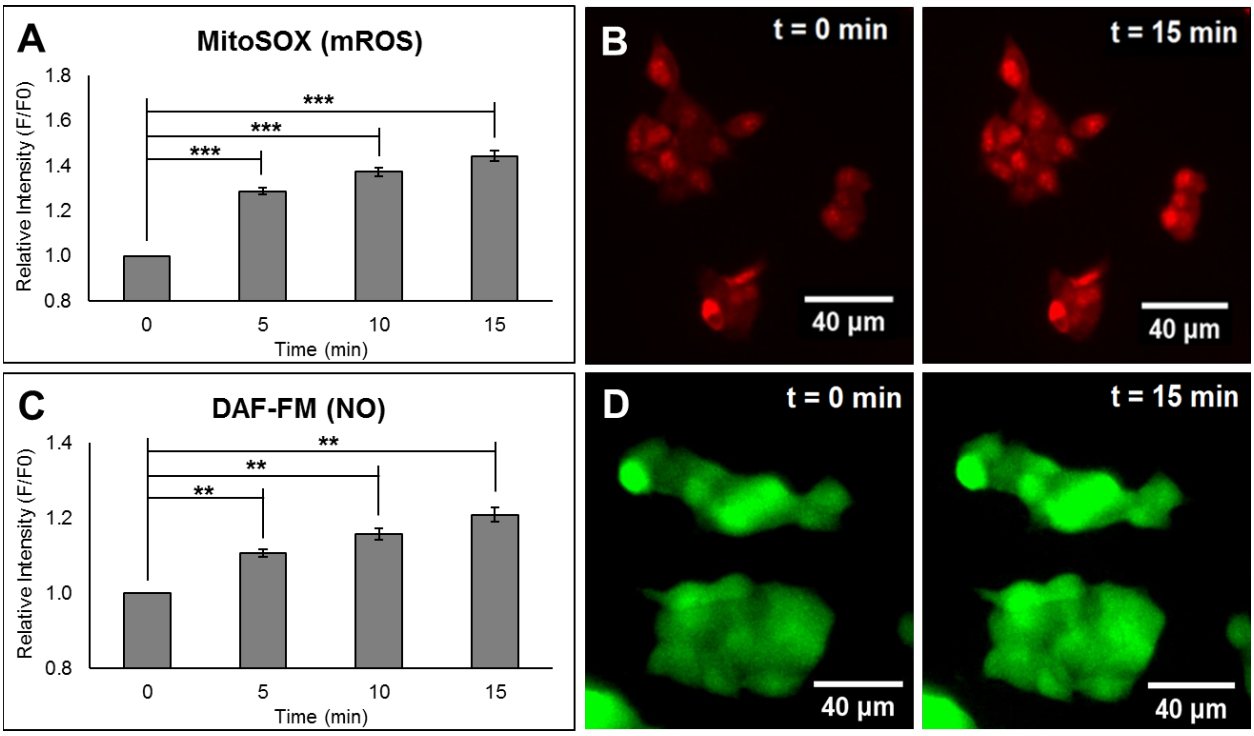

Figure 3-4: (A) Relative rise in Mitosox intensity over baseline value following PBM irradiation for 12 independent samples. (B) Representative images demonstrating the rise in Mitosox intensity pre-irradiation and 15 minutes post-irradiation. (C) Percent rise in DAF-FM intensity over baseline value following PBM irradiation for 5 independent samples. (D) Representative images demonstrating the rise in DAF-FM intensity pre-irradiation and 15 minutes post-irradiation. All data represents mean +/- standard error mean. * $p<0.05$, ** $p<0.01$, *** $p<0.001$.

receptor mediated intracellular calcium release. While the spiking frequency of dantrolene-treated samples was decreased in comparison to the control, this difference was only noticeable at the 15-minute mark. (Fig. 3-3A) However, a treatment with 2-APB to inhibit the IP_3-receptor-mediated pathway was shown to significantly impede such an increase in the calcium spiking frequency by PBM. (Fig. 3-3B)

ROS and NO Elevations: In addition to apparent direct effects on TRP channels by PBM (see Fig. 3-2), it is well documented that CCO activity can also be increased by PBM. This should result in an increased production of ROS and NO. To verify this, we used the superoxide fluorescent probe MitoSOX to observe changes in mROS (superoxide). Following PBM

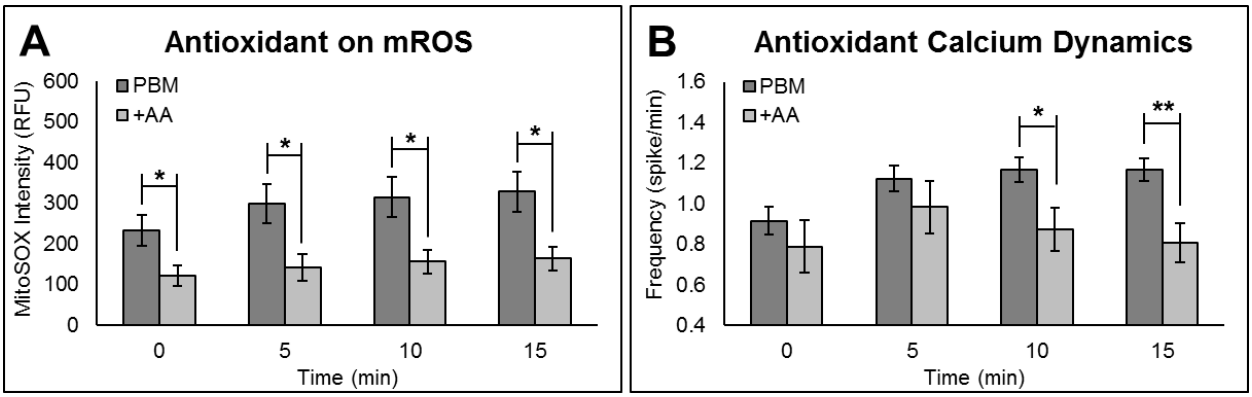

Figure 3-5: (A) MitoSOX intensity between PBM and +AA (Ascorbic Acid) groups following exposure, indicating the effect of AA (2.5 mM) on mROS. (B) Change in calcium spiking frequency following exposure after treatment with AA. Samples included 8 independent samples involving ~110 active cells. All data represents mean +/- standard error mean. * $p<0.05$, ** $p<0.01$, *** $p<0.001$.

irradiation, we observed a maximum rise of 44.3 ± 2.3% at the 15-minute mark over the baseline level. (Fig. 3-4A and 3-4B) In the same PBM-induced CCO activation model, cytosolic NO is also expected to increase as NO dissociates from the heme group of CCO. We then used the molecular probe DAF-FM to measure the relative levels of cytosolic NO. Measuring its fluorescent intensity, we observed a maximum rise of 20.8 ± 1.8% in 15 minutes. (Fig. 3-4C and 3-4D) These results are consistent with and support the mechanism of PBM on CCO activity in β-cells by dissociating NO and resulting in an increase in mROS.

Antioxidants to reverse PBM-induced ROS increases: Given the influence ROS has on calcium dynamics, we aimed to determine how the suppression of mROS would affect the calcium spiking frequency. Therefore, we treated the samples with ascorbic acid (AA) and observed a significant reduction in the MitoSOX intensity, as expected. (Fig. 3-5A) We next analyzed the spiking frequency of active cells treated with AA. There was no significant difference in the calcium spiking frequency analysis between the AA-treated and control cells until the 10-minute time point. (Fig. 3-5B) It would appear that an increase in the ROS level at the early stage of PBM stimulation (< 10 minutes) may be abrogated by AA and yet has no significant impact of the

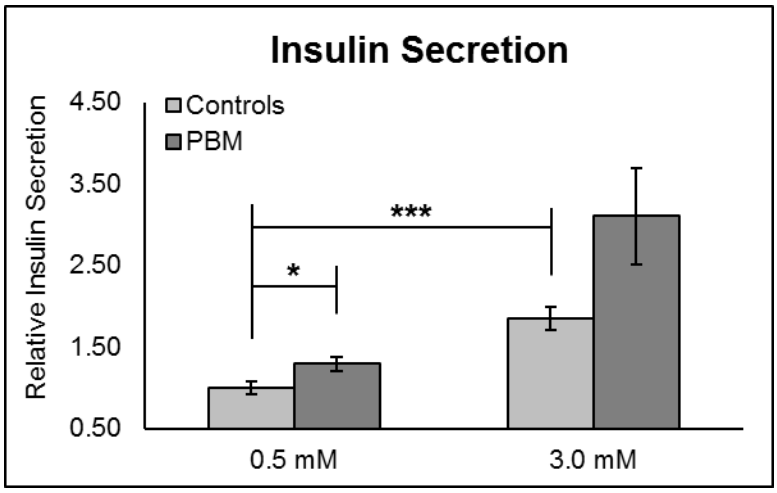

Figure 3-6: Relative Insulin secretion at 0.5 mM and 3.0 mM glucose in Krebs ringer buffer with and without PBM exposure. All groups included 8 independent samples. All data represents mean +/- standard error mean. * $p<0.05$, ** $p<0.01$, *** $p<0.001$.

calcium dynamics, suggesting ROS is not interfering with activation of the calcium channels at the cell membrane level. At later stages (> 10 min), ROS-mediated calcium release from intracellular calcium stores is potentially inhibited by AA and therefore diminishes the calcium spiking activity.[31] Thus, mROS may act to sustain the calcium spiking patterns through ROS-dependent intracellular calcium release pathways.

Insulin Secretion: Finally, we aimed to determine how the stimulation of PBM-induced calcium dynamics would affect insulin secretion. βTC-6 cells have been shown to have a maximum secretion at 3 mM with a half-maximum at 0.5 mM glucose loads.[26] For both the control and PBM-treated groups, the samples were washed in Krebs Ringer Buffer (KRB) at 0 mM glucose for 1 hour, and then mounted onto the chamber. Following laser irradiation, the samples were allowed to secrete for 15 minutes. The samples exposed to PBM in a 0.5 mM glucose solution demonstrated a 30% increase in insulin secreted over the control samples. PBM exposure of cells in a 3 mM solution also appeared to increase insulin secretion by ~ 70% over the control group. However, the amount of secreted insulin was not found to be significantly different than that measured among the 3 mM control group ($p > 0.05$). (Fig. 3-6)

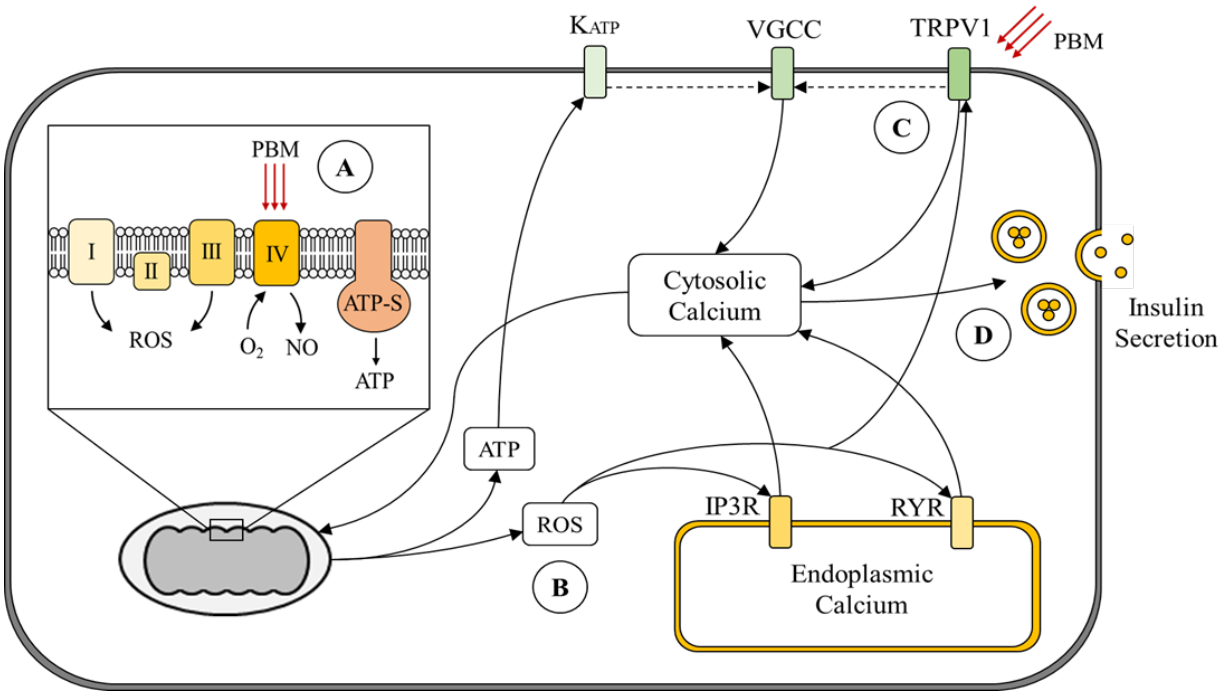

Figure 3-7: (A) PBM likely dissociates NO from CCO increasing O2 consumption and flux through the ETC. This results in an increase in mROS and likely ATP. (B) While the metabolic changes may instigate depolarization via the canonical pathway, ROS may play a role by activating IP3Rs, RYRs, and TRPV channels. (C) It is likely that PBM activates TRPV channels directly as well resulting in depolarization events with calcium influx. (D) The resulting increase in calcium spiking activity alongside the metabolic shift likely induces pulsatile insulin secretion by the β-cells.

Discussion

It was clear from the results that 810 nm PBM was capable of stimulating the calcium dynamics in βTC-6 cells, as the calcium spiking frequency and the active proportion of the population was increased. This response is similar to what is found in glucose-stimulated insulin secretion (GSIS) in that both the frequency increased along with the number of cells actively spiking.[32] In GSIS, this response is due to an increased rate of depolarization events caused by ATP-sensitive potassium channels in the cell membrane. Membrane depolarization can open the VGCCs allowing an calcium influx, which influences the rate of calcium spiking events.[33]

However, the mechanisms by which PBM modulates the calcium dynamics in β-cells are yet to be fully elucidated.

Much of the work performed by the Hamblin group, has demonstrated that NIR-PBM likely affects intracellular calcium via activation and opening of TRPV channels. In this mechanism, light is absorbed by structured water surrounding the channels, heating it and opening the channels.[34] While the TRPV channels allow for calcium influx, other cations such as sodium and potassium are also able to proceed down their electrochemical gradients resulting in membrane depolarization.[35] Since the calcium currents for TRPV channels is relatively low, it is more likely that the depolarization by TRPV channels leads to the activation of VGCCs resulting in much stronger calcium currents.[36] Capsazepine is stated to be membrane impermeable, suggesting the TRPV1 channels at the cell surface are one of the likely targets that responds to PBM. Thus, our findings imply that the activation of TRPV1 channels at the surface is more likely involved in the early stage of calcium spiking than other TRP channels that are expressed on the endoplasmic reticulum. Overall, these results support the model that both membrane surface TRPV1 and L-type VGCC channels mediate the response of modulating calcium dynamics by PBM.

It was demonstrated that very short pulses of NIR light were able to bring about calcium spikes in cardiomyocytes.[17] In this work, blocking the Ryanodine receptors that generally control calcium induced calcium release (CICR) did not significantly affect the calcium spiking frequency but did reduce the amplitude. In addition, IP_3-receptor blocking by 2-APB appeared to disrupt calcium spiking. It was also shown that 2-APB inhibits the PBM-induced calcium dynamics in glioblastoma cells.[37] It was then proposed that PBM is able to stimulate the phospholipase C/IP_3 pathway that regulates CICR by involving intracellular calcium stores. The results from these previous reports support our findings in that Ryanodine receptor blocking does diminish but not

abolish the calcium spiking in response to PBM. However, the IP_3-receptor pathway appears critical in the overall stimulation of calcium spiking (see Fig. 3-3).

Our results from the present study help clarify the mechanisms in which PBM affects the calcium response, but do not necessarily explain the sustained calcium activity out to a 15-minute time point. Thus, we considered the metabolic mechanism(s). It has been shown that NO plays an inhibitory role in the energy production of the mitochondria. Higher concentrations of NO lead to an increase in reversible binding to CCO, thus slowing its binding to O_2 and leading to a reduced flux in the electron transport chain (ETC).[38] When laser photons are absorbed by CCO, NO is dissociated from CCO and increases its O_2 consumption. This allows for an increase in flux through the ETC, corresponding with an increase in ATP and ROS production.[12] Our results demonstrated an increase in intensity from both MitoSOX (O^{-}_2) and DAF-FM (NO) indicating elevations in available superoxide and nitric oxide, respectively. These findings are consistent with the theory that PBM increases CCO activity in the mitochondria in addition to exerting effects on ion channels. While the calcium channels may be responsible for the initial stage of calcium influx across the cell membrane, an elevation in mROS is postulated to contribute to and sustain the increased calcium dynamics beyond the initial stimulation induced by PBM through activation of TRP channels in endoplasmic recticulum, IP_3- and Ryanodine-receptors.[39]

Intracellular concentrations of ROS can be both therapeutic and pathological depending on the concentration and the amount of time present.[40] For instance, chronic glucose load brought about by insulin resistance is well known to cause β-cell oxidative stress via ROS production that leads to the cell's dysfunction and apoptosis.[41] Alternatively, mROS production has been shown to help stimulate the release on insulin, and therefore acting as a signal of glucose load in β-cells.[42] ROS formation can induce calcium spiking along with insulin secretion in β-cells via endoplasmic

calcium release.[43] Our results demonstrate that the antioxidant AA is able to suppress the superoxide concentration, which inhibits the calcium spiking frequency at later time points. (see Fig. 3-5) A plausible explanation is emerging that localized water heating around TRPV1 channels initially activates the channels with subsequent VGCC activation via membrane depolarization. Moreover, a metabolic shift that increases the intracellular ROS levels may act to sustain the calcium spiking activity in response to PBM via ROS-mediated activation of Ryanodine- and IP3-receptor and TRPV channels.

Finally, based on these changes to calcium dynamics in β-cells, 810 nm PBM is expected to modulate insulin secretion. A previous report demonstrated that 810 nm is capable of inducing insulin secretion from primary islets, and that the concentration of glucose likely alters the response.[5] Similarly, our results demonstrated an increase in insulin secretion in response to PBM at a lower glucose load. (see Fig. 3-6) While PBM exposure appeared to substantially increase the insulin secretion at a higher glucose load, it was not statistically significant. Thus, it is plausible that PBM can induce insulin secretion, but that the exact parameters have yet to be optimized. The number of combinatory PBM parameters will exponentially grow if one considers potential dependence on the wavelength, fluence and also the rate of energy deposit. It would be helpful to develop computational models to predict the several molecular coupling pathways that were outlined in the current study.

Conclusions:

Our work here demonstrates that PBM can stimulate the calcium spiking frequency and activity in β-cells. Together with previously reported findings, we propose a working model that incorporates several mechanisms we identified. (Fig. 3-7) PBM is postulated to activate TRPV1

channels at the cell surface and mediate ion fluxes across the cell membrane. Changes in the ion concentrations may lead to membrane depolarization and activate electrically operating channels such as L-type VGCCs. Combined effects of TRVP1 channel and VGCC activation initiate and enhance calcium spiking. In tandem, PBM couples to COO and increases intracellular mROS that can potentially release calcium from intracellular calcium stores primarily through the IP_3-receptor pathway. Such an elevation in mROS may sustain and extend the calcium spiking response beyond the initial stage. Taken collectively, these events lead to insulin secretion and support the ability of NIR PBM to alter both the calcium and insulin dynamics in β-cells with potential therapeutic applications to promote the functionality of islets. Finally, the laser exposure apparatus we employed in the current study was designed to determine and elucidate potential coupling mechanisms in a short 15-minute observation time window. Increases in the insulin secretion under two glucose loadings could be interpreted as facilitated exocytosis of the pre-packaged vesicles rather than translational synthesis of insulin. Experimental designs of additional apparatuses are currently underway to expose β-cells to PBM for a longer period of time (e.g., 9 J/cm^2 per day over several days).

Acknowledgments:

We would like to acknowledge and thank Drs. Alfred and Janet Potvin for providing financial support for this work.

References:

1. Zein, R., Selting, W. and Hamblin, M., Review of light parameters and photobiomodulation efficacy: dive into complexity. *Journal of Biomedical Optics*, 2018; 23(12), p.1.

2. Sharma, S., Kharkwal, G., Sajo, M., Huang, Y., De Taboada, L., McCarthy, T. and Hamblin, M., Dose response effects of 810 nm laser light on mouse primary cortical neurons. *Lasers in Surgery and Medicine,* 2011; 43(8), pp.851-859.

3. McColloch, A., Liebman, C., Liu, H. and Cho, M., Altered Adipogenesis of Human Mesenchymal Stem Cells by Photobiomodulation Using 1064 nm Laser Light. *Lasers in Surgery and Medicine*. 2020.

4. Irani, S., Mohseni Salehi Monfared, S., Akbari-Kamrani, M., Ostad, S., Abdollahi, M. and Larijani, B., Effect of Low-Level Laser Irradiation on In Vitro Function of Pancreatic Islets. *Transplantation Proceedings,* 2009; 41(10), pp.4313-4315.

5. Meulenaer, E., Louchami, K., Zhang, Y., Bulur, N., Sener, A., Malaisse, W., Effects of infrared light on insulin release, cationic fluxes and cellularity in insulin-producing cells. *Metabolic and Functional Research on Diabetes,* 2009; Vol. 2, pp 63-70.

6. Hedeskov, C., Mechanism of glucose-induced insulin secretion. Physiological Reviews, 1980; 60(2), pp.442-509.

7. Fridlyand, L., Tamarina, N. and Philipson, L., Bursting and calcium oscillations in pancreatic β-cells: specific pacemakers for specific mechanisms. American Journal of Physiology-Endocrinology and Metabolism, 2010; 299(4), pp.E517-E532.

8. Ramadan, J., Steiner, S., O'Neill, C. and Nunemaker, C., The central role of calcium in the effects of cytokines on beta-cell function: Implications for type 1 and type 2 diabetes. Cell Calcium, 2011; 50(6), pp.481-490.

9. Gilon P, Ravier M, Jonas J, Henquin J. Control Mechanisms of the Oscillations of Insulin Secretion In Vitro and In Vivo. Diabetes. 2002;51(Supplement 1):S144-S151.

10. Bertram, R., Sherman, A. and Satin, L., Electrical Bursting, Calcium Oscillations, and Synchronization of Pancreatic Islets. Advances in Experimental Medicine and Biology, 2010; pp.261-279.

11. Yadav, A. and Gupta, A., Noninvasive red and near-infrared wavelength-induced photobiomodulation: promoting impaired cutaneous wound healing. Photodermatology, Photoimmunology & Photomedicine, 2017; 33(1), pp.4-13.

12. Hamblin, M., Mechanisms and Mitochondrial Redox Signaling in Photobiomodulation. Photochemistry and Photobiology, 2018; 94(2), pp.199-212.

13. Leloup, C., Tourrel-Cuzin, C., Magnan, C., Karaca, M., Castel, J., Carneiro, L., Colombani, A., Ktorza, A., Casteilla, L. and Penicaud, L., Mitochondrial Reactive Oxygen Species Are Obligatory Signals for Glucose-Induced Insulin Secretion. Diabetes, 2009; 58(3), pp.673-681.

14. Rahman, F., Park, D., Joe, Y., Jang, K., Chung, H. and Kim, U., Critical Roles of Carbon Monoxide and Nitric Oxide in Ca2+ Signaling for Insulin Secretion in Pancreatic Islets. Antioxidants & Redox Signaling, 2019; 30(4), pp.560-576.

15. de Freitas, L. and Hamblin, M., Proposed Mechanisms of Photobiomodulation or Low-Level Light Therapy. IEEE Journal of Selected Topics in Quantum Electronics, 2016; 22(3), pp.348-364.

16. Amaroli, A., Ferrando, S. and Benedicenti, S., Photobiomodulation Affects Key Cellular Pathways of all Life-Forms: Considerations on Old and New Laser Light Targets and the Calcium Issue. Photochemistry and Photobiology, 2018; 95(1), pp.455-459.

17. Dittami, G., Rajguru, S., Lasher, R., Hitchcock, R. and Rabbitt, R., Intracellular calcium transients evoked by pulsed infrared radiation in neonatal cardiomyocytes. The Journal of Physiology, 2011; 589(6), pp.1295-1306.

18. Moreau, D., Lefort, C., Pas, J., Bardet, S., Leveque, P. and O'Connor, R., Infrared neural stimulation induces intracellular Ca2+ release mediated by phospholipase C. Journal of Biophotonics, 2017; 11(2).

19. Salehpour, F., Mahmoudi, J., Kamari, F., Sadigh-Eteghad, S., Rasta, S. and Hamblin, M., Brain Photobiomodulation Therapy: a Narrative Review. Molecular Neurobiology, 2018; 55(8), pp.6601-6636.

20. Lim, J., Ali, Z., Sanders, R., Snyder, A., Eells, J., Henshel, D. and Watkins, J., Effects of low-level light therapy on hepatic antioxidant defense in acute and chronic diabetic rats. Journal of Biochemical and Molecular Toxicology, 2009; 23(1), pp.1-8.

21. Peplow, P. and Baxter, G., Defining a Therapeutic Window for Laser Irradiation (810 nm) Applied to the Inguinal Region to Ameliorate Diabetes in Diabetic Mice. Photomedicine and Laser Surgery, 2014; 32(9), pp.500-504.

22. Yu, W., Chi, L., Naim, J. and Lanzafame, R., Improvement of host response to sepsis by photobiomodulation. Lasers in Surgery and Medicine, 1997; 21(3), pp.262-268.

23. Liebman, C., Vu, T., Phillips, A., Chen, B. and Cho, M., Altered β-Cell Calcium Dynamics via Electric Field Exposure. Annals of Biomedical Engineering, 2020.

24. Fan, L., Zhang, F., Fan, H. and Zhang, C., Brief review of image denoising techniques. Visual Computing for Industry, Biomedicine, and Art, 2019; 2(1).

25. García-Montalvo, E., H. Reyes-Pérez, and L. Del Razo. Fluoride exposure impairs glucose tolerance via decreased insulin expression and oxidative stress. Toxicology, 2009; 263:75-83.

26. Poitout, V., Stout, L., Armstrong, M., Walseth, T., Sorenson, R. and Robertson, R., Morphological and functional characterization of beta TC-6 cells--an insulin-secreting cell line derived from transgenic mice. Diabetes, 1995; 44(3), pp.306-313.

27. Iglewicz, B., and D. C. Hoaglin. How to Detect and Handle Outliers, American Society for Quality Control. 1993.

28. Dubitzky W., Wolkenhauer O., Cho KH., Yokota H., Holm-Bonferroni Method. In: (eds) Encyclopedia of Systems Biology. 2013.

29. Charles Zaiontz., The data analysis for this paper was generated using the Real Statistics Resource Pack software (Release 6.2). Copyright, 2013 – 2019.

30. Dittami, G., Rajguru, S., Lasher, R., Hitchcock, R. and Rabbitt, R., Intracellular calcium transients evoked by pulsed infrared radiation in neonatal cardiomyocytes. The Journal of Physiology, 2011; 589(6), pp.1295-1306.

31. Song MY, Makino A, Yuan JX., Role of reactive oxygen species and redox in regulating the function of transient receptor potential channels. Antioxid Redox Signal. 2011; 15(6):1549-1565.

32. Dolenšek, J., Klemen, M., Gosak, M., Križančić-Bombek, L., Pohorec, V., Rupnik, M., Stožer, A. Glucose-dependent activation, activity, and deactivation of beta cell networks in acute mouse pancreas tissue slices. 2020. Preprint available at: https://doi.org/10.1101/2020.03.11.986893

33. Braun, M., Ramracheya, R., Bengtsson, M., Zhang, Q., Karanauskaite, J., Partridge, C., Johnson, P. and Rorsman, P., Voltage-Gated Ion Channels in Human Pancreatic - Cells: Electrophysiological Characterization and Role in Insulin Secretion. Diabetes, 2008; 57(6), pp.1618-1628.

34. Tsai, S. and Hamblin, M., Biological effects and medical applications of infrared radiation. Journal of Photochemistry and Photobiology B: Biology, 2017; 170, pp.197-207.

35. Takayama, Y., Uta, D., Furue, H. and Tominaga, M., Pain-enhancing mechanism through interaction between TRPV1 and anoctamin 1 in sensory neurons. Proceedings of the National Academy of Sciences, 2015; 112(16), pp.5213-5218.

36. Gees, M., Colsoul, B. and Nilius, B., The Role of Transient Receptor Potential Cation Channels in Ca2+ Signaling. Cold Spring Harbor Perspectives in Biology, 2010; 2(10), pp.a003962-a003962.

37. Moreau, D., Lefort, C., Pas, J., Bardet, S., Leveque, P. and O'Connor, R., Infrared neural stimulation induces intracellular Ca2+ release mediated by phospholipase C. Journal of Biophotonics, 2017; 11(2), p.e201700020.

38. Brown, G., Regulation of mitochondrial respiration by nitric oxide inhibition of cytochrome c oxidase. Biochimica et Biophysica Acta (BBA) - Bioenergetics, 2001; 1504(1), pp.46-57.

39. Song, M., Makino, A. and Yuan, J., Role of Reactive Oxygen Species and Redox in Regulating the Function of Transient Receptor Potential Channels. Antioxidants & Redox Signaling, 2011; 15(6), pp.1549-1565.

40. Tiganis, T., Reactive oxygen species and insulin resistance: the good, the bad and the ugly. Trends in Pharmacological Sciences, 2011; 32(2), pp.82-89.

41. Kaneto, H., Katakami, N., Matsuhisa, M. and Matsuoka, T., 2010. Role of Reactive Oxygen Species in the Progression of Type 2 Diabetes and Atherosclerosis. Mediators of Inflammation, 2010; pp.1-11.

42. Leloup, C., Tourrel-Cuzin, C., Magnan, C., Karaca, M., Castel, J., Carneiro, L., Colombani, A., Ktorza, A., Casteilla, L. and Penicaud, L., Mitochondrial Reactive Oxygen Species Are Obligatory Signals for Glucose-Induced Insulin Secretion. Diabetes, 2009; 58(3), pp.673-681.

43. Llanos, P., Contreras-Ferrat, A., Barrientos, G., Valencia, M., Mears, D. and Hidalgo, C., Glucose-Dependent Insulin Secretion in Pancreatic β-Cell Islets from Male Rats Requires Ca2+ Release via ROS-Stimulated Ryanodine Receptors. PLOS ONE, 2015; 10(6), p.e0129238.

CHAPTER 4:

AN INTEGRATED MODEL FOR PREDICTING THE FUNCTIONAL EFFECTS OF ELECTRICAL AND PHOTONIC STIMULI ON β-CELLS

Caleb Liebman and Michael Cho

In preparation for submission

Abstract:

Electric field stimulation (EFS) and Photobiomodulation (PBM) have both been shown to have therapeutic potential in several disease states. Recently, our work with these physical stimuli have demonstrated an ability to affect the cellular functionality of insulin secreting β-cells. Herein, we explore how these modalities may exert their effects using an integrated numerical simulation. Aside from providing insight into how EFS and PBM could affect the β-cell physiology, these simulations could prove useful in optimizing synergistic parameters for use in diabetic therapies. Our model predicts the effects of EFS on calcium dynamics and their waveforms, along with an early model of PBM effects that implies a potential activation of Glucokinase increasing the β-cell's glucose consumption. The results of this model indicate that PBM and EFS can act together to induce both calcium spiking and glucose uptake at lower glucose loads, while providing differential effects at higher glucose concentrations. Taken together, this model elucidates the effects of these physical stimuli on the β-cell physiology and its insulin secretion.

Introduction:

It has been well established that cells are able to sense and respond to their local environment, with insulin secreting β-cells being no exception.[1] While many efforts have focused on the biologic environment, few reports have demonstrated how these cells may respond to various physical stimuli. Previous research has demonstrated that cellular functionality can be altered by physical stimuli such as electrical fields and laser therapy.[2,3] Electric fields are natively found in several biological processes from wound healing to neural signaling,[4] while cellular responses to light are commonplace in the eye and skin.[5] Depending on the parameters, exogenous

EFS and PBM have demonstrated therapeutic potential by altering various aspects of cellular physiology.[6,7]

EFS has been used to improve wound healing alongside therapies such as deep brain stimulation.[8,9] EFS affects the polarity of the cellular membrane leading to changes with the cell's electrophysiology with respect to depolarization event timing and cation flux.[10,11] At biologically relevant electric field (EF) strengths (~ 1 – 5 V/cm),[12] a slow increase in calcium entry has been demonstrated and is likely mediated by the opening of voltage gated calcium channels (VGCCs).[13] When the EF strengths are orders of magnitude higher, electroporation can occur with applications for transfection and instigating cellular death.[14] While we focus on direct current (DC) EFs given their biologic mimicry, many other groups have demonstrated therapeutic benefits with pulsed DC- and alternating current (AC-) EFs.[15,16] While biologically relevant DC-EFs only affect the cellular membrane's polarity, pulsed and AC EFs are capable of affecting intracellular physiology, thus increasing the complexity of the cellular response.[17]

While the mechanisms of EFS are relatively well established, the mechanisms for PBM have yet to be fully elucidated. Some of the leading mechanisms of PBM include the activation of TRP channels, dissociation of nitric oxide (NO) from the functional heme binding site on cytochrome C oxidase (CCO) leading to an increase in electron transport chain (ETC) flux, and release of calcium from the endoplasmic reticulum via IP3- or Ryanodine- receptor channels.[18,19] Regardless of the mechanisms, PBM has demonstrated the ability to increase various intracellular signaling molecules such as calcium, reactive oxygen species (ROS) including superoxide and NO, and metabolic signals such as the ATP/ADP ratio.[20]

Of particular interest here, previous work has demonstrated electrophysiological and insulin secretory changes in the β-cell phenotype by EFS and PBM exposure.[21] In an effort to

predict the effects of these stimuli along with any synergistic or antagonistic responses, we developed an integrated numerical model to simulate calcium and insulin responses to these modalities independently and in combination. By elucidating these interactions, these modalities may be able to stimulate β-cell insulin secretion for use in various therapeutic applications.

Methods:

Modeling and Simulation: The electrophysiological model was replicated in Matlab from the 2003 Fridlyand model for β-cell calcium dynamics.[22] The ATP production in this model was then replaced with the output of the 2010 Fridlyand model for a β-cell's mitochondrial function.[23] These two models were then integrated with a previously developed model of insulin secretion.[24] Some modifications were made to the insulin secretion model to account for maximal secretion rates and maximum refilling rates for readily releasable pools based on a previous report.[25] In addition, the oxygen acceptor kinetic factor (FAe) of was set to 0.6 from 1.0 to account for an assumed NO inhibition (50 nM) of CCO activity and thus an inhibited capacity for ETC flux and oxygen consumption.[26,27] An illustration of the overall model's components can be found in Fig. 4-1.

Electrical stimulation was modeled using the equation for membrane potential by external electric fields by Schoenbach.[28] Given the hyper- and hypo- polarization between the anode and cathode facing sides respectively, the hyper-polarized side was neglected, while the depolarized side was accounted for by assuming the average depolarization to be the average value from $-\pi/2$ to $\pi/2$, resulting in a multiplier of $2/\pi$. The averaged membrane potential then becomes $1/\pi$ of the maximal value when halved considering only the depolarized side. Thus the change in membrane voltage and its differential equation become:

$$V_m = \frac{1}{\pi}\, f_c\, E\, r$$

$$\frac{dV_m}{dt} = \frac{\sum I_m}{-C_m} + \frac{1}{\pi}\, f_c\, E\, r$$

Where V_m is membrane voltage, f_c (1.5) is the spherical form factor, E is electric field strength, and r is the cellular radius with 7μm used for β-cells. The I_m are the plasma membrane currents with C_m being the overall membrane conductance.

Given that the exact mechanisms of photobiomodulation aren't fully elucidated, we firstly incorporated various potential mechanism into the model and varied their parameters to observe how the calcium dynamics would be affected. Since TRPV antagonist such as Capsazepine have demonstrated the role of TRPV1 in PBM's effects on calcium dynamics, we added this channel to the model to investigate its impact by varying its open fraction. The equations for its ionic currents were determined by its previously reported conductance elsewhere.[29]

While TRPV1 may be activated by other factors such as ROS signaling and pH levels, the most well established dependency is temperature. Using a simple thermal model for a cell along with a cellular convective heat loss estimate found elsewhere, we simulated the temperature rise in a cell by light exposure.[30] This assumed light was absorbed by the cell via its cross sectional area and with heat loss to the surrounding media via its surface area. Additionally, the temperature of the media was allowed to rise by its absorption via its cross sectional area with an assumed surface heat convection loss of 50 W/m^{2}K. This was then compared to experimentally determined temperature elevations of the bulk media. The differential equation for the cellular temperature rise is:

$$\frac{dT_{cell}}{dt} = \frac{\alpha\, I_r\, A_c - h_c\, A_{sc}(T_{cell} - T_{med})}{m_c\, C_p}$$

Where α is the absorbance of water at 810 nm, I_r is the irradiant flux, A_c is the cross sectional area for the cell, and h_c was the convective heat loss to the media from the cell[30] T_{cell} and T_{med} are the temperatures for the cell and media respectively, with m_c being the cell's mass, and C_p being the specific heat of water. The temperature change for the media was determined by:

$$\frac{dT_{med}}{dt} = \frac{\alpha\, I_r\, A_m - h_m\, A_{sm}(T_{med} - T_{sur})}{m_{med}\, C_p}$$

Where A_m is the cross sectional area for the media, h_m being the convective heat loss to the surrounding from the media's surface A_{sm}, and m_{med} being the media's mass.

The cytosolic calcium influx by PBM has also been shown to originate from intracellular stores, in particular from IP3-Receptors on the ER membrane in some cell types.[31] Since, the electrophysiological model already included equations for the calcium release via these channels, we simply multiplied its calcium flux by a factor to determine how a potential increase of the open fraction from the IP3-receptor channels would contribute to the overall calcium dynamics.

For the activity of CCO by PBM, the integrated mitochondrial model includes an equation for proton pumping related to ETC flux:

$$J_{hres} = V_{me} F_{De} F_{Ae} F_{Te}$$

Where V_{me} is the optimal rate of proton flux with, F_{De} accounting for NADH availability, F_{Te} accounting for mitochondrial membrane potential, and the modified F_{Ae} oxygen availability for binding to CCO completing ETC flux. While the original model kept F_{Ae} at maximum ($F_{Ae} = 1$), we varied this parameter in the model from 0.6 to 1 to see how the availability of oxygen binding to CCO would affect the calcium dynamics. Thus demonstrating the effect of PBM on CCO's activity into the model

Based on these results, we attempted to model PBM by its fluence through a combination of these parameters to match experimentally observed data. CCO activity was estimated by a 2nd

order polynomial fitted to experimentally estimated CCO activity by fluence at 660 nm from a previous report.[32] We then accounted for the difference between 660 nm and 810 nm by their respective CCO absorbance.[33] Thus the multiplier for CCO was determined by the following:

$$\Delta FAe = 1 + \ 1.6\ [\alpha_{CCO}\ I_r] - \ 0.9\ [\alpha_{CCO}\ I_r]^2$$

With FAe being 0.6 multiplied by this change in CCO activity by PBM.

While CCO appeared to be the dominant factor affecting the calcium spiking, it did not adequately account for the observed rise in spiking frequency. Thus we assumed that PBM could be modulating Glucokinase activity (GKA) and thereby increasing the rate limiting factor for glucose consumption. Small variations in Glucokinase (GK) capacity were able to substantially affect the calcium dynamics. To better match the data, a multiplier of $1 + \ FAe(\Delta FAe - 1\ )/14$ was added to the model with a maximum increase of 5% in GKA at peak PBM values.

Simulation Plots: Results from the model were generated over a range of parameter values, with the results being subtracted from the control values. These difference values were then color coded with green represented a reduction from the control and red representing an increase, with black being no change. A box mean blur was then performed to attempt an interpolation between the given simulations. The color intensity was adjusted between the negative and positive values for the absolute maximum value from the data.

Bulk Temperature Experimentation: Using an Omega HH42A thermistor, bulk temperature measurements were taken of the HBSS before and after the 1 minute exposure to PBM with the fluences 4.5, 9.0, and 18.0 J/cm^2. The total volume of Hank's balanced salt solution (HBSS) in the chamber was 2 mL, which was the same as the sample runs. All fluences incorporated 6 experimental runs with initial temperature readings as similar as possible.

Cell Culture: Mouse insulinoma β-TC6 cells from ATCC were grown in high glucose (4.5 g/L) Dulbecco's modified eagle's medium (DMEM) from sigma and supplemented with 15% fetal bovine serum (FBS) from Gibco and 1% penicillin-sterptomyosin (P-S) from Sigma. Cultures were incubated at a humid 37 °C with 5% CO2. Samples were prepared using 0.25% Trypsin-EDTA solution from Sigma and seeded on glass coverslips at a density of 40,000 cells per cm^2 in low glucose (1 g/L) DMEM supplemented with 15% FBS and 1% P-S. Samples were then used within 2 – 4 days after seeding.

Sample Staining: Half an hour before imaging, samples were washed with HBSS from Sigma and then incubated for 30 minutes with a staining solution containing 0.8 μM Fluo-8 (Abcam) and 1 drop/mL Nucblue (Thermo). Samples were then washed and mounted to the PBM chamber immersed in HBSS. Samples from the PBM groups included Mitosox (μM) for the superoxide measurements in our previous reports.

Fluorescent Imaging: Baseline calcium spiking was measured using a 2 minute video before PBM/EFS exposure and then at 5, 10, and 15 minutes for PBM and just at 15 for EFS. Static images for calcium rise and nuclear position were taken at the baseline and these time points as well. For EFS imaging, the samples were mounted to the chamber as previously described elsewhere and imaged.[21] While for PBM, samples were first imaged, then moved for PBM exposure, and followed by replacement and imaging of the same cells. Details on the PBM chamber and the experimental procedure can also be found in the Chapter 3.

Image Analysis: Samples from previous works were reanalyzed for comparison with the model's predictions. Regions of interest (ROI) were made on the location of cellular nuclei and then overlaid on the calcium spiking videos to measure the mean intensity of Fluo-8 per cell over time. Using a spike threshold of 10% above the moving average mean (n=10), spikes per cell were

recorded with time and used to determine the average frequency of active cells demonstrating at least one spike. Calcium rise was determined by generating ROIs on the cell clusters and measuring the mean calcium at each time point. PBM calcium rise results used the peak intensity over the baseline for the relative values. EFS calcium rise was simply post- over pre- exposure intensities.

Insulin Secretion and Measurement: Experimental samples from our previous reports were used and reported as the relative increase in insulin secretion from their respective controls.[21] Samples were first washed in Krebs Ringer Buffer (KRB) without glucose and incubated for an hour. Samples were then mounted to their respective chambers in KRB. Fifteen minutes after exposure to either PBM or EFS, the surrounding KRB was taken and eventually measured in an insulin ELISA. Normalization was performed using a Cyquant assay to measure DNA content to adjust for the number of cells per sample.

Statistical Analysis: Simple student's paired t-tests were performed between the time points following stimulation with a significant p-value cutoff at 0.05.

Results:

Model Baseline Response: To determine the model's response to normal stimuli, we ran the simulation results for mean intracellular calcium, the calcium spiking frequency, and the percent of total insulin for variations in glucose load. As can be seen in Fig. 4-2. A-C, the mean calcium, spiking frequency, and insulin secretion all respond appropriately to the glucose load. The rise in calcium spiking and insulin secretion begin to accelerate as the glucose loads increased is critical to normal β-cell physiology.[34] To demonstrate the temporal characteristics of the

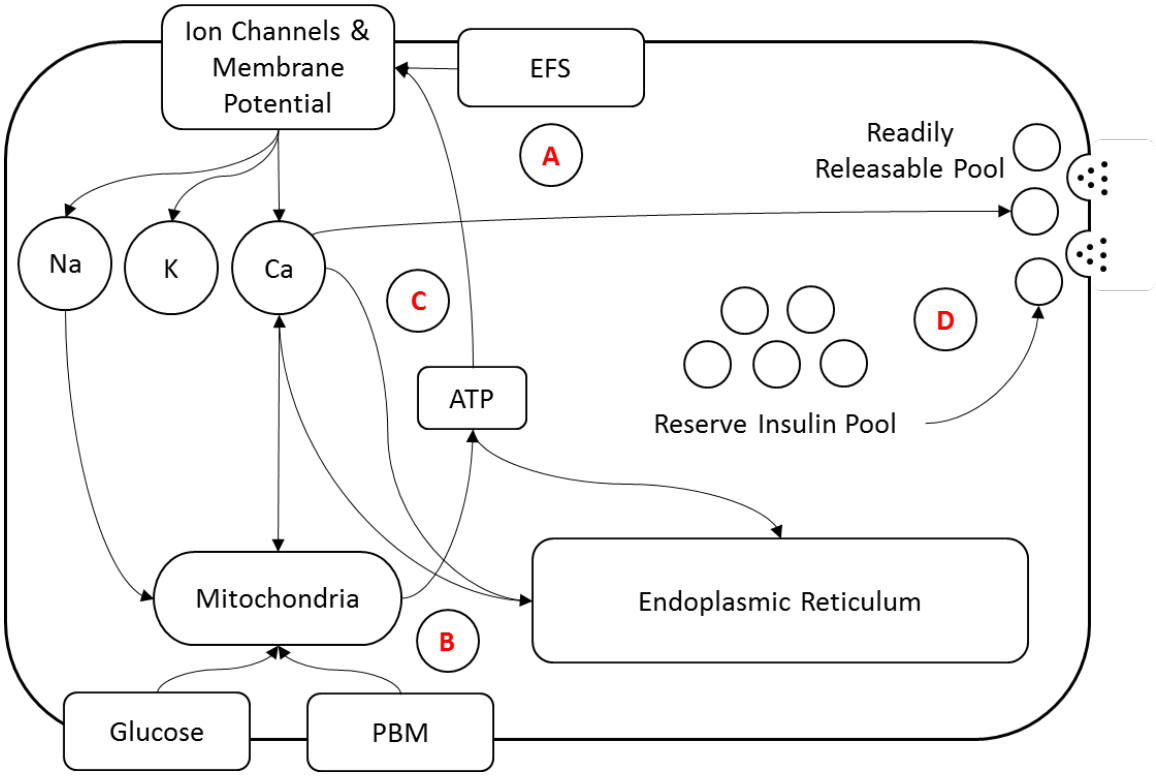

Figure 4-1: (A) EFS is capable of altering the membrane potential and thus affection cationic currents into the cell. (B) PBM likely exerts its effects on CCO activity increasing ETC flux and ATP production. (C) Due to interactions between EFS and PBM, the calcium dynamics are altered within the cell. (D) These calcium dynamics directly spur insulin secretion from the readily releasable pool followed by replenishment from the reserve insulin pool.

simulation, response curves for calcium and insulin secretion are shown in Fig. 4-2. D-E. At 100 mg/dL, no calcium spiking is observed, mean intracellular calcium is in a steady state, and insulin secretion is low. When the glucose load is increased to 200 mg/dL, calcium spiking begins and is tightly correlated with insulin secretion, with the overall insulin secretion being orders of magnitude higher than the low glucose condition.

EFS versus Glucose Load: Simulation plots were generated crossing glucose load against EFS strength to determine how EFS alone affects the mean calcium, calcium spiking frequency, and insulin secretion, referred to from here on as the standard responses. These plots can be seen in Fig. 4-3. A-C. Mean calcium appears to follow a positive linear relationship between glucose

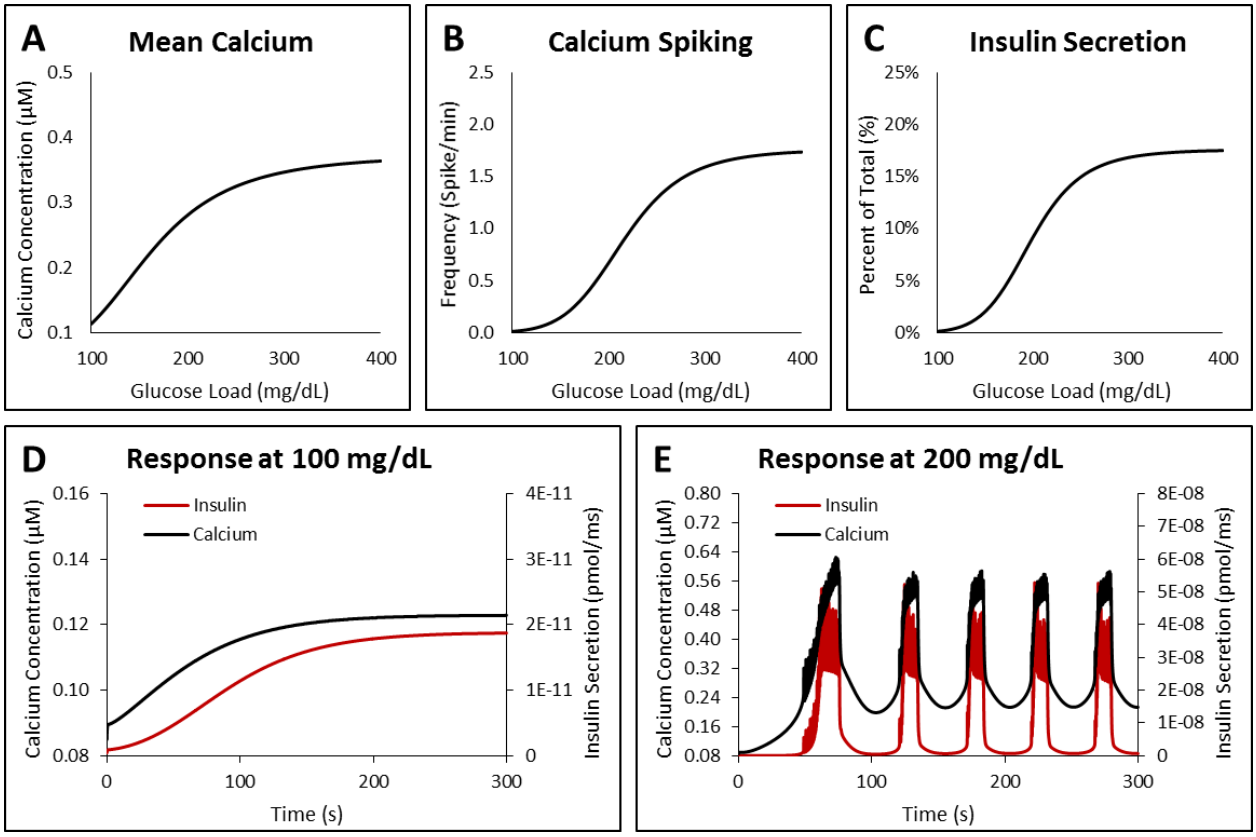

Figure 4-2: (A) Simulated mean calcium at various levels of glucose load. (B) Simulated calcium spiking rates versus glucose load. (C) Insulin secretion as a measure of % of total insulin content by glucose load. (D) Temporal response of calcium and insulin secretion at normal glucose levels (100 mg/dL). (E) Temporal response of calcium and insulin secretion at elevated glucose levels (200 mg/dL).

load and EFS strength. These simulations correspond well with the observations seen in Fig. 4-3. D.

The relationship between glucose load and EF strength on calcium spiking is more complex. Firstly, EFS can start calcium spiking at lower than basal glucose loads by its depolarizing effects. We previously reported this phenomena by which the percent of active cells could be increased by EFS.[21] Depending on the glucose load, the rise in calcium spiking occurs between particular EFS values. This type of pattern could explain the observations made where calcium spiking was found to increase at 1 and 2 V/cm but then begin to decrease at 3 V/cm as

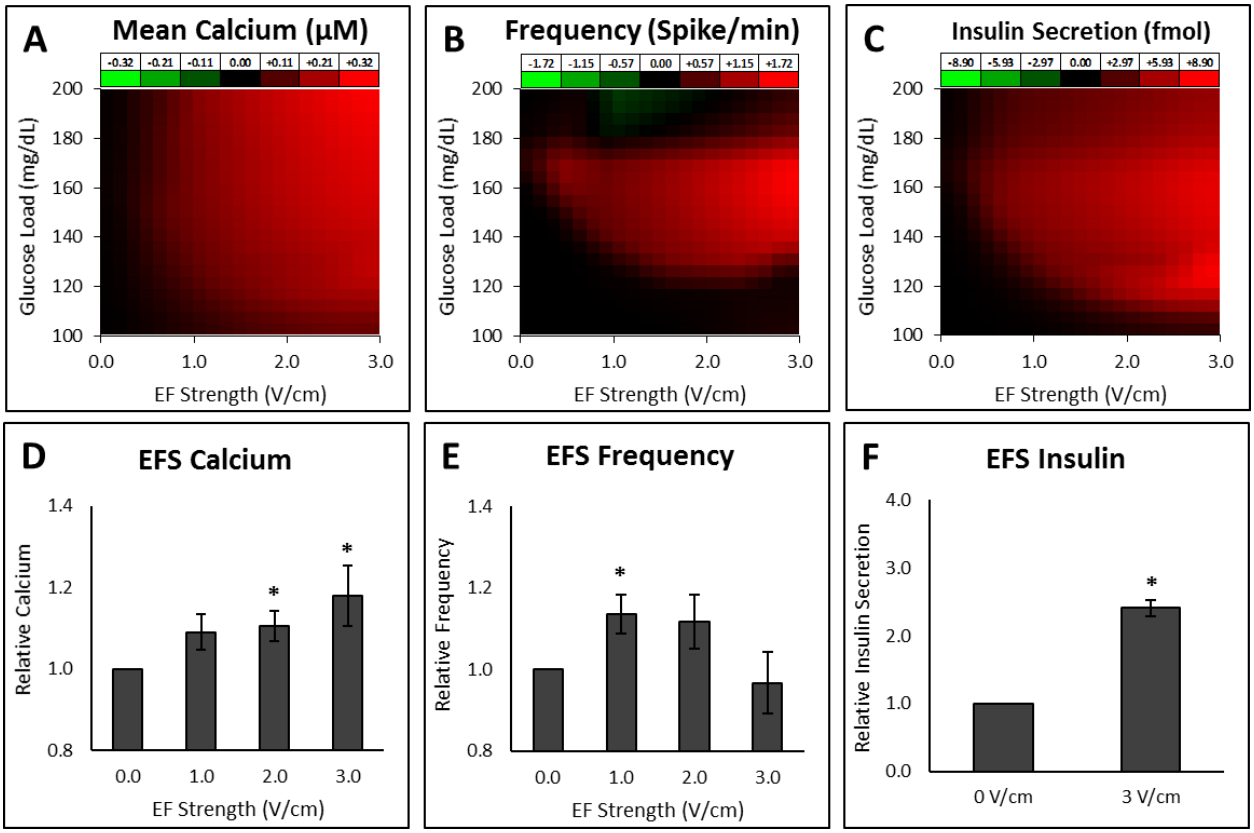

Figure 4-3: (A-C) Heat maps for the difference (positive = Red, negative = Green) between simulation results and baseline values for mean calcium, spiking frequency, and insulin secretion against glucose load versus electric field strengths. (D) Experimental results demonstrating a rise in intracellular calcium versus EFS strength. (E) Experimentally determined changes in spiking frequency under different EFS strengths. **(F)** Relative insulin secretion between control group and a 3 V/cm field without glucose.

seen in Fig. 4-3. E. Another observation is that the simulation predicts a slight decrease in calcium spiking at higher glucose loads.

The relationship between EFS and glucose load on insulin secretion appears to be relatively straightforward. Given that calcium dynamics drive insulin secretion, it would seem reasonable that higher glucose loads and greater EF strengths would increase the overall insulin secretion rate. A note is to be made that the difference plot demonstrated a greater increase in insulin secretion at low glucose with higher EF strengths. Simulations within these regions predicted the ability of stronger EFs to induce a few calcium spikes but greatly elevate the background calcium

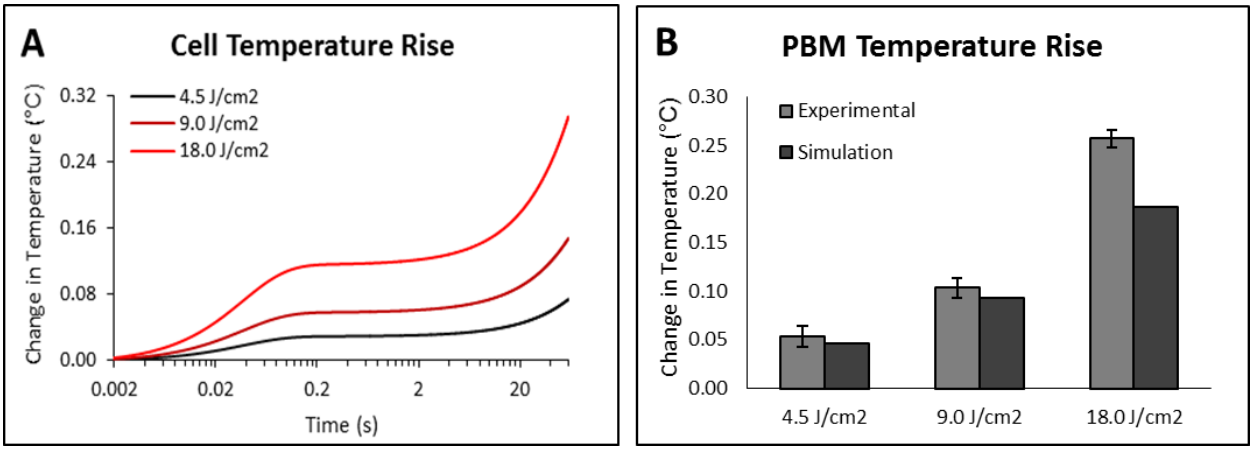

Figure 4-4: (A) Thermal model predictions for the change in cellular temperature over log(time). Within 200 ms the cellular temperature matches the extracellular temperature and rises proportionally with it. (B) Experimentally measured bulk temperature change following 1 minute of laser exposure at various fluences versus the model predictions.

concentration. Thus leading to a bursting effect of insulin secretion but without sustained calcium spiking events. Given the significant increase in insulin secretion by 3 V/cm in the absence of extracellular glucose shown in Fig. 4-3. F, this could be a possibility.

Temperature and TRPV1 Simulations: Given that TRPV1's primary activators are vanilloids and temperature, we estimated the potential temperature rise of a given cell and environment by the 810 nm laser at various strengths. It appeared that the cell's temperature would rise quickly, but would reach its steady state with the surrounding media within ~200 ms of PBM irradiation as seen in Fig. 4-4. A. After this, the cell's temperature would gradually rise as the temperature of the surrounding fluid increased. The model predicted a final temperature rise of 0.046, 0.093, and 0.187 °C for 4.5, 9.0, and 18.0 J/cm^2 respectively. While the cell's change in temperature was approximately 162% of the bulk temperature in these simulation, this is likely negligible with respect to TRPV1 activation give that the cell's max temperatures would be 37.08, 37.15, and 37.30 °C for 4.5, 9.0, and 18.0 J/cm^2 respectively. The measured bulk temperatures

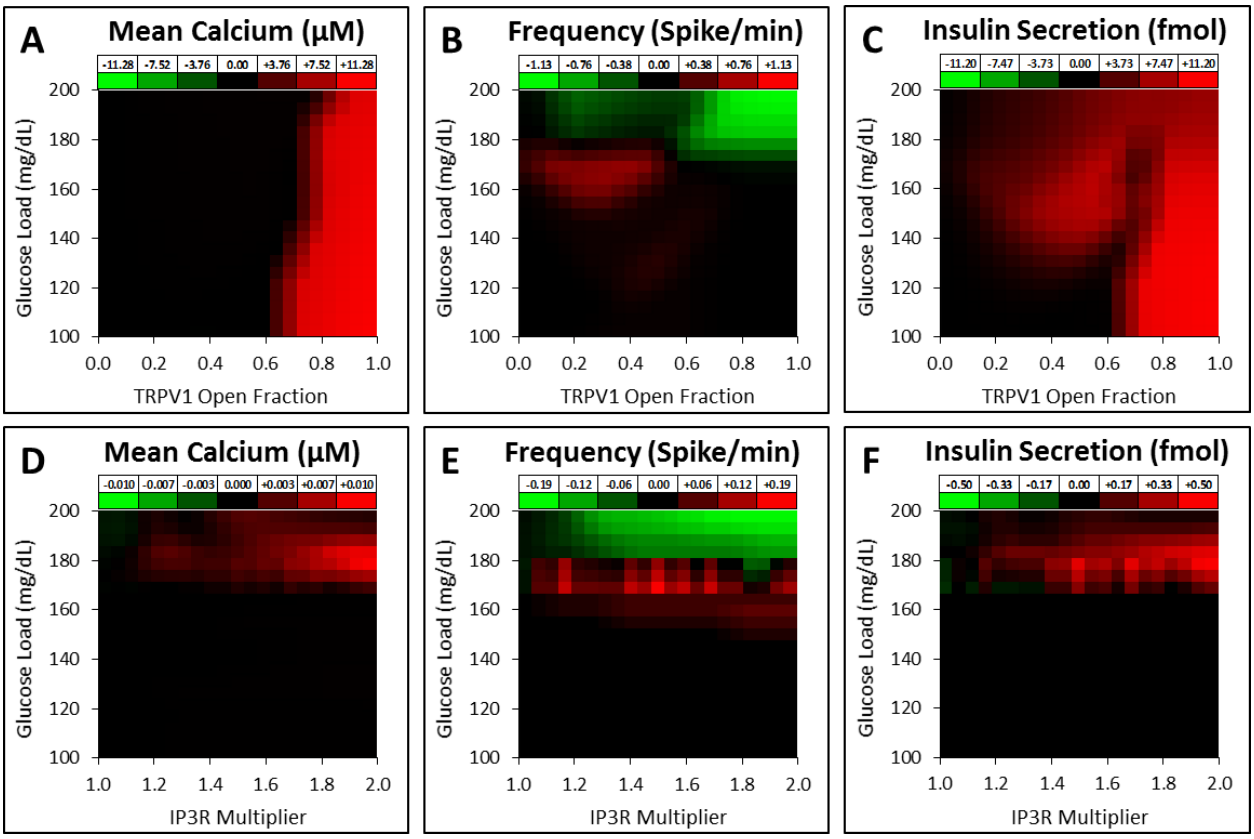

Figure 4-5: (A-C) Simulation plots for the difference in mean calcium, spiking frequency, and insulin secretion against glucose load versus TRPV1 open fraction. (D-F) Simulation plots for the differences in mean calcium, spiking, and insulin secretion against glucose load versus an IP3R multiplier.

following PBM exposure seen in Fig. 4-4. B, match well with the predicted values from the model. If we assume a 37 °C initial temperature, the temperature following 300 mW/cm^2 for a 1 minute exposure (18.0 J/cm^2) is predicted to be 37.3 °C leading to a change in TPRV1 open fraction from 0.0026 to 0.0033 using an equation from another report.[35]

Nevertheless, an ionic current for TRPV1 was added to the model along with its cationic conductance values obtained elsewhere.[36] The open fraction was then compared to the standard responses. Mean calcium was slightly increased at all open fractions, but when the open fraction was approximately greater than 0.7, the cell would be flooded with intracellular calcium as seen in Fig. 4-5. A. TRPV1 was found to modestly increase spiking frequency at medium glucose loads

between 0.0 and 0.4 open fractions, while at higher glucose loads or greater open fractions it could reduce the spiking frequency as seen in Fig. 4-5. B. In Fig. 4-5. C, insulin secretion could be increased at medium glucose loads with lower open fractions likely due to the small increases in calcium spiking and intracellular calcium. At high open fractions, the flooding of intracellular calcium would lead to an insulin burst, with the maximal insulin secretion rate being reached.

IP3-Receptor Activation: The simulation plots were made for the standard responses with IP3R being sensitized up to a 2 fold increase in its calcium flux Fig. 4-6. A-C. As for the mean calcium, increasing the sensitivity to opening lead to an increase in intracellular calcium. This is expected, but the increase in calcium was at most 0.01 μM equating to about a 3% rise from basal. Spiking frequency appeared to increase when sensitized for lower glucose loads, which was likely due to activation of spiking near the glucose load threshold rather than a true increase in spiking frequency, while higher glucose loads decreased the change in frequency. As with the calcium, the difference between the sensitized channel and the basal response was low, increasing at most by 0.18 spikes/min. Finally the change in insulin followed the same trend as the change in the mean intracellular calcium. As the receptors were sensitized, insulin secretion would increase, yet to a relatively small difference between it and the basal response.

CCO Activity: The primary mechanism by which PBM affects the cell is believed to be through CCO activation by dissociating NO from its functional heme group. Given that the estimated activity for our model at basal conditions was set to approximately 60% (FAe = 0.6), PBM was expected to increase this value up to its optimal conditions near 100%. As explained in the methods section, we estimated the increase in FAe based on a previous report with PBM and CCO activity.[37] Since our basal conditions were set at 0.6, a reduction from this activity would thus inhibit the standard responses. When CCO activity is increased as seen in Fig. 4-6. A-C, both

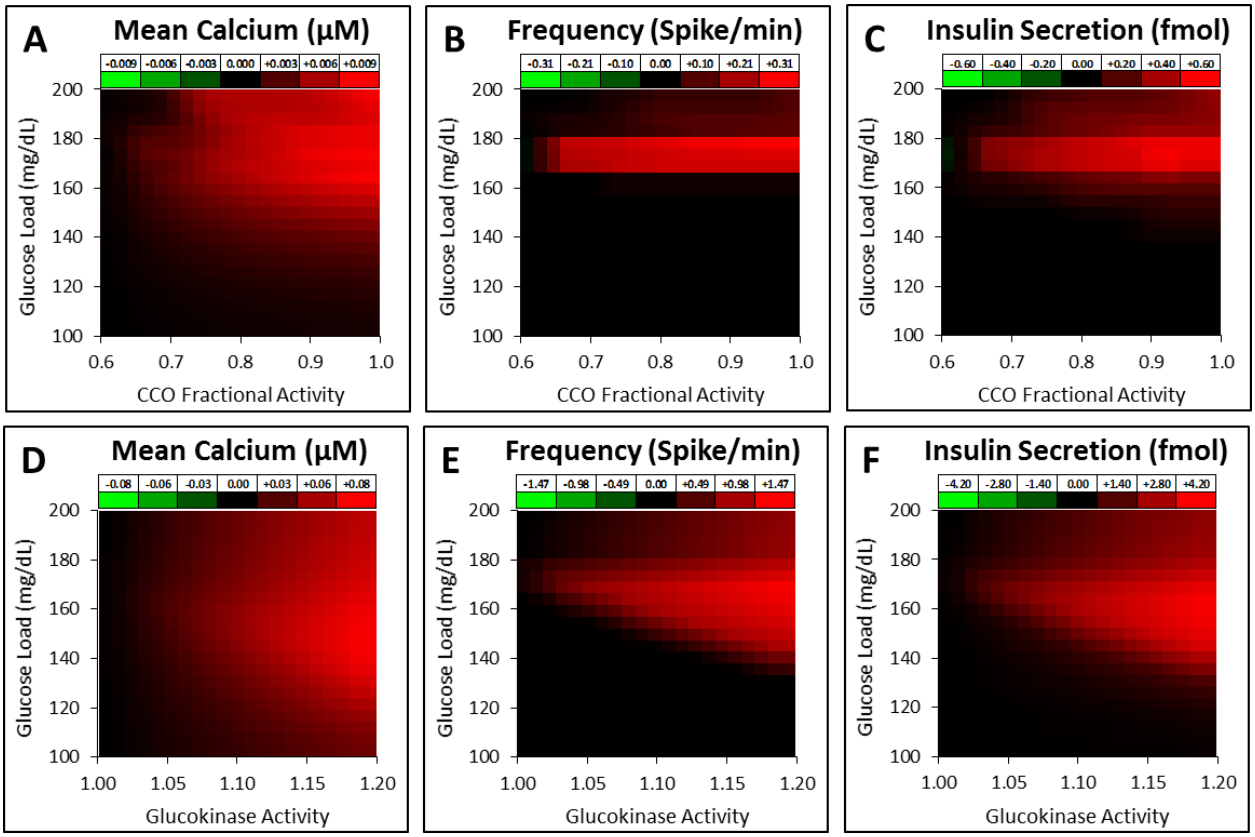

Figure 4-6: (A-C) Simulation plots for the difference in calcium, spiking, and insulin secretion against CCO fractional activity. (D-E) Simulation plots for the difference in calcium, spiking, and insulin secretion against glucose load versus fractional glucokinase activity.

insulin secretion and calcium spiking is modestly increased. Similar to results from the IP3-Receptor simulations, the activation of calcium spiking is possible near the threshold value for glucose. Unlike IP3-receptor simulations, increases in CCO activity do not inhibit spiking or insulin at any glucose load and had a greater increase in calcium spiking.

Glucokinase Activity Simulation: Under the assumption that PBM could increase the activity of GK, the sensitivity of the cell to its glucose load would be increased. We modeled the standard responses by a multiplier of GK from 1 to 1.2 seen in Fig. 4-6. D-F. While the increase in the mean calcium was small, the spiking frequency could be greatly increased by GKA. The increase in its activity could also lead to the activation of calcium spiking at lower than basal

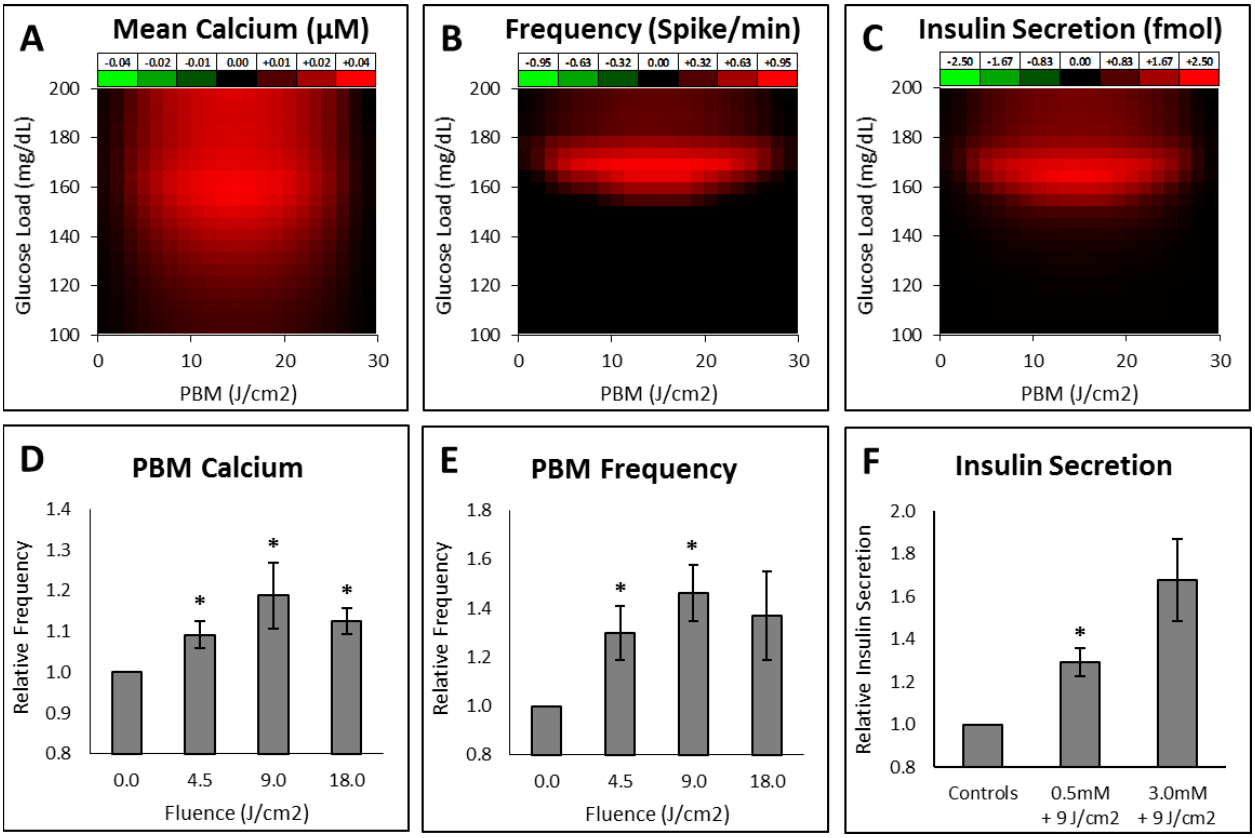

Figure 4-7: (A-C) Simulation plots for the difference in mean calcium, spiking, and insulin secretion against glucose load versus PBM fluence based on CCO and GK activation. (D) Experimentally derived relative changes in mean calcium following PBM irradiation at various fluences. (E) Relative change in frequency following PBM exposure. (F) Percent total insulin secretion following 9 J/cm2 PBM exposure at 0.5 and 3.0 mM glucose loads.

threshold levels. This strong increase in calcium dynamics was able to increase the insulin secretion beyond the basic rise in background calcium.

PBM Model for Stimulation: Given the results from TRPV1, IP3R, CCO, and GK stimulation, we assumed that the dominant factors that could result in the spiking rise observed would be the stimulation of CCO and GKA. TRPV1 was excluded from the PBM model since the thermal rise was far too small to lead to significant opening of these channels. Beyond this, both TRPV1 and IP3-Receptor activation within the model did not result in the large rise in calcium spiking observed with experimentation. Following these assumptions, the standard responses were

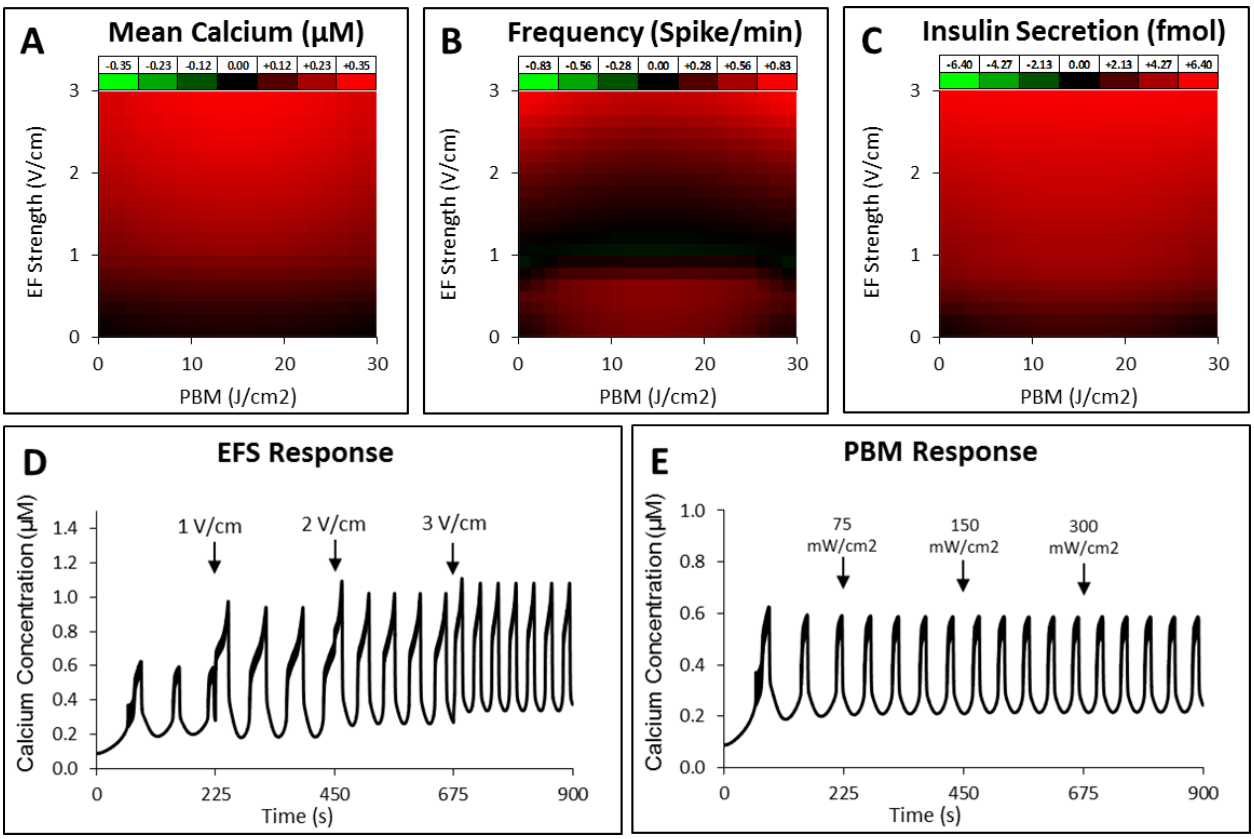

Figure 4-8: (A-C) Simulation plots for the difference in mean calcium, spiking, and insulin secretion with EFS strengths versus PBM fluence at 180 mg/dL demonstrating potentially optimal therapeutic windows for synergistic cooperation. (D) Temporal plots of calcium and insulin secretion for 180 mg/dL, with sequential increases in EF strength demonstrating the change in calcium waveforms and frequency. (E) Temporal plot for intracellular calcium at 180 mg/dL, with sequential increases in PBM irradiance demonstrating the change in frequency derived by PBM's effects.

plotted shown in Fig. 4-7. A-C. While the effects of PBM demonstrate an increase in intracellular calcium, the change was much less than the simulated effects of EFS. For calcium spiking, the greatest increase appeared near the glucose threshold, likely indicating an activation of the calcium dynamics when at basal conditions spiking would not occur. Insulin secretion demonstrated peaks with calcium spiking rather than elevations in intracellular calcium.

The simulations demonstrated similar patterns to the data presented in Fig. 4-7. D-F. The mean calcium along with spiking frequency increased with fluence and then began to decrease at

higher strengths. While the simulations demonstrate an optimal range between 10 – 20 J/cm^2, the data seems to suggest that the peak may be closer to 10 J/cm^2 with a more narrow range. This could be due to differences between how isolated mitochondria and intracellular mitochondria respond to PBM. The experimental results for insulin secretion were increased following PBM exposure and demonstrated the influence of glucose load with PBM.

EFS with PBM: Finally, in an attempt to determine interactions on the cellular response between EFS and PBM, multiple plots were generated and shown in Fig. 4-8. A-C. Both mean calcium and insulin secretion were maximized when the simulation's optimal fluence (15 J/cm^2) and greatest EF strength (3 V/cm) were applied. All of these plots were generated at a glucose load of 180 mg/dL since this is the threshold for spiking to begin. The plot for calcium spiking frequency was the most diverse, with a section around 1 V/cm and the PBM window having the lowest increase in spiking. Also worth noting, the calcium spiking was greatest within the PBM window at low EF strengths, but was the least at higher EF strengths.

To observe the temporal responses to these stimuli, Fig. 4-8. D-E plotted the calcium response to sequentially increasing EFS and PBM stimulations respectively. EFS caused an increase in frequency with greater EF strengths, but also increased the amplitude and reduced the spike duration as the EF's strengths increased. Similar to EFS, PBM was able to increase spiking frequency at higher fluences, but unlike the EFS response the spikes' morphologies and amplitudes appeared unchanged.

Discussion:

EFS likely exerts the majority of its effects by altering the membrane potential leading to an increase in the open fraction of any voltage dependent channels.[38] Given the previous report

demonstrating the involvement of VGCCs in EFS instigated calcium influx, it seems reasonable to assume that it is the dominant driver, yet several other cationic channels present in β-cells could also be affected.[39] While this could explain the influx of intracellular calcium from the extracellular space, it does not account for the change in the spiking frequency. Therapies utilizing EFs with neurological processes have demonstrated that fields as weak as 0.05 V/cm can affect the depolarization events of neuronal cell.[40] It seems that the small shift in membrane polarity is able to reduce the delay between depolarization events by increasing the voltage driving force for the ionic currents. This increase in the depolarization frequency should lead to shorter and more frequent calcium spikes, given their dependency on depolarization events.

When investigating the effects of EFS with respect to the model's predictions, it appeared that by increasing the EF strength under a constant glucose load, the frequency would continue to rise until a dropping point was reached that depended on the particular glucose load. When applying even greater EF strengths, the model predicted a region where spiking would cease and the cell would be flooded by an influx of calcium. This is likely due to a driving force inducing calcium influx that surpasses the cell's capacity to sequester or remove calcium from the cytosolic space.[41] This has been well documented with stronger EFs as a method to induce cellular death via calcium cytotoxicity.[42] Another region occurred with glucose loads greater than around 180 mg/dL under constant EF strengths, where the spiking did not increase and even decreased at lower EF strengths. Looking at the temporal plots in this region, it appeared that the duration between each spike was in fact reduced, but because of the increased amplitude of each spike, its width became longer than its period and thus reduced the overall frequency.

The insulin secretion appeared greatest at higher field strengths with a strong increase in calcium spiking, but another area also appeared at lower glucose concentrations with elevated EF

strengths. The temporal plots indicated that the calcium influx likely overwhelmed the cellular machinery to remove calcium from the cytosol given that one large spike occurred followed by a steady elevated level of intracellular calcium which lead to a strong burst of insulin secretion. Since repolarization events and the resting membrane potential require ATP dependent ionic pumps, these outward currents were likely insufficient to overcome the influx of cations brought about by EFS.[43]

While others along with our previous work have demonstrated the involvement of TRPV1 channels with PBM's effects, the lack of temperature rise is unlikely to induce their opening.[44] It is possible that other TRPV channels could also be involved since they are able to respond to lower temperature levels.[45] Alternatively, it has been reported that the drug Capsazepine can inhibit VGCCs alongside TRPV1.[46] Since VGCCs are critical to the electrophysiology of β-cells, it may be possible that this inhibition could guise itself as TRPV1 inactivation. It may also be possible PBM induces elevations in ROS leading to the activation of TRP channels.[47] Since the peak of calcium spiking commonly occurred around the 10 minute mark following irradiation in the experimentation, this may be a possibility; however, the opening of TRPV1 alone does not seem to account for the effects given by the model's predictions.

Previous publications reported that cardiomyocytes can be stimulated to by high intensity pulsed laser to drive calcium spikes.[48] Furthermore, it was suggested that sarcoplasmic release of calcium was the more likely source of cytoplasmic influx. Another report concluded that PBM was able to induce IP3-Receptor calcium release from the endoplasmic reticulum.[49] While IP3-Receptor activation may be induced by PBM exposure, the model did not predict significant changes in the calcium dynamics of these cells. It seems reasonable that drugs to inactivate IP3-

Receptors could be interfering with oscillatory machinery instead of simply blocking the effects of PBM.[50]

The primarily cited mechanism of action is the stimulation of CCO leading to elevations in ATP, ROS, and NO.[51] Depending on the amount of inhibition by NO on CCO, this mechanism could explain some of the findings, yet if there is little NO inhibition to begin with, it wouldn't seem likely to have a great effect. Our model demonstrated an increase in calcium spiking and insulin secretion brought about by a shift in CCO activity, yet the magnitude of the effects was lacking in comparison with the experimental observations. Looking for another explanation, it was assumed that the increased metabolic state of the cell could increase the activity of Glucokinase thereby increasing ATP production. GKA has been shown to be adjusted by the cell within minutes depending on the activity of the GK regulatory proteins.[52] These proteins inactivate and transport GK inside the nucleus at low glucose condition, but when glucose is plentiful, GK can be transported into the cytosol thereby increasing glycolytic flux.[53] GK acts as the rate limiting factor in glucose uptake by β-cells and thus presented as a likely mediator for the observed effects.[54] Additionally, other groups have demonstrated that cytosolic NO along with calcium release from the endoplasmic reticulum can lead to an increase in GKA.[55,56] Thus the increase in GKA could be an observed effect of IP3-Receptor release with PBM.

While EFS has a strong ability to affect the electrophysiology of the cell, it is unable to affect many of the intracellular processes. In contrast, PBM appears to directly affect the metabolic state of the cell while also affecting a plethora of other potential chromophores.[57] Since metabolic shifts along with elevations in ROS have been shown to affect insulin dynamics,[58] it seems reasonable that PBM could also lead to insulin secretion via different mechanisms than EFS. The results from the model indicate that through the combination of EFS and PBM, β-cells could be

stimulated to secrete insulin and respond to lower glucose levels as if they were higher glucose concentrations. While at elevated glucose concentrations, EFS and PBM could only induce smaller changes in the cell's immediate response.

Given that calcium dynamics play a major role in controlling the functions of various transcription factors and enzymatic activity, the ability to augment it via non-invasive modalities may prove a powerful therapeutic tool, especially for *ex vivo* or stem cell interventions. Another group has demonstrated beneficial outcomes from the combination laser therapy with magnetic fields to improve mesenchymal stem cell proliferation thus validating the possibility of a synergistic action between these modalities.[59] Low strength EFS could improve insulin secretion similar to the electro-physiologic mechanisms of Sulfonylurea.[60] While multiple PBM exposures have been shown to increase SOD2 expression, and thus could be used as a preventive measure to glucose toxicity and oxidative stress in diabetes.[61]

Based on the results from the model, it would seem that the optimal parameters depend very much on the desired physiologic outputs and the metabolic state of the cell. At lower glucose levels a combination of increasing the metabolic state by PBM with an amplified insulin secretion by EFS is likely optimal, while at higher glucose concentrations PBM may not be as necessary, as EFS had stronger effects with this regime. The results of this model give insight towards a synergistic methodology utilizing these modalities for use in diabetic therapies.

References:

1. Alessandra, G., Algerta, M., Paola, M., Carsten, S., Cristina, L., Paolo, M., Elisa, M., Gabriella, T. and Carla, P., 2020. Shaping Pancreatic β-Cell Differentiation and Functioning: The Influence of Mechanotransduction. *Cells*, 9(2), p.413.

2. Thrivikraman, G., Boda, S. and Basu, B., 2018. Unraveling the mechanistic effects of electric field stimulation towards directing stem cell fate and function: A tissue engineering perspective. *Biomaterials*, 150, pp.60-86.

3. de Freitas, L. and Hamblin, M., 2016. Proposed Mechanisms of Photobiomodulation or Low-Level Light Therapy. *IEEE Journal of Selected Topics in Quantum Electronics*, 22(3), pp.348-364.

4. Li, L. and Jiang, J., 2011. Stem cell niches and endogenous electric fields in tissue repair. *Frontiers of Medicine*, 5(1), pp.40-44.

5. Haltaufderhyde, K., Ozdeslik, R., Wicks, N., Najera, J. and Oancea, E., 2014. Opsin Expression in Human Epidermal Skin. *Photochemistry and Photobiology*, 91(1), pp.117-123.

6. Miller, J., Eldabe, S., Buchser, E., Johanek, L., Guan, Y. and Linderoth, B., 2016. Parameters of Spinal Cord Stimulation and Their Role in Electrical Charge Delivery: A Review. *Neuromodulation: Technology at the Neural Interface*, 19(4), pp.373-384.

7. Zein, R., Selting, W. and Hamblin, M., 2018. Review of light parameters and photobiomodulation efficacy: dive into complexity. *Journal of Biomedical Optics*, 23(12), p.1.

8. Chao, P., Lu, H., Hung, C., Nicoll, S. and Bulinski, J., 2007. Effects of Applied DC Electric Field on Ligament Fibroblast Migration and Wound Healing. *Connective Tissue Research*, 48(4), pp.188-197.

9. Amon, A. and Alesch, F., 2017. Systems for deep brain stimulation: review of technical features. *Journal of Neural Transmission*, 124(9), pp.1083-1091.

10. Mycielska, M. and Djamgoz, M., 2004. Cellular mechanisms of direct-current electric field effects: galvanotaxis and metastatic disease. *Journal of Cell Science*, 117(9), pp.1631-1639.

11. Radman, T., Su, Y., An, J., Parra, L. and Bikson, M., 2007. Spike Timing Amplifies the Effect of Electric Fields on Neurons: Implications for Endogenous Field Effects. *Journal of Neuroscience*, 27(11), pp.3030-3036.

12. Funk, R., 2015. Endogenous electric fields as guiding cue for cell migration. *Frontiers in Physiology*, 6.

13. Pall, M., 2013. Electromagnetic fields actviaactivation of voltage-gated calcium channels to produce beneficial or adverse effects. *Journal of Cellular and Molecular Medicine*, 17(8), pp.958-965.

14. Weaver, J. and Chizmadzhev, Y., 1996. Theory of electroporation: A review. *Bioelectrochemistry and Bioenergetics*, 41(2), pp.135-160.

15. Beebe, S., Blackmore, P., White, J., Joshi, R. and Schoenbach, K., 2004. Nanosecond pulsed electric fields modulate cell function through intracellular signal transduction mechanisms. *Physiological Measurement*, 25(4), pp.1077-1093.

16. Cho, M., Thatte, H., Lee, R. and Golan, D., 1994. Induced redistribution of cell surface receptors by alternating current electric fields. *The FASEB Journal*, 8(10), pp.771-776.

17. Schoenbach, K., Beebe, S. and Buescher, E., 2001. Intracellular effect of ultrashort electrical pulses. *Bioelectromagnetics*, 22(6), pp.440-448.

18. Hamblin, M., 2018. Mechanisms and Mitochondrial Redox Signaling in Photobiomodulation. *Photochemistry and Photobiology*, 94(2), pp.199-212.

19. Dittami, G., Rajguru, S., Lasher, R., Hitchcock, R. and Rabbitt, R., 2011. Intracellular calcium transients evoked by pulsed infrared radiation in neonatal cardiomyocytes. *The Journal of Physiology*, 589(6), pp.1295-1306.

20. R Hamblin, M., 2017. Mechanisms and applications of the anti-inflammatory effects of photobiomodulation. *AIMS Biophysics*, 4(3), pp.337-361.

21. Liebman, C., Vu, T., Phillips, A., Chen, B. and Cho, M., 2020. Altered β-Cell Calcium Dynamics via Electric Field Exposure. *Annals of Biomedical Engineering*.

22. Fridlyand, L., Tamarina, N. and Philipson, L., 2003. Modeling of Ca2+ flux in pancreatic β-cells: role of the plasma membrane and intracellular stores. *American Journal of Physiology-Endocrinology and Metabolism*, 285(1), pp.E138-E154.

23. Fridlyand, L. and Philipson, L., 2010. Glucose sensing in the pancreatic beta cell: a computational systems analysis. *Theoretical Biology and Medical Modelling*, 7(1).

24. Kang, H., Jo, J., Kim, H., Choi, M., Rhee, S. and Koh, D., 2005. Glucose metabolism and oscillatory behavior of pancreatic islets. *Physical Review E*, 72(5).

25. Rorsman, P. and Renström, E., 2003. Insulin granule dynamics in pancreatic beta cells. *Diabetologia*, 46(8), pp.1029-1045.

26. Poderoso, J., Carreras, M., Lisdero, C., Riobó, N., Schöpfer, F. and Boveris, A., 1996. Nitric Oxide Inhibits Electron Transfer and Increases Superoxide Radical Production in Rat Heart Mitochondria and Submitochondrial Particles. *Archives of Biochemistry and Biophysics*, 328(1), pp.85-92.

27. Pannala, V., Camara, A. and Dash, R., 2016. Modeling the detailed kinetics of mitochondrial cytochrome c oxidase: Catalytic mechanism and nitric oxide inhibition. *Journal of Applied Physiology*, 121(5), pp.1196-1207.

28. K.H. Schoenbachk, R., n.d. Ultrashort electrical pulses open a new gateway into biological cells. *Conference Record of the Twenty-Sixth International Power Modulator Symposium, 2004 and 2004 High-Voltage Workshop.*

29. Samways, D. and Egan, T., 2011. Calcium-dependent decrease in the single-channel conductance of TRPV1. *Pflügers Archiv - European Journal of Physiology*, 462(5), pp.681-691.

30. Song, P., Gao, H., Zhang, M., Yang, F., Li, S., Kang, B., Xu, J. and Chen, H., 2019. Transient microscopy for measuring heat transfer in single cells. *ArVix.org*, [online] Available at: <https://arxiv.org/abs/1901.00141> [Accessed 13 August 2020].

31. Moreau, D., Lefort, C., Pas, J., Bardet, S., Leveque, P. and O'Connor, R., 2017. Infrared neural stimulation induces intracellular Ca2+ release mediated by phospholipase C. *Journal of Biophotonics*, 11(2), p.e201700020.

32. Houreld, N., Masha, R. and Abrahamse, H., 2012. Low-intensity laser irradiation at 660 nm stimulates cytochrome c oxidase in stressed fibroblast cells. *Lasers in Surgery and Medicine*, 44(5), pp.429-434.

33. Mason, M., Nicholls, P. and Cooper, C., 2014. Re-evaluation of the near infrared spectra of mitochondrial cytochrome c oxidase: Implications for non invasive in vivo monitoring of tissues. *Biochimica et Biophysica Acta (BBA) - Bioenergetics*, 1837(11), pp.1882-1891.

34. Colsoul, B., Schraenen, A., Lemaire, K., Quintens, R., Van Lommel, L., Segal, A., Owsianik, G., Talavera, K., Voets, T., Margolskee, R., Kokrashvili, Z., Gilon, P., Nilius, B., Schuit, F. and Vennekens, R., 2010. Loss of high-frequency glucose-induced Ca2+ oscillations in pancreatic islets correlates with impaired glucose tolerance in Trpm5-/- mice. *Proceedings of the National Academy of Sciences*, 107(11), pp.5208-5213.

35. Yao, J., Liu, B. and Qin, F., 2009. Heat Activation of Temperature-Gated Ion channels Studied by Fast Temperature Jumps. *Biophysical Journal*, 96(3), p.267a.

36. Samways, D. and Egan, T., 2011. Calcium-dependent decrease in the single-channel conductance of TRPV1. *Pflügers Archiv - European Journal of Physiology*, 462(5), pp.681-691.

37. Poderoso, J., Carreras, M., Lisdero, C., Riobó, N., Schöpfer, F. and Boveris, A., 1996. Nitric Oxide Inhibits Electron Transfer and Increases Superoxide Radical Production in Rat Heart Mitochondria and Submitochondrial Particles. *Archives of Biochemistry and Biophysics*, 328(1), pp.85-92.

38. Thrivikraman, G., Boda, S. and Basu, B., 2018. Unraveling the mechanistic effects of electric field stimulation towards directing stem cell fate and function: A tissue engineering perspective. *Biomaterials*, 150, pp.60-86.

39. Mycielska, M. and Djamgoz, M., 2004. Cellular mechanisms of direct-current electric field effects: galvanotaxis and metastatic disease. *Journal of Cell Science*, 117(9), pp.1631-1639.

40. Radman, T., Su, Y., An, J., Parra, L. and Bikson, M., 2007. Spike Timing Amplifies the Effect of Electric Fields on Neurons: Implications for Endogenous Field Effects. *Journal of Neuroscience*, 27(11), pp.3030-3036.

41. Mogami, H., Gardner, J., Gerasimenko, O., Camello, P., Petersen, O. and Tepikin, A., 1999. Calcium binding capacity of the cytosol and endoplasmic reticulum of mouse pancreatic acinar cells. *The Journal of Physiology*, 518(2), pp.463-467.

42. Orrenius, S. and Nicotera, P., 1994. The calcium ion and cell death. *Neural Transm Suppl.*, 43, pp.1-11.

43. Morth, J., Pedersen, B., Buch-Pedersen, M., Andersen, J., Vilsen, B., Palmgren, M. and Nissen, P., 2010. A structural overview of the plasma membrane Na+,K+-ATPase and H+-ATPase ion pumps. *Nature Reviews Molecular Cell Biology*, 12(1), pp.60-70.

44. Zhang, F., Jara-Oseguera, A., Chang, T., Bae, C., Hanson, S. and Swartz, K., 2017. Heat activation is intrinsic to the pore domain of TRPV1. *Proceedings of the National Academy of Sciences*, 115(2), pp.E317-E324.

45. Ferrandiz-Huertas, C., Mathivanan, S., Wolf, C., Devesa, I. and Ferrer-Montiel, A., 2014. Trafficking of ThermoTRP Channels. *Membranes*, 4(3), pp.525-564.

46. Docherty, R., Yeats, J. and Piper, A., 1997. Capsazepine block of voltage-activated calcium channels in adult rat dorsal root ganglion neurones in culture. *British Journal of Pharmacology*, 121(7), pp.1461-1467.

47. Taylor-Clark, T., 2016. Role of reactive oxygen species and TRP channels in the cough reflex. *Cell Calcium*, 60(3), pp.155-162.

48. Dittami, G., Rajguru, S., Lasher, R., Hitchcock, R. and Rabbitt, R., 2011. Intracellular calcium transients evoked by pulsed infrared radiation in neonatal cardiomyocytes. *The Journal of Physiology*, 589(6), pp.1295-1306.

49. Yan, X., Liu, J., Zhang, Z., Li, W., Sun, S., Zhao, J., Dong, X., Qian, J. and Sun, H., 2016. Low-level laser irradiation modulates brain-derived neurotrophic factor mRNA transcription through calcium-dependent activation of the ERK/CREB pathway. *Lasers in Medical Science*, 32(1), pp.169-180.

50. Chen, J., Tao, R., Sun, H., Tse, H., Lau, C. and Li, G., 2009. Multiple Ca2+signaling pathways regulate intracellular Ca2+activity in human cardiac fibroblasts. *Journal of Cellular Physiology*.

51. Karu, T., 2014. Cellular and Molecular Mechanisms of Photobiomodulation (Low-Power Laser Therapy). *IEEE Journal of Selected Topics in Quantum Electronics*, 20(2), pp.143-148.

52. Whitticar, N. and Nunemaker, C., 2020. Reducing Glucokinase Activity to Enhance Insulin Secretion: A Counterintuitive Theory to Preserve Cellular Function and Glucose Homeostasis. *Frontiers in Endocrinology*, 11.

53. Guigas, B., Bertrand, L., Taleux, N., Foretz, M., Wiernsperger, N., Vertommen, D., Andreelli, F., Viollet, B. and Hue, L., 2006. 5-Aminoimidazole-4-Carboxamide-1- -D-Ribofuranoside and Metformin Inhibit Hepatic Glucose Phosphorylation by an AMP-Activated Protein Kinase-Independent Effect on Glucokinase Translocation. *Diabetes*, 55(4), pp.865-874.

54. German, M., 1993. Glucose sensing in pancreatic islet beta cells: the key role of glucokinase and the glycolytic intermediates. *Proceedings of the National Academy of Sciences*, 90(5), pp.1781-1785.

55. Rizzo, M. and Piston, D., 2003. Regulation of β cell glucokinase by S-nitrosylation and association with nitric oxide synthase. *Journal of Cell Biology*, 161(2), pp.243-248.

56. Markwardt, M., Seckinger, K. and Rizzo, M., 2015. Regulation of Glucokinase by Intracellular Calcium Levels in Pancreatic β Cells. *Journal of Biological Chemistry*, 291(6), pp.3000-3009.

57. Passarella, S. and Karu, T., 2014. Absorption of monochromatic and narrow band radiation in the visible and near IR by both mitochondrial and non-mitochondrial photoacceptors results in photobiomodulation. *Journal of Photochemistry and Photobiology B: Biology*, 140, pp.344-358.

58. Leloup, C., Tourrel-Cuzin, C., Magnan, C., Karaca, M., Castel, J., Carneiro, L., Colombani, A., Ktorza, A., Casteilla, L. and Penicaud, L., 2008. Mitochondrial Reactive Oxygen Species Are Obligatory Signals for Glucose-Induced Insulin Secretion. *Diabetes*, 58(3), pp.673-681.

59. Nurković, J., Zaletel, I., Nurković, S., Hajrović, Š., Mustafić, F., Isma, J., Škevin, A., Grbović, V., Filipović, M. and Dolićanin, Z., 2016. Combined effects of electromagnetic field and low-level laser increase proliferation and alter the morphology of human adipose tissue-derived mesenchymal stem cells. *Lasers in Medical Science*, 32(1), pp.151-160.

60. Proks, P., Reimann, F., Green, N., Gribble, F. and Ashcroft, F., 2002. Sulfonylurea Stimulation of Insulin Secretion. *Diabetes*, 51(Supplement 3), pp.S368-S376.

61. McColloch, A., Liebman, C., Liu, H. and Cho, M., 2020. Alterted Adipogenesis of Human Mesenchymal Stem Cells by Photobiomodulation Using 1064 nm Laser Light. *Lasers in Surgery and Medicine*.

CHAPTER 5:

CONCLUSIONS AND DISCUSSION

Therapeutic Electric Field Stimulation:

EFS has demonstrated its ability to affect cellular functionality along with more complex processes such as stem cell differentiation and cell migration.[1] While its therapeutic potential has been explored for many cell types, its effects on the insulin producing β-cell had not been well investigated. Our work herein demonstrated the capacity of EFS to affect both the calcium and insulin dynamics in β-cells which was dependent on field strength and cellular location within its respective cluster. This knowledge gives insight into how this type of stimulation could be used with islet transplantation procedures. Further work into the long term epigenetic and physiologic changes by this type of modality will further expand the potential of EFS in diabetes.

It was shown that by increasing EF strength, a greater rise in intracellular calcium could be achieved. Given that insulin secretion was significantly stimulated in the absence of extracellular glucose, it seems reasonable that the calcium influx was the dominate driver for its secretion. It was also shown that calcium influx was mediated by L-type VGCCs which is in accord other research groups.[2] Given its effects on depolarization events, it makes sense that EFS was able to increase calcium spiking activity and thus the likelihood of stimulating insulin secretion. It was also interesting that the level of relative calcium activity decreased at higher EF strengths. Since there is a limited ability of cells to sequester their intracellular calcium, it may be that the stronger EFs surpassed this capacity.[3]

A prolonged elevation of intracellular calcium brought about by these higher EFs could certainly have negative effects along with cell death, a phenomena known as calcium cytotoxicity.[4]

The elevation in calcium increases mitochondrial activity along with ROS. These mechanisms are part of the process that leads to the inhibition of BCL-2 and the release of cytochrome c, activating the apoptotic pathways leading to cellular death.[5] This type of cellular stress has also been implicated in β-cell dysfunction in T2D.[6] Thus we investigated the survival rate of these cells a day after EFS. It was shown that even our highest strength was still well tolerated by this cell type. Other groups have used even higher EF strengths and saw beneficial effects, but differences in EF application and cell type would certainly change the capacity of these cells to tolerate this stimulation.[7]

As previously stated, the effects of the EFS appear to depend on the position of each cell within its cluster. This has even greater implications with respect to islet clusters as they are commonly larger (100 – 200 μm) than the clusters imaged here.[8] β-cells contain various types of gap junctions that allow depolarization events and calcium exchange to take place between neighboring cells.[9] This type of interaction has been observed in mature islets as calcium waves propagating throughout the islet.[10] Managing these cellular interactions, it was discovered that a specific sub-population of β-cells act as pacemaker cells appearing to coordinate calcium dynamics between islet cells.[11] While this type of DC-EFS will mostly affect the outer shell cells due to the electrical shielding, the signals could still be transduced to the interior of the islet via these specific gap junctions and thus affect the entire islet's physiologic functionality.

While the short term effects of EFS include the induction of insulin secretion along with an increase in intracellular calcium dynamics, the longer term effects of EFS on β-cells has not yet been investigated. However, a large body of work exists demonstrating the capacity of EFS to improve the long term efficacy of various therapeutic methods.[12] With respect to regenerative medicine, EFS has demonstrated its capacity to affect stem cell differentiation,[13] along with

affecting early fate determination in embryonic stem cells.[14] This makes since given that endogenous electric fields have been associated with the limb formation and cell localization via migration.[15] Multiple types of EFS have shown longer term effects in the form of increased proliferation and cell survival.[16] This could prove useful for expanding adult stem cells or other extracted cell types prior to implantation. These effects likely result from the coupling between EFs and intracellular signaling affecting transcription factor activity.[17] In addition, EFs have been shown to stimulate the secretion of various hormones and neurotransmitters which may play a large role in the effects at a tissue level.[18,19]

Aside from the increased activity of various calcium dependent proteins, prolonged EF exposure is able to migrate and sensitize various charged surface receptors.[20] The migration of these receptors may play a role in the differences in direction during galvanotaxis between cell types, as some migrate towards the cathode while others to the anode.[21] Additionally, the migration of ion channels during prolonged EFS could further alter the electrophysiology of the cell for prolonged periods of time.[22]

Therapeutic Photobiomodulation:

PBM originally called low level laser therapy (LLLT), has been used for decades for various applications. While it has been shown to have therapeutic benefits, the lack of knowledge about its cellular mechanisms along with a large variation in parameters has limited its therapeutic use.[23] Recently, much of the work by the Hamblin group has spurred the investigation of the cellular mechanisms of this type of physical stimulus.[24] Our work focused on how β-cells might be affected by PBM along with its potential mechanisms. It was found that PBM can significantly enhance the calcium spiking frequency for at least 15 minutes past the exposure event, along with

an increase in ROS and NO. It appeared that ROS may play a strong role in the calcium dynamics, as the redox state affects many types of calcium channels.[25] This was further demonstrated when the addition of ascorbic acid reduced both ROS and calcium spiking frequency. As with the EFS, PBM could instigate insulin secretion, but appeared to have a lower effect with a potential dependency on glucose concentration given its metabolic mechanisms.

Much of the work by Hamblin implicated the effects of light on cytochrome c oxidase and calcium influx via TRPV channels.[26] Through these and other mechanisms, PBM has been shown to provide beneficial effects such as reduced inflammation, improved would healing, along with improved cellular proliferation and cell survival. These effects are likely mediated by the fact that PBM has been shown to down regulate the expression of various inflammatory proteins such as TNF-α, IL-1β, and IL-8.[27] In juxtaposition, PBM has been shown to increase the expression of BLC-2 and Cyclin Ds, thereby improving cell survivability and proliferation.[28] Improved antioxidant capacity has also been shown through PBM via increases in SOD2 and other antioxidant enzymes.[29] Through this, PBM has also been shown to significantly affect fate determination in mesenchymal stem cell differentiation.[30]

By the inhibition of calcium spiking by Capsazepine in our work along with Hamblin's work demonstrating an inhibition in calcium influx, it would appear that TRPVs are part of the mechanisms by which PBM affects the calcium dynamics.[26] How these TRPVs are activated would need to be further elucidated, as it has been theorized that structured water heating could induce their opening.[24] Yet the heat loss to the local environment would be rapid and likely not remain elevated beyond the bulk media temperature out to 15 minutes. Measurements of bulk temperature immediately following the 1 minute 150 mW/cm^2 exposure to 810 nm light was only elevated on average by 0.08 °C. Thus other PBM mechanisms must be in play.

Another potential PBM mechanism that might potentially offer an alternate explanation is the involvement of intracellular calcium release. While we demonstrated that extracellular calcium was required for the changes in calcium dynamics by PBM, other groups demonstrated that high intensity near-infrared laser could induce the release of endoplasmic calcium.[31] Thus we used the inhibitors Dantrolene and 2-APB to inhibit Ryanodine- and IP3- receptors, respectively. While the 2-ABP concentration we used (10 μM) was consistent with what was reported in literature, it should be noted that 2-APB at low concentrations (< 20 μM) can activate store operated calcium entry (SOCE) and inhibit the same entry pathway at higher concentrations.[32] Furthermore, 2-APB has also been shown to inhibit most TRP channels and yet activate the subgroup of TRPV channels depending on the concentration used.[33] These observations indicate that the effects of 2-APB are rather complex and may activate or inhibit multiple entry calcium entries in addition to the IP3-receptor pathway. Use of knockout model should further illuminate the role of various intracellular calcium pathways that respond to PBM.

The current model predicts that NO becomes dissociated from CCO following its absorption of PBM's photons.[34] Given that NO acts as an inhibitor of cellular respiration, this dissociation would result in an increased ETC flux, thus a greater amount of ATP and ROS.[35] The elevation in cytosolic ROS has been shown to increase many ion channel's activity and open fractions.[36] Mitochondrial ROS has also been shown to be an important mediator for insulin secretion, as it signals an increase in the metabolic state of the cell.[37] In particular, NO has been shown to affect a wide array of cellular processes and is well known to play a critical role in blood pressure dynamics.[38] In β-cells, the enzyme glucokinase acts as the rate limiting factor in glucose consumption and thus the sensor for the insulin secretion response. Interestingly, its activity has

been shown to increase in the presence of elevated cytosolic NO concentrations.[39] Given the number of proteins that could act as a chromophore, it seems reasonable that many cellular pathways could be either directly or indirectly affected by PBM exposure.

Cellular Responses to Calcium and ROS:

Calcium dynamics play a critical role in a plethora of cellular processes by acting as a ubiquitous secondary messenger.[40] As for the calcium dynamics in β-cells, it plays a primary role in insulin secretion, but various other calcium dependent enzymes can also be activated leading to alterations in the transcription factor regulation.[41] The rise in intracellular calcium activates Calcineurin leading to the activation and translocation of the cytosolic nuclear factor of activated T-cells (NFAT) into the nucleus.[42] In β-cells, this increased activity of NFAT in the nucleus can upregulate many of the functional genes associated with β-cell functionality (e.g. PDX1, INS, and GLUT2) along with an increase in cell proliferation via the upregulation of Cyclins.[43] Thus when β-cells are induced to secrete insulin via elevated calcium dynamics alongside metabolic inputs, NFAT and mitogen activated protein kinases (MAPKs) can upregulate insulin promoter genes leading to an increase in insulin production in the preparation of future stimulation of insulin secretion.[44] Given this, the increase in calcium dynamics brought about by either EFS or PBM could alter the expression of these genes providing therapeutic benefits.

A successful drug in T2 diabetes has been the GLP-1 receptor agonist Dulaglutide that can sensitize β-cells and improve their insulin secretion capacity.[45] It has been shown that NFAT is one of the functional pathways that the growth factor glucagon like peptide (GLP-1) improves β-cell functionality.[46] While intracellular calcium dynamics can activate NFAT and other transcription factors, an old question has always remained on how the cell interpret these calcium

spiking events. Without the ability to directly control these calcium spiking events, it has been difficult to determine if the frequency, amplitude, or duration were more important in the cellular response.[47] Recently, an optogenetic study involving the calcium dynamics effects on NFAT concluded that the dominant parameter appeared to be the duty cycle of calcium spikes rather than their frequency or amplitude.[48]

Through the activation of calmodulins (CaMs) and calcium dependent protein kinases (CDPKs), calcium is able to affect a large number of intracellular processes.[49] Particular to β-cells, the CaM dependent kinase IV has been shown to increase cAMP response element-binding protein (CREB) activity resulting in an amplification of proliferation and survival signals mediated by insulin receptor substrate 2's (IRS-2) interaction with insulin like growth factor receptors (IGFs).[50] Since intracellular calcium modulates several pathways shared by receptors such as IGF-1, a fertile area of research related to this work, is the combined effects of calcium modulation by EFS and/or PBM with biological agonists such as the previously mentioned GLP-1. Thus it may be possible that there are synergistic interaction between therapeutic biologics and the physical modalities of EFS and PBM.

A critical link between cytosolic calcium and ROS is the mitochondria. As cytosolic calcium increases, the mitochondria uptake some of this calcium via the mitochondrial uniporter (MCU-1).[51] The mitochondria has its own electrophysiology containing a large array of ion channels to maintain the mitochondrial membrane potential (MMP). Elevations in mitochondrial calcium stimulates the enzymes involved in ETC flux resulting in an increase in ATP and mitochondrial ROS.[52] Thus, there is a strong interplay between ROS and calcium with respect to the mitochondria. As previously stated, ROS can modulate a large number of calcium channels including IP3- and Ryanodine- receptors alongside many of the TRP channel family.[36] Thus a

complex system emerges, were the calcium dynamics resulting from these interactions can further affect the production or ROS within the cell, thus requiring tight regulation to prevent various forms of pathology.[53]

Simulations and Potential Mechanisms:

Utilizing several previously developed numerical models of β-cell physiology, we incorporated them together with models for EFS and PBM in order to elucidate the potential effect, mechanisms, and optimal doses of these physical modalities. The results of the simulations followed a similar pattern to the collected data save a few particular instances. As for EFS, the intracellular calcium rose with EF strength as it did with the experimental results. The calcium spiking, was similar to the results, but with different peak dosage. As the EFS may increase the calcium driving force, the cell must rectify these spikes by removing calcium from the cytosol.[54] At increased spiking rates, the increased frequency of depolarization likely allows for more calcium spiking events to occur. In addition, stronger EFs increased the amplitude and duration of each spike which would result in a delay between each spike as the cell must remove the intracellular calcium. This delay may overtake the increase in depolarization spike timing and thus start to slow down the spiking frequency. Running the simulation at much higher EF strengths resulted in a massive increase in calcium with a loss of spiking. This is likely due to the driving force of calcium influx superseding the ability of the cell to remove or sequester the calcium.

A benefit of the model produced is its ability to predict the effects on calcium from some of the potential PBM mechanisms. For instance, the effect of TRPV1 activation could significantly increase intracellular calcium if the open fraction was significantly increased; however, bulk thermal predictions precluded this from being a possibility. While the proposed PBM mechanisms

theorize structured water heating, it is unlikely that this heating would persist once the exposure event concluded. The results of these mechanistic studies in the model indicated that the predicted increase in CCO activity, is the most likely mechanism. However, it alone did not account for the increase in calcium spiking frequency seen in the experiments. Thus we hypothesized that the increase in cytosolic NO could increase the activity of glucokinase, thereby affecting the calcium dynamics in this cell type.[36]

Another benefit of developing this model is its ability to predict optimal EFS and PBM parameters given a desired calcium or insulin response. Given that active calcium dynamics along with the stimulation of insulin secretion can benefit the functionality of β-cells, one would likely want the greatest release of insulin and calcium influx. Yet as previously stated, excessive calcium influx can lead to dysfunction or cellular death and insulin secretion has a maximum rate dependent on the primed content of the readily releasable pool.[55] Additionally, the model demonstrated that the extracellular glucose concentration is an important factor in the response, and thus optimal dosages would likely depend on the context of the glucose load.

One deficiency of this model is that it does not account for the insulin dynamic modulations brought about by the metabolic changes due to PBM. While transient elevations of ROS by PBM have been shown to improve cellular antioxidant capacity by increasing the expression of SOD2, too great of an increase in transient ROS could lead to cellular death or DNA damage.[56] The simulation predicts an optimal window of PBM between 10 – 20 J/cm^2, while other reports have indicated that 10 J/cm^2 may be an upper limit before negative effects become apparent.[57] A recent report by Hamblin attempted to determine optimal parameters based on a large collection of previous reports, with a similar conclusion. He additionally indicated that the cell's phenotype and mitochondrial count likely play a significant role in the optimal response range.[58] As for the EFS

parameters, it would seem reasonable to maintain the range of DCEF within the physiologic range of 1 – 5 V/cm.[59]

Islet Transplantation and Future Prospects:

Islet transplantation is a surgical procedure that involves gathering isolated cadaveric islets and implanting them into the hepatic portal vein of the T1D patient. Early methods lacked efficacy and thus resulted in the loss of insulin independence within the first year. Steady improvements to the transplantation such as the Edmonton protocol, improved the results of the procedure. Despite these improvements, it is still considered an experimental procedure.[60] Major challenges include cell sourcing, cell survival, and maintaining cellular functionality.[61] Given the large size diversity of islets, the islet equivalent (IEQ) is used as a dosing parameter with an assumed average 150 μm of the islets. Unfortunately, the requirement of multiple donors for one patient worth of IEQ has not been uncommon.[62] A major reason for high IEQ dosages is that a large portion of islet cells will die following transplantation due to cellular stress, inflammation, and lack of oxygenation.[63] Thus any procedures to increase cell count or prevent cellular death would ameliorate this issue.

To this end, both PBM and EFS have demonstrated the ability to protect cells from apoptosis and induce cell proliferation.[64,16] EFS likely exerts its effects predominantly through its effects on calcium dynamics, while PBM likely affects the metabolic state of the cell more than its effects on calcium dynamics. Following the extraction form the cadaveric donors, the islets are kept *in vitro* for purification and quality assessment, but the ex vivo conditions lower the efficacy of the treatment and thus should not be more than several days depending on the methods employed.[65] The loss of functionality by these explanted islets is likely caused by the disruption

to the extracellular matrix, as it has been shown to be critically important for preserving islet functionality.[66]

As for post-transplantation, the majority of cellular loss has been attributed to apoptosis due to inflammation and hypoxia. Interestingly, experiments involving mild heating and electrical stimulation on MIN6 β-cells with *in vivo* experiments demonstrated a significant improvement with cell survival following 6-hour treatment with TNF-α, along with the upregulation of heat shock protein 72 (HSP72) and β-cell critical genes PDX1, GLUT2, and IRS-2.[67] Pre-transplant photobiomodulation using 810 nm light has also been shown to improve the antioxidant capacity of HEI-O1C auditory cells and protect them from inflammatory apoptosis.[68] In addition to the therapeutic potential for islet transplantation, both EFS and PBM are either non- or minimally-invasive modalities that could also be used to treat T2D.

Final Remarks:

The research performed herein, demonstrated the ability for both EFS and PBM to modulate the intracellular calcium dynamics of the β-cell phenotype and induce insulin secretion. EFS had strong potential in inducing calcium influx with the capacity to instigate insulin secretion even in the absence of extracellular glucose. PBM was also shown to affect intracellular calcium dynamics via different mechanisms, likely via changes with the metabolic state of the mitochondria. Further, the mechanisms by which PBM exerts its effects on calcium spiking frequency were investigated via multiple pharmacologic blocking experiments. To further explore the effects of EFS and PBM, an integrated model involving β-cell electrophysiology, mitochondrial metabolism, and insulin secretion into a single numerical simulation. Using this, the effects on intracellular calcium, calcium spiking, and insulin secretion by varied EF strengths and

potential mechanisms of PBM were investigated. This resulted in a novel PBM model that hypothesized the involvement of another potential target of PBM, which needs to be explored in future work.

While this research is illuminating on how EFS and PBM affect the β-cell physiology, there are several limitations to this work. Firstly, the insulinoma cell line used throughout this work has a lower glucose threshold for insulin secretion than that of *in vivo* β-cells. In addition, the fact that they are insulinomas implies a pathological increase in insulin production and secretion. There are also well known differences between mouse and human β-cells and their responses to glucose. While the integrated model derived from the Fridlyand lab predicted its effects with normal physiologic parameters, they also validated their work via an earlier insulinoma cell line, βTC-3.

Despite the potential differences between these cells and those extracted from donors, the results from this work, along with the results from previous reports, indicate that the effects of EFS and PBM could be used to improve the survivability, proliferation, and functionality of β-cell before islet implantation. While the scope of this work was limited to the short term effects and biophysical mechanisms of these physical stimuli, work should be continued to demonstrate the long term benefits from these stimulatory methods. Following this, further work involving *in vivo* experimentation on the pre-treatment of islet transplants would be warranted. Overall, both EFS and PBM have the potential to give bioengineering control over β-cell calcium dynamics and lead to various modes of diabetic therapies.

References:

1. Love, M., Palee, S., Chattipakorn, S. and Chattipakorn, N., 2017. Effects of electrical stimulation on cell proliferation and apoptosis. *Journal of Cellular Physiology*, 233(3), pp.1860-1876.

2. Pall, M., 2013. Electromagnetic fields actviaactivation of voltage-gated calcium channels to produce beneficial or adverse effects. *Journal of Cellular and Molecular Medicine*, 17(8), pp.958-965.

3. Berridge, M., Bootman, M. and Roderick, H., 2003. Calcium signalling: dynamics, homeostasis and remodelling. *Nature Reviews Molecular Cell Biology*, 4(7), pp.517-529.

4. Nicotera, P., Bellomo, G. and Orrenius, S., 1992. Calcium-Mediated Mechanisms in Chemically Induced Cell Death. *Annual Review of Pharmacology and Toxicology*, 32(1), pp.449-470.

5. Polster, B. and Fiskum, G., 2004. Mitochondrial mechanisms of neural cell apoptosis. *Journal of Neurochemistry*, 90(6), pp.1281-1289.

6. Ramadan, J., Steiner, S., O'Neill, C. and Nunemaker, C., 2011. The central role of calcium in the effects of cytokines on beta-cell function: Implications for type 1 and type 2 diabetes. *Cell Calcium*, 50(6), pp.481-490.

7. Kloth, L., 2005. Electrical Stimulation for Wound Healing: A Review of Evidence From In Vitro Studies, Animal Experiments, and Clinical Trials. *The International Journal of Lower Extremity Wounds*, 4(1), pp.23-44.

8. Wang, Y., Paushter, D., Wang, S., Barbaro, B., Harvat, T., Danielson, K., Kinzer, K., Zhang, L., Qi, M. and Oberholzer, J., 2011. Highly Purified versus Filtered Crude Collagenase: Comparable Human Islet Isolation Outcomes. *Cell Transplantation*, 20(11-12), pp.1817-1825.

9. Farnsworth, N. and Benninger, R., 2014. New insights into the role of connexins in pancreatic islet function and diabetes. *FEBS Letters*, 588(8), pp.1278-1287.

10. Benninger, R., Zhang, M., Head, W., Satin, L. and Piston, D., 2008. Gap Junction Coupling and Calcium Waves in the Pancreatic Islet. *Biophysical Journal*, 95(11), pp.5048-5061.

11. Johnston, N., Mitchell, R., Haythorne, E., Pessoa, M., Semplici, F., Ferrer, J., Piemonti, L., Marchetti, P., Bugliani, M., Bosco, D., Berishvili, E., Duncanson, P., Watkinson, M., Broichhagen, J., Trauner, D., Rutter, G. and Hodson, D., 2016. Beta Cell Hubs Dictate Pancreatic Islet Responses to Glucose. *Cell Metabolism*, 24(3), pp.389-401.

12. McCaig, C., Rajnicek, A., Song, B. and Zhao, M., 2005. Controlling Cell Behavior Electrically: Current Views and Future Potential. *Physiological Reviews*, 85(3), pp.943-978.

13. Titushkin, I. and Cho, M., 2009. Controlling cellular biomechanics of human mesenchymal stem cells. *2009 Annual International Conference of the IEEE Engineering in Medicine and Biology Society*.

14. Yamada, M., Tanemura, K., Okada, S., Iwanami, A., Nakamura, M., Mizuno, H., Ozawa, M., Ohyama-Goto, R., Kitamura, N., Kawano, M., Tan-Takeuchi, K., Ohtsuka, C., Miyawaki, A., Takashima, A., Ogawa, M., Toyama, Y., Okano, H. and Kondo, T., 2006. Electrical Stimulation Modulates Fate Determination of Differentiating Embryonic Stem Cells. *STEM CELLS*, 25(3), pp.562-570.

15. Hopyan, S., 2017. Biophysical regulation of early limb bud morphogenesis. *Developmental Biology*, 429(2), pp.429-433.

16. Love, M., Palee, S., Chattipakorn, S. and Chattipakorn, N., 2017. Effects of electrical stimulation on cell proliferation and apoptosis. *Journal of Cellular Physiology*, 233(3), pp.1860-1876.

17. Tong, J., Sun, L., Zhu, B., Fan, Y., Ma, X., Yu, L. and Zhang, J., 2017. Pulsed electromagnetic fields promote the proliferation and differentiation of osteoblasts by reinforcing intracellular calcium transients. *Bioelectromagnetics*, 38(7), pp.541-549.

18. Liebano, R. and Machado, A., 2014. Vascular Endothelial Growth Factor Release Following Electrical Stimulation in Human Subjects. *Advances in Wound Care*, 3(2), pp.98-103.

19. Lee, K., Chang, S., Roberts, D. and Kim, U., 2004. Neurotransmitter release from high-frequency stimulation of the subthalamic nucleus. *Journal of Neurosurgery*, 101(3), pp.511-517.

20. Cho, M., Thatte, H., Lee, R. and Golan, D., 1994. Induced redistribution of cell surface receptors by alternating current electric fields. *The FASEB Journal*, 8(10), pp.771-776.

21. Allen, G., Mogilner, A. and Theriot, J., 2013. Electrophoresis of Cellular Membrane Components Creates the Directional Cue Guiding Keratocyte Galvanotaxis. *Current Biology*, 23(7), pp.560-568.

22. Kindzelskii, A. and Petty, H., 2005. Ion channel clustering enhances weak electric field detection by neutrophils: apparent roles of SKF96365-sensitive cation channels and myeloperoxidase trafficking in cellular responses. *European Biophysics Journal*, 35(1), pp.1-26.

23. Hamblin, M., 2016. Photobiomodulation or low-level laser therapy. *Journal of Biophotonics*, 9(11-12), pp.1122-1124.

24. De Freitas, L. and Hamblin, M., 2016. Proposed Mechanisms of Photobiomodulation or Low-Level Light Therapy. *IEEE Journal of Selected Topics in Quantum Electronics*, 22(3), pp.348-364.

25. Görlach, A., Bertram, K., Hudecova, S. and Krizanova, O., 2015. Calcium and ROS: A mutual interplay. *Redox Biology*, 6, pp.260-271.

26. Wang, Y., Huang, Y., Wang, Y., Lyu, P. and Hamblin, M., 2016. Photobiomodulation (blue and green light) encourages osteoblastic-differentiation of human adipose-derived stem cells: role of intracellular calcium and light-gated ion channels. *Scientific Reports*, 6(1).

27. R Hamblin, M., 2017. Mechanisms and applications of the anti-inflammatory effects of photobiomodulation. *AIMS Biophysics*, 4(3), pp.337-361.

28. Ahrabi, B., Rezaei Tavirani, M., Khoramgah, M., Noroozian, M., Darabi, S., Khoshsirat, S. and Abbaszadeh, H., 2019. The Effect of Photobiomodulation Therapy on the Differentiation, Proliferation, and Migration of the Mesenchymal Stem Cell: A Review. *Journal of Lasers in Medical Sciences*, 10(5), pp.S96-S103.

29. Li, F., Liu, Y., Qin, F., Luo, Q., Yang, H., Zhang, Q. and Liu, T., 2014. Photobiomodulation on Bax and Bcl-2 Proteins and SIRT1/PGC-1αAxis mRNA Expression Levels of Aging Rat Skeletal Muscle. *International Journal of Photoenergy*, 2014, pp.1-8.

30. McColloch, A., Liebman, C., Liu, H. and Cho, M., 2020. Alterted Adipogenesis of Human Mesenchymal Stem Cells by Photobiomodulation Using 1064 nm Laser Light. *Lasers in Surgery and Medicine*.

31. Dittami, G., Rajguru, S., Lasher, R., Hitchcock, R. and Rabbitt, R., 2011. Intracellular calcium transients evoked by pulsed infrared radiation in neonatal cardiomyocytes. *The Journal of Physiology*, 589(6), pp.1295-1306.

32. Putney, J., 2010. Pharmacology of Store-operated Calcium Channels. Molecular Interventions, 10(4), pp.209-218.

33. Colton, C. and Zhu, M., n.d. 2-Aminoethoxydiphenyl Borate as a Common Activator of TRPV1, TRPV2, and TRPV3 Channels. Transient Receptor Potential (TRP) Channels, pp.173-187.

34. Hamblin, M., 2018. Mechanisms and Mitochondrial Redox Signaling in Photobiomodulation. *Photochemistry and Photobiology*, 94(2), pp.199-212.

35. Sarti, P., Forte, E., Giuffrè, A., Mastronicola, D., Magnifico, M. and Arese, M., 2012. The Chemical Interplay between Nitric Oxide and Mitochondrial CytochromecOxidase: Reactions, Effectors and Pathophysiology. *International Journal of Cell Biology*, 2012, pp.1-11.

36. Song, M., Makino, A. and Yuan, J., 2011. Role of Reactive Oxygen Species and Redox in Regulating the Function of Transient Receptor Potential Channels. *Antioxidants & Redox Signaling*, 15(6), pp.1549-1565.

37. Leloup, C., Tourrel-Cuzin, C., Magnan, C., Karaca, M., Castel, J., Carneiro, L., Colombani, A., Ktorza, A., Casteilla, L. and Penicaud, L., 2008. Mitochondrial Reactive Oxygen Species Are Obligatory Signals for Glucose-Induced Insulin Secretion. *Diabetes*, 58(3), pp.673-681.

38. Chen, K., Pittman, R. and Popel, A., 2008. Nitric Oxide in the Vasculature: Where Does It Come From and Where Does It Go? A Quantitative Perspective. *Antioxidants & Redox Signaling*, 10(7), pp.1185-1198.

39. Seckinger, K., Rao, V., Snell, N., Mancini, A., Markwardt, M. and Rizzo, M., 2018. Nitric Oxide Activates β-Cell Glucokinase by Promoting Formation of the "Glucose-Activated" State. *Biochemistry*, 57(34), pp.5136-5144.

40. Giorgi, C., Danese, A., Missiroli, S., Patergnani, S. and Pinton, P., 2018. Calcium Dynamics as a Machine for Decoding Signals. *Trends in Cell Biology*, 28(4), pp.258-273.

41. Sabatini, P., Speckmann, T. and Lynn, F., 2019. Friend and foe: β-cell Ca2+ signaling and the development of diabetes. *Molecular Metabolism*, 21, pp.1-12.

42. Hogan, P., 2003. Transcriptional regulation by calcium, calcineurin, and NFAT. *Genes & Development*, 17(18), pp.2205-2232.

43. Heit, J., Apelqvist, Å., Gu, X., Winslow, M., Neilson, J., Crabtree, G. and Kim, S., 2006. Calcineurin/NFAT signalling regulates pancreatic β-cell growth and function. *Nature*, 443(7109), pp.345-349.

44. Lawrence, M., Borenstein-Auerbach, N., McGlynn, K., Kunnathodi, F., Shahbazov, R., Syed, I., Kanak, M., Takita, M., Levy, M. and Naziruddin, B., 2015. NFAT Targets Signaling Molecules to Gene Promoters in Pancreatic β-Cells. *Molecular Endocrinology*, 29(2), pp.274-288.

45. Mathieu, C., Del Prato, S., Botros, F., Thieu, V., Pavo, I., Jia, N., Haupt, A., Karanikas, C. and García-Pérez, L., 2018. Effect of once weekly dulaglutide by baseline beta-cell function in people with type 2 diabetes in the AWARD programme. *Diabetes, Obesity and Metabolism*, 20(8), pp.2023-2028.

46. Lawrence, M., Bhatt, H. and Easom, R., 2002. NFAT Regulates Insulin Gene Promoter Activity in Response to Synergistic Pathways Induced by Glucose and Glucagon-Like Peptide-1. *Diabetes*, 51(3), pp.691-698.

47. Smedler, E. and Uhlén, P., 2014. Frequency decoding of calcium oscillations. *Biochimica et Biophysica Acta (BBA) - General Subjects*, 1840(3), pp.964-969.

48. Hannanta-anan, P. and Chow, B., 2016. Optogenetic Control of Calcium Oscillation Waveform Defines NFAT as an Integrator of Calcium Load. *Cell Systems*, 2(4), pp.283-288.

49. Kahl, C. and Means, A., 2003. Regulation of Cell Cycle Progression by Calcium/Calmodulin-Dependent Pathways. *Endocrine Reviews*, 24(6), pp.719-736.
50. Liu, B., Barbosa-Sampaio, H., Jones, P., Persaud, S. and Muller, D., 2012. The CaMK4/CREB/IRS-2 Cascade Stimulates Proliferation and Inhibits Apoptosis of β-Cells. *PLoS ONE*, 7(9), p.e45711.

51. Raffaello, A., De Stefani, D. and Rizzuto, R., 2012. The mitochondrial Ca2+ uniporter. *Cell Calcium*, 52(1), pp.16-21.

52. Camello-Almaraz, C., Gomez-Pinilla, P., Pozo, M. and Camello, P., 2006. Mitochondrial reactive oxygen species and Ca2+ signaling. *American Journal of Physiology-Cell Physiology*, 291(5), pp.C1082-C1088.

53. Brookes, P., Yoon, Y., Robotham, J., Anders, M. and Sheu, S., 2004. Calcium, ATP, and ROS: a mitochondrial love-hate triangle. *American Journal of Physiology-Cell Physiology*, 287(4), pp.C817-C833.

54. Balke, C., Egan, T. and Wier, W., 1994. Processes that remove calcium from the cytoplasm during excitation-contraction coupling in intact rat heart cells. *The Journal of Physiology*, 474(3), pp.447-462.

55. Rorsman, P. and Renström, E., 2003. Insulin granule dynamics in pancreatic beta cells. *Diabetologia*, 46(8), pp.1029-1045.

56. Bardaweel, S., Gul, M., Alzweiri, M., Ishaqat, A., ALSalamat, H. and Bashatwah, R., 2018. Reactive Oxygen Species: the Dual Role in Physiological and Pathological Conditions of the Human Body. *The Eurasian Journal of Medicine*, 50(3), pp.193-201.

57. Yu, W., Chi, L., Naim, J. and Lanzafame, R., 1997. Improvement of host response to sepsis by photobiomodulation. *Lasers in Surgery and Medicine*, 21(3), pp.262-268.

58. Zein, R., Selting, W. and Hamblin, M., 2018. Review of light parameters and photobiomodulation efficacy: dive into complexity. *Journal of Biomedical Optics*, 23(12), p.1.

59. Funk, R. Endogenous electric fields as guiding cue for cell migration. Front. Physiol. 2015. https://doi.org/10.3389/fphys.2015.00143/full.

60. Shapiro, A., Pokrywczynska, M. and Ricordi, C., 2016. Clinical pancreatic islet transplantation. *Nature Reviews Endocrinology*, 13(5), pp.268-277.

61. Rickels, M. and Robertson, R., 2018. Pancreatic Islet Transplantation in Humans: Recent Progress and Future Directions. *Endocrine Reviews*, 40(2), pp.631-668.

62. Al-Adra, D., Gill, R., Imes, S., O'Gorman, D., Kin, T., Axford, S., Shi, X., Senior, P. and Shapiro, A., 2014. Single-Donor Islet Transplantation and Long-term Insulin

Independence in Select Patients With Type 1 Diabetes Mellitus. *Transplantation*, 98(9), pp.1007-1012.

63. Gamble, A., Pepper, A., Bruni, A. and Shapiro, A., 2018. The journey of islet cell transplantation and future development. *Islets*, 10(2), pp.80-94.

64. Liang, J., Liu, L. and Xing, D., 2012. Photobiomodulation by low-power laser irradiation attenuates Aβ-induced cell apoptosis through the Akt/GSK3β/β-catenin pathway. *Free Radical Biology and Medicine*, 53(7), pp.1459-1467.

65. Daoud, J., Rosenberg, L. and Tabrizian, M., 2010. Pancreatic Islet Culture and Preservation Strategies: Advances, Challenges, and Future Outlook. *Cell Transplantation*, 19(12), pp.1523-1535.

66. Daoud, J., Petropavlovskaia, M., Rosenberg, L. and Tabrizian, M., 2010. The effect of extracellular matrix components on the preservation of human islet function in vitro. *Biomaterials*, 31(7), pp.1676-1682.

67. Kondo, T., Sasaki, K., Matsuyama, R., Morino-Koga, S., Adachi, H., Suico, M., Kawashima, J., Motoshima, H., Furukawa, N., Kai, H. and Araki, E., 2012. Hyperthermia With Mild Electrical Stimulation Protects Pancreatic β-Cells From Cell Stresses and Apoptosis. *Diabetes*, 61(4), pp.838-847.

68. Bartos, A., Grondin, Y., Bortoni, M., Ghelfi, E., Sepulveda, R., Carroll, J. and Rogers, R., 2016. Pre-conditioning with near infrared photobiomodulation reduces inflammatory cytokines and markers of oxidative stress in cochlear hair cells. *Journal of Biophotonics*, 9(11-12), pp.1125-1135.

APPENDIX

Simulation Flow Chart:

All values used the following untis: Time (ms), Concentration (μM), Volume (pL), Potential (mV), Current (fA), Capacitance (fF), and Conductance (pS). All simulations were performed on a Dell Latitude E7470 with an Intel i7-6600 with 8 GB of DDR4 RAM using MATLAB Version: 9.2.0.556344 (R2017a). Each run of the full model was timed at 5.17088 (s), the thermal model being 0.013769 (s), and the frequency count code taking 0.005511 (s). Each plot run for the standard parameters would include approximately 441 simulation runs under different parameters, thus taking approximately 38 minutes.

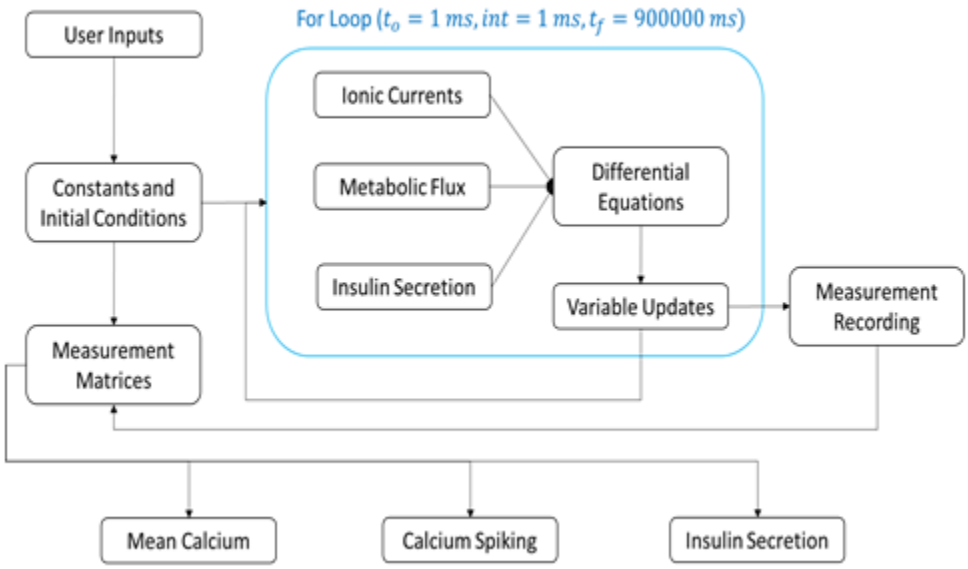

Figure A-1: Flowchart for simulations, with user inputs and constants fed into a for loop solving for ionic currents, metabolic fluxes, and insulin secretion. These values are then fed into the differential equations and followed by the variables being updated. Measurements are taken at each time point and used to determine the output results.

Electrophysiology Model:

All of the following equations and parameters in this section were from:

Fridlyand, L., Tamarina, N. and Philipson, L., 2003. Modeling of Ca2+ flux in pancreatic β-cells: role of the plasma membrane and intracellular stores. *American Journal of Physiology-Endocrinology and Metabolism*, 285(1), pp.E138-E154

Ion Flux Equations:

The Nernst potential equations for ions were derived from the following equation:

$$V_{ion} = \frac{RT}{z_{ion}F} \ln \frac{[ion]_{outside}}{[ion]_{inside}}$$

Where V_{ion} is the Nernst potential for a particular ion (i.e. Ca^{2+}, Na^{+}, K^{+}), R is the universal gas constant, T is the temperature, z is the charge for the particular ion, F is Faraday's constant, $[ion]_{outside}$ is the concentration of the particular ion outside the cell, and $[ion]_{inside}$ is the concentration of the particular ion in the cytosol.

The following equations are for ion flux for calcium:

$$I_{VCa} = (GmVCa)\ (PVCa)(V - V_{Ca})$$

$$PVCa = \frac{1}{1 + e^{\frac{VCah - V}{KCah}}}$$

Where $GmVCa$ is the whole cell conductance for VGCCs, $PVCa$ is the open fraction for VGCC, $VCah$ is the half-activated voltage, and $KCah$ is the slope for the half-activated voltage.

$$I_{Capump} = PmCap \frac{{[Ca]_i}^2}{KCap^2 + {[Ca]_i}^2}$$

Where $PmCap$ is the maximum current for the calcium pumps, $[Ca]_i$ is the cytosolic calcium concentration, and $KCap$ is the half-maximum pump activity.

$$I_{Na,Ca} = gNaCa \frac{{[Ca]_i}^5}{{[Ca]_i}^5 + {K_{NaCa}}^5} (V - V_{NaCa})$$

$$V_{NaCa} = \frac{RT}{F}\left(3 \ln \frac{[Na]_o}{[Na]_i} - \ln \frac{[Ca]_o}{[Ca]_i}\right)$$

Where gNaCa is the maximum conductance for all sodium calcium exchangers, $[Na]_o$ and $[Na]_i$ being the concentration of sodium outside and inside the cell respectively, and K_{NaCa} being the affinity constant for calcium for these channels.

The interactions between cytosolic calcium and endoplasmic calcium are shown here:

$$J_{ER} = P_{CaER} \frac{[Ca]_i^{\,2}}{[Ca]_i^{\,2} + K_{Carp}^{\,2}}$$

$$J_{Out} = \left(P_{leak} + P_{IP3} O_{inf}\right)\left([Ca]_{ER}^{\,2} - [Ca]_i\right)$$

$$O_{inf} = \frac{[Ca]_i}{[Ca]_i + K_{RCa}} \frac{[IP3]_i^{\,3}}{[IP3]_i^{\,3} + K_{IP3}^{\,3}}$$

Where J_{ER} is calcium flux into the endoplasmic reticulum by SERCA pumps, P_{CaER} is the maximum rate, and K_{Carp} is the half-maximum activity. J_{Out} is the release of ER calcium, P_{leak} is the rate of calcium that leaks out of the ER, P_{IP3} is the rate of calcium from IP3-Receptor channels, O_{inf} is the open fraction for P_{IP3} channels, $[Ca]_{ER}$ is the ER calcium concentration, K_{RCa} is the affinity constant for calcium, and K_{IP3} is the binding constant for IP3 to these channels.

The following equations are for ion flux for sodium:

$$I_{Cran} = f_{cran}\, p_{cran}\, (V - V_{Na})$$

$$f_{cran} = \frac{-g_{mcran}}{1 + e^{\frac{[Ca]_{ER} - K_{Car}}{3}}}$$

$$p_{cran} = (V - V_{Cran})$$

Where f_{cran} and p_{cran} are the voltage-independent and voltage-dependent portions of the open probability, g_{mcran} is the conductance of these channels, $[Ca]_{ER}$ is the calcium concentration of the endoplasmic reticulum, K_{Car} is the half-activation with respect to ER calcium, and V_{Cran} is the reverse potential.

$$I_{Na} = g_{mNa}\, p_{Na} (V - V_{Na})$$

$$p_{Na} = \frac{1}{1 + e^{\frac{104+V}{8}}}$$

Where g_{mNa} is the total sodium channel conductance and p_{Na} is the voltage dependent open probability.

$$I_{Na,K} = P_{NaK}\frac{(F_1 f_2 f_3 F_4 F_5 f_6 - b_1 B_2 B_3 B_4 b_5 B_6)}{D}$$

$$D = f_2 f_3 F_4 F_5 f_6 + b_1 f_3 F_4 F_5 f_6 + b_1 B_2 F_4 F_5 f_6 + b_1 B_2 B_3 F_5 f_6 + b_1 B_2 B_3 B_4 f_6 + b_1 B_2 B_3 B_4 b_5$$

$$F_1 = f_1[Na]_i^{\,3}\,,\ F_4 = f_4[K]_i^{\,2}\,,\ F_5 = f_5[ATP]_i\,,\ B_2 = b_2[ADP]_i\,,\ B_3 = b_3[Na]_o^{\,3},\ B_4 = b_4[P]\,,$$

$$B_6 = b_6[K]_i^{\,2}\,,\ f_5 = {f_5}^* e^{\frac{VF}{2RT}}\,,\ b_5 = {b_5}^* e^{\frac{-VF}{2RT}}$$

Where P_{NaK} is the maximum current, $[ATP]_i$ and $[ADP]_i$ are the ATP and ADP concentrations respectively, $[P]$ is the concentration of phosphate, the remainder of the parameters were fitting constants from experimental results and are listed in table A-2.

The following equations are for ion flux for potassium:

$$I_{kDr} = g_{mKdr}\, n\, (V - V_K)$$

Where g_{mKdr} is the conductance for the voltage gated potassium channels and n is the open probability that changes with voltage. This parameter is updated according to its differential equations in the respective section.

$$I_{KCa} = g_{mKCa}\, f_{Ca}\, (V - V_K)$$

$$f_{Ca} = \frac{[Ca]_i^{\,4}}{[Ca]_i^{\,4} - {K_{KCa}}^4}$$

Where g_{mKCa} is the conductance for the calcium sensitive potassium channels, f_{Ca} is their open probability, and K_{KCa} is the affinity constant for calcium.

$$I_{KATP} = g_{mKATP}\, O_{KATP}(V - V_K)$$

$$O_{KATP} = \frac{0.08\left(1 + 0.33\frac{[ADP]_i}{K_{dd}}\right) + 0.89\left(1.65\frac{[ADP]_i}{K_{dd}}\right)^2}{\left(1 + 0.165\frac{[ADP]_i}{K_{dd}}\right)^2\left(1 + 0.135\frac{[ADP]_i}{K_{td} + \frac{0.05[ATP]_i}{K_{tt}}}\right)}$$

Where g_{mKATP} is the ATP sensitive potassium channel's conductance, O_{KATP} being the open fraction dependent on ATP concentration, and K_{dd}, K_{td}, and $K_{tt}$are dissociation constants.

Differential Equations:

Change in membrane voltage:

$$\frac{dV}{dt} = \frac{I_{VCa} + I_{Capump} + I_{Na,Ca} + I_{Cran} + I_{Na} + I_{Na,K} + I_{kDr} + I_{KCa} + I_{KATP}}{-C_m}$$

Where V is membrane voltage, t is time, I_{VCa} is the current due to voltage gated calcium channels, I_{Capump} is the current due to membrane calcium pumps, $I_{Na,Ca}$ is the current due to membrane sodium calcium exchangers, I_{Cran} is the current due to non-selective ion current controlled by endoplasmic calcium storage, I_{Na} is the current due to background sodium currents, $I_{Na,K}$ is the current due to membrane sodium potassium exchangers, I_{kDr} is the current due to voltage dependent potassium channels, I_{KCa} is the current due to calcium activated potassium channels, I_{KATP} is the current due to ATP sensitive potassium channels, and C_m is the whole cell membrane capacitance.

Change in cytosolic calcium:

$$\frac{d[Ca]_i}{dt} = f_i\left(\frac{-I_{VCa} + 2I_{NaCa} - 2I_{Capump}}{2FV_i} - J_{ER} + \frac{J_{out}}{V_i}\right) - K_{sg}[Ca]_i$$

Where f_i is the fractional free unbound intracellular calcium and V_i is the cytosolic volume.

Change in ER calcium:

$$\frac{d[Ca]_{ER}}{dt} = \frac{f_{ER}}{V_{ER}}(J_{ER}\,V_i - J_{out})$$

Where f_{ER} is the ER fractional free calcium and V_{ER} is the ER volume.

Change in cytosolic sodium:

$$\frac{d[Na]_i}{dt} = \frac{-3I_{NaCa} - 3I_{NaK} - I_{Na} - I_{Cran}}{FV_i}$$

Change in IP3:

$$\frac{d[IP3]_i}{dt} = K_{IP}\frac{[Ca]_i{}^2}{[Ca]_i{}^2 - K_{IPCa}{}^2} - K_{dIP}[IP3]_i$$

Where K_{IP} is the constant rate of IP3 generation, K_{IPCa} is the half-maximum rate of production by calcium, and K_{dIP} is the rate of IP3 degradation.

Change in ATP:

$$\frac{d[ATP]_i}{dt} = K_{ADP}[ADP]_i - \frac{I_{Na,K} + I_{Capump}}{FV_i} - \frac{J_{ER}}{2} - (K_{ATPCa}[Ca]_i + K_{ATP})[ATP]_i$$

Where K_{ADP} is the rate of ATP production from ADP, K_{ATPCa} is the rate of ATP consumption dependent on calcium, and K_{ATP} is the base constant for ATP consumption.

The amount of adenine $[A]_i$ within the cell was assumed constant and conserved between ATP and ADP, thus:

$$[ATP]_i + [ADP]_i = [A]_i$$

For I_{kDr}, the change in n with time is:

$$\frac{dn}{dt} = \frac{n_{inf} - n}{\tau_n}$$

$$n_{inf} = \frac{1}{1 + e^{\frac{(V_n - V)}{S_n}}}$$

$$\tau_n = \frac{c}{e^{\frac{(V - V_\tau)}{a}} + e^{\frac{(V_\tau - V)}{b}}}$$

Where V_n is the half-activation voltage, S_n is the slope at half-maximum, and the rest are experimentally derived coefficients listed in table A-2.

Variables and Parameters:

Table A-1: Variables and initial conditions for electrophysiology model.

Variable	Initial Value
V	-60.9
$[Ca]_i$	0.085
$[Na]_i$	9858
$[IP3]_i$	0.33
$[ATP]_i$	932.1
$[Ca]_{ER}$	22.8
n	0.00123

Table A-2: Parameters and constants for electrophysiology equations.

Parameter	Value	Parameter	Value	Parameter	Value
g_{mVCa}	770	K_{RCa}	0.077	f_5^*	0.002
V_{Cah}	-19	K_{IP3}	3.2	f_6	11.5
K_{Cah}	9.5	K_{sg}	0.0001	b_1	100
P_{mCap}	2000	$[A]_i$	4000	b_2	0.0002
K_{Cap}	0.1	K_{ADP}	Removed	b_3	$1.72\text{x}10^{-17}$
g_{NaCa}	271	K_{ATPCa}	0.00005	b_4	0.0002
K_{NaCa}	0.75	K_{ATP}	0.00005	b_5^*	0.03
g_{mCran}	0.7	V_i	0.764	b_6	$6\text{x}10^{-7}$
V_{Cran}	0	V_{ER}	0.28	K_{dd}	17
K_{Car}	200	P_{IP3}	0.0012	K_{td}	26
g_{mNa}	1200	$[K]_i$	132400	K_{tt}	1
P_{NaK}	600	$[K]_o$	8000	$T\ (Kelvin)$	310
g_{mKDr}	0.1	$[Ca]_o$	2600	R	8.314
g_{mKCa}	130	$[Na]_o$	140000	F	96485
K_{KCa}	0.1	C_m	6158	V_n	-14
g_{mKATP}	24000	f_i	0.01	S_n	7
P_{CaER}	0.105	f_{ER}	0.03	a	65
K_{Carp}	0.5	$[P]$	4950	b	20
K_{IP}	0.0003	f_1	$2.5\text{x}10^{-10}$	c	20
K_{dIP}	0.00004	f_2	10	V_τ	-75
K_{IPCa}	0.4	f_3	0.172		
P_{leak}	0.0001	f_4	$1.5\text{x}10^{-8}$		

Metabolic Model:

All of the following equations and parameters in this section were from:

Fridlyand, L. and Philipson, L., 2010. Glucose sensing in the pancreatic beta cell: a computational systems analysis. *Theoretical Biology and Medical Modelling*, 7(1).

Metabolic Equations:

For glucose entry consumption:

$$J_{glu} = V_{mglu}\left(\frac{[ATP]_i}{[ATP]_i + K_{mATP}}\right)\left(\frac{[Glu]^{hgl}}{[Glu]^{hgl} + K_{mgl}{}^{hgl}}\right)$$

Where J_{glu} is the glucokinase reaction rate, V_{mglu} is the maximum glucose consumption, $[Glu]$ is the extracellular glucose concentration, K_{mATP} is the Michaelis-Menten rate constant, K_{mgl} is the half-maximum glucose concentration, and hgl is the hill coefficient.

For glycolytic reactions with NAD/NADH:

$$J_{gpd} = V_{mGPD}\left(\frac{[G3P]}{[G3P] + K_{mG3P}}\right)\left(\frac{[NAD]_i/[NADH]_i}{K_{gNc} + [NAD]_i/[NADH]_i}\right)$$

Where J_{gpd} is the glycolytic flux, $[G3P]$ is the cytosolic concentration of glucose-3-phosphate, V_{mGPD} is the maximum activity for G3P dehydrogenase, K_{mG3P} is the Michaelis-Menten constant, $[NAD]_i$ and $[NADH]_i$ are the cytosolic NAD and NADH concentrations respectively, and K_{gNc} is the half-maximum rate constant.

$$J_{LDH} = V_{mLDH}\left(\frac{[PYR]}{[PYR] + K_{mLD}}\right)\left(\frac{[NAD]_i/[NADH]_i}{K_{LNc} + [NAD]_i/[NADH]_i}\right)$$

Where J_{LDH} is the flux through lactate dehydrogenase (LDH), V_{mLDH} is the maximal activity of LDH, K_{mLD} is the Michaelis-Menten constant, $[PYR]$ is the pyruvate concentration, and K_{LNc} is the half-maximal rate.

The Pyruvate consumption by the mitochondria:

$$J_{PYR} = V_{mPDH}\, F_{PYR}\, F_{PNAD}\, F_{PCa}$$

$$F_{PYR} = \left(\frac{[PYR]}{K_{mPYR} + [PYR]}\right)$$

$$F_{PNAD} = \left(\frac{[NAD]_m/[NADH]_m}{K_{PNm} + [NAD]_m/[NADH]_m}\right)$$

$$F_{PCa} = \left(\frac{1}{1 + u_2(1 + u_1(1 + [Ca]_m/K_{Cam})^{-2})}\right)$$

Where J_{PYR} is the pyruvate consumption by the mitochondria, V_{mPDH} is the maximal activity of pyruvate dehydrogenase, K_{mPYR} is the Michaelis-Menten constant, $[NAD]_m$ and $[NADH]_m$ are the NAD/NADH concentrations in the mitochondria, K_{PNm} is the half-maximal NAD/NADH ratio for NADH production, $[Ca]_m$ is the mitochondrial calcium concentration, and K_{Cam}, u_1, u_2, are given parameters.

For proton pumping rate by ETC:

$$J_{hres} = V_{me} F_{De} F_{Ae} F_{Te}$$

$$F_{De} = \frac{[NADH]_m}{K_{mNH} + [NADH]_m}$$

$$F_{Ae} = 1$$

$$F_{Te} = \frac{K_{AT}\, \psi_m + 1}{K_{BT}\, \psi_m + 1}$$

Where V_{me} is the optimal conditions rate, F_{De} is the kinetic factor by NADH electron transfer, F_{Ae} is the oxygen availability factor (later changed), F_{Te} being a thermodynamic potential factor, K_{mNH} being an affinity constant, ψ_m being the mitochondrial membrane potential, and K_{BT} and K_{AT} being experimentally derived coefficients.

For proton flux through ATP-Synthase:

$$J_{ph} = V_{mph} A_D A_T A_{Ca}$$

$$A_D = \frac{[mgADP]_i{}^{hph}}{K_{mADP}{}^{hph} + [mgADP]_i{}^{hph}}$$

$$A_T = \frac{\psi_m{}^{hp}}{K_{ph}{}^{hp} + \psi_m{}^{hp}}$$

$$A_{Ca} = 1 - \frac{1}{e^{[Ca]_m/K_{PCam}}}$$

Where V_{mph} is the optimal rate, $[mgADP]_i$ is the free cytosolic ADP concentration, hph is the hill coefficient, K_{mADP} is the constant for activation rate, K_{ph} is the half-maximal ATP production rate by the mitochondrial membrane voltage, $[Ca]_m$ is the mitochondrial calcium concentration, with K_{PCam} being a calcium binding coefficient.

For proton leak:

$$J_{hl} = (P_{lb} + P_{lr})e^{(K_{lp}\psi_m)}$$

Where P_{lb} is basal leak rate, P_{lr} is the regulated leak, and K_{lp} is a membrane voltage coefficient.

For the NAD/NADH flux in and out of the mitochondria:

$$J_{TNADH} = T_{NADH}\left(\frac{[NADH]_i/[NAD]_i}{K_{TNi} + [NADH]_i/[NAD]_i}\right)\left(\frac{[NAD]_m/[NADH]_m}{K_{TNm} + [NAD]_m/[NADH]_m}\right)$$

Where T_{NADH} is the maximum transfer rate, and K_{TNi} and K_{TNm} are affinity constants for cytosol and mitochondria respectively.

Calcium entry into the mitochondria by uniporter:

$$J_{uni} = P_{Ca}\frac{Z_{Ca}\psi_m}{T_V}\frac{\alpha_m[Ca]_m e^{(-Z_{Ca}\psi_m/T_V)} - \alpha_i[Ca]_i}{e^{(-Z_{Ca}\psi_m/T_V)^{-1}}}$$

Where P_{Ca} is the permeability of calcium via the uniporter, T_V being thermal voltage, and α_m and α_i being activity constants.

Sodium and calcium exchange via the mitochondrial exchanger:

$$J_{NaCa} = \frac{V_{mNC} e^{(0.5\psi_m \alpha_1 / T_V)} - e^{(0.5\psi_m \alpha_2 / T_V)}}{1 + \alpha_1 + \alpha_2 + \frac{[Na]_i{}^3}{K_{Naj}{}^3} + \frac{[Ca]_m}{K_{Caj}} + \frac{[Na]_m{}^3}{K_{Naj}{}^3} + \frac{[Ca]_i}{K_{Caj}}}$$

$$\alpha_1 = \frac{[Na]_i{}^3 [Ca]_m}{K_{Naj}{}^3 K_{Caj}}$$

$$\alpha_2 = \frac{[Na]_m{}^3 [Ca]_i}{K_{Naj}{}^3 K_{Caj}}$$

Where V_{mNC} is the maximal exchange rate, with K_{Naj} and K_{Caj} being binding constants for Na and Ca respectively.

Metabolic Differential Equations:

For the rate change of G-3-P concentration:

$$\frac{d[G3P]}{dt} = \frac{2J_{glu} - J_{gpd}}{V_i} - K_{gpd}[G3P]$$

With K_{gpd} is the G3P consumption rate.

The rate change of pyruvate:

$$\frac{d[PYR]}{dt} = \frac{J_{gpd} - J_{PYR} - J_{LDH}}{V_i + V_{mmit}}$$

With V_{mmit} being the mitochondrial volume.

Rate change for NADH in the mitochondria:

$$\frac{d[NADH]_m}{dt} = \frac{4.6J_{PYR} - J_{TNADH} - 0.1J_{hres}}{V_{mit}} - K_{NADHm}[NADH]_m$$

With K_{NADHm} being the rate of NADH consumption.

Rate change for NADH in the cytosol:

$$\frac{d[NADH]_i}{dt} = \frac{J_{gpd} - J_{TNADH} - J_{LD}}{V_i} - K_{NADHc}[NADH]_c$$

With K_{NADHc} being the rate of NADH consumption.

Additionally, with nucleotides being conserved in their respective compartments:

$$N_{Tm} = [NAD]_m - [NADH]_m$$

$$N_{Ti} = [NAD]_i - [NADH]_i$$

With N_{Tm} and N_{Ti} being the total NAD in the mitochondria and cytosol respectively.

For the mitochondrial membrane potential:

$$\frac{d\psi_m}{dt} = \frac{J_{hres} - J_{ph} - J_{hl} - J_{NaCa} - 2J_{uni}}{C_{mit}}$$

With C_{mit} being the mitochondrial membrane capacitance.

The rate change of mitochondrial calcium being:

$$\frac{d[Ca]_m}{dt} = \frac{-f_m(J_{uni} - J_{NaCa})}{V_{mit}}$$

With $f_m$being the fraction of free calcium in the mitochondria. Additionally, the change of mitochondrial calcium was used to update the electrophysiological equation for cytosolic calcium to:

$$\frac{d[Ca]_i}{dt} = f_i\left(\frac{-I_{VCa} + 2I_{NaCa} - 2I_{Capump}}{2FV_i} - J_{ER} + \frac{J_{out}}{V_i} - \frac{d[Ca]_m}{dt}\right) - K_{sg}[Ca]_i$$

The rate change in ATP production being:

$$\frac{d[ATP]_i}{dt} = \frac{2J_{glu} + 0.231J_{pf}}{V_i} - (K_{ATP} + K_{ATPCa}[Ca]_i)[ATP]_i$$

This was then incorporated into the differential equation for ATP from the electrophysiology model:

$$\frac{d[ATP]_i}{dt} = \frac{2J_{glu} + 0.231J_{pf}}{V_i} - \frac{J_{ER}}{2} - \frac{I_{Na,K} + I_{Capump}}{FV_i} - (K_{ATPCa}[Ca]_i + K_{ATP})[ATP]_i$$

The ratio of magnesium bound ADP to unbound ADP was maintained via:

$$[MgADP]_i = 0.055[ADP]_i$$

Variables and Parameters:

Table A-3: Variables and initial conditions for metabolic model.

Variable	Initial Value
$[G3P]$	2.79
$[PYR]$	8.62
$[NADH]_i$	0.97
ψ_m	94.7
$[NADH]_m$	57.2
$[Ca]_m$	0.242

Table A-4: Parameters and constants for metabolic equations.

Parameter	Value	Parameter	Value	Parameter	Value
V_{mmit}	0.0144	K_{mpyr}	47.5	K_{lp}	0.0305
V_{mit}	0.06	K_{PNm}	81	T_{NADH}	0.05
f_m	0.0003	u_1	1.5	K_{TNm}	16.78
$[Na]_m$	5000	u_2	1.1	P_{Ca}	0.004
T_V	26.73	K_{Cam}	0.05	a_m	0.2
N_{tm}	2200	V_{me}	22	a_i	0.341
N_{ti}	2000	K_{mNH}	3000	V_{mNC}	0.025
V_{mglu}	0.011	K_{AT}	-0.00492	K_{Naj}	8000
K_{mATP}	500	K_{BT}	-0.00443	K_{Caj}	8
K_{mgl}	7	V_{mph}	8	K_{TNi}	0.002
hgl	1.7	K_{mADP}	20	K_{gpd}	0.00001
V_{mGPD}	0.5	hph	2	K_{NADHm}	0.0001
V_{mG3P}	200	hp	8	K_{NADHi}	0.0001
V_{mLD}	1.2	K_{Ph}	131.4	K_{ATP}	0.00004
K_{mLD}	47.5	K_{PCam}	0.165	K_{ATPCa}	0.00009
K_{LNc}	1	P_{lb}	0.0012		
V_{mPDH}	0.3	P_{lr}	0.0012		

Insulin Secretion Model:

All of the following equations and parameters in this section were from:

Kang, H., Jo, J., Kim, H., Choi, M., Rhee, S., & Koh, D. (2005). Glucose metabolism and oscillatory behavior of pancreatic islets. *Physical Review E, 72*(5). doi:10.1103/physreve.72.051905

Insulin Model Equations:

For the rate of insulin secretion:

$$R_s = R_o \bar{C_i}^4 \frac{S_R}{S_{max}}$$

$$\bar{C_i} = (C_i - C_b)/C_o$$

Where R_o is an insulin secretion coefficient, S_R is the insulin primed at the readily releasable pool, S_{max} is the maximum value for the readily releasable pool, C_b and C_o being calcium coefficients, and C_i being the intracellular calcium concentration.

For the refilling rate from the reserve pool:

$$R_r = \alpha_r (S_{max} - S_R)$$

Where α_r is the refill rate coefficient.

Insulin Differential Equation:

For the change in the readily releasable pool:

$$\frac{dS_R}{dt} = R_r - R_s$$

Parameters for Insulin Model:

Table A-5: Parameters for insulin secretion.

Parameter	Value
C_0	0.1
C_b	0.06
S_{max}	0.000036
R_o	1.2×10^{-10}
α_r	2

<u>Equation Updates for EFS and PBM:</u>

EFS Equations:

During the parameter updates, the membrane voltage changed by:

$$V(t+1) = V(t) + \frac{dV}{dt} + (E_m\ EFS)$$

$$E_m = \frac{1}{\pi}\ f_c\ r$$

Where EFS is the strength of the electric field set by the user in V/cm. E_m being the coefficient derived explained in chapter 4 for assuming an average membrane depolarization, with f_c being the spherical form factor (1.5) and r being the radius of the cell (7 μm).

This equation was derived from the equation given in:

Schoenbach, K., et al. Ultrashort electrical pulses open a new gateway into biological cells. Proc. IEEE 92:1122–1137, 2004.

PBM Equations:

The effects of PBM were via CCO activation utilized the equation:

$$J_{hres} = V_{me} F_{De} DF_{Ae} F_{Te}$$

With the basal F_{Ae} being changed from 1.0 to 0.6 based on the activity of CCO at 50 nM nitric oxide concentration from:

Poderoso, J., Carreras, M., Lisdero, C., Riobó, N., Schöpfer, F. and Boveris, A., 1996. Nitric Oxide Inhibits Electron Transfer and Increases Superoxide Radical Production in Rat Heart Mitochondria and Submitochondrial Particles. Archives of Biochemistry and Biophysics, 328 (1), pp.85-92.

The change in F_{Ae} by PBM was determined by:

$$DF_{Ae} = F_{Ae}\ \left(1 + (1.6A_e) - \left(0.9{A_e}^2\right)\right)$$

$$A_e = \ Abs_{CCO}\ PBM_{ir}\ EXP\ (10^{-3})$$

Where DF_{Ae} is the updated F_{Ae} under PBM, Abs_{CCO} being the absorption of CCO for 810 nm light, PBM_{ir} being the irradiance in (mW/cm^2), EXP being the duration of PBM (s), and (10^{-3}) to convert to model units.

The change in CCO activity was interpolated via a 2nd order polynomial for the experimental data found here:

Houreld, N., Masha, R. and Abrahamse, H., 2012. Low-intensity laser irradiation at 660 nm stimulates cytochrome c oxidase in stressed fibroblast cells. Lasers in Surgery and Medicine, 44(5), pp.429-434.

The effects of PBM on glucokinase activity modified the glucose consumption equation to:

$$J_{glu} = HKA\left(1 + \frac{\left((1.6A_e) - \left(0.9{A_e}^2\right)\right)}{14}\right)V_{mglu}\left(\frac{[ATP]_i}{[ATP]_i + K_{mATP}}\right)\left(\frac{[Glu]^{hgl}}{[Glu]^{hgl} + {K_{mgl}}^{hgl}}\right)$$

Where HKA was the glucokinase fractional activity (1 at basal) with PBM's effects increasing it by at most 5%.

For TRPV1, the open fraction was manipulated by the user with the following equations added:

$$I_{TRPVCa} = G_{TRPVCa}\, PoTRPV\, (V - V_{ca})$$

$$I_{TRPVNa} = G_{TRPVNa}\, PoTRPV\, (V - V_{Na})$$

Where I_{TRPVCa} and I_{TRPVNa} are the TRPV currents for calcium and sodium respectively, G_{TRPVCa} and G_{TRPVNa} being the conductance values for TRPV for each ion, and $PoTRPV$ being the open fraction for TRPV1 channels.

This led to the change in the following differential equations:

$$\frac{d[Ca]_i}{dt} = f_i\left(\frac{-I_{VCa} + 2I_{NaCa} - 2I_{Capump} - I_{TRPVCa}}{2FV_i} - J_{ER} + \frac{J_{out}}{V_i} - \frac{d[Ca]_m}{dt}\right) - K_{sg}[Ca]_i$$

$$\frac{d[Na]_i}{dt} = \frac{-3I_{NaCa} - 3I_{NaK} - I_{Na} - I_{Cran} - I_{TRPVNa}}{FV_i}$$

Insulin Equations:

Maximum insulin dynamic rates were found from the following paper:

Rorsman, P. and Renström, E., 2003. Insulin granule dynamics in pancreatic beta cells. Diabetologia, 46(8), pp.1029-1045.

This led to the following if statement conditions:

$$if\ R_r\ \geq I_t\ 1.4 \times 10^{-6}\ \ and\ t \leq 300000\ , then\ R_r = \ I_t\ 1.4 \times 10^{-6}$$

$$if\ R_r\ \geq I_t\ 5.0 \times 10^{-7}\ \ and\ t > 300000\ , then\ R_r = \ I_t\ 5.0 \times 10^{-7}$$

$$else\ R_r = \alpha_r(S_{max} - S_R)$$

Table A-6: Parameters for updated and custom equations.

Parameter	Value	Reference
f_c	1.5	A1
r	7 (μm)	A2
Abs_{CCO}	0.06	A3
PBM_{ir}	User Defined	
EXP	User Defined	
G_{TRPVCa}	15	A4
G_{TRPVNa}	63	A4
I_t	0.0222	A1

Table A-6 references:

A1. K.H. Schoenbachk, R., n.d. Ultrashort electrical pulses open a new gateway into biological cells. *Conference Record of the Twenty-Sixth International Power Modulator Symposium, 2004 and 2004 High-Voltage Workshop.*

A2. Dean, P. (1973). Ultrastructural morphometry of the pancreatic β-cell. *Diabetologia*, *9*(2), 115-119. doi: 10.1007/bf01230690

A3. Mason, M., Nicholls, P. and Cooper, C., 2014. Re-evaluation of the near infrared spectra of mitochondrial cytochrome c oxidase: Implications for non invasive in vivo monitoring of tissues. *Biochimica et Biophysica Acta (BBA) - Bioenergetics*, 1837(11), pp.1882-1891.

A4. Samways, D. and Egan, T., 2011. Calcium-dependent decrease in the single-channel conductance of TRPV1. *Pflügers Archiv - European Journal of Physiology*, 462(5), pp.681-691.

Thermal Simulation Equations:

The change in temperature in the cell was determined by:

$$\frac{dT_{cell}}{dt} = \frac{\alpha\ I_r\ A_c - h_c\ A_{sc}(T_{cell} - T_{med})}{m_c\ C_p}$$

Where α is water absorbance at 810 nm, I_r is the irradiance (W/cm^2), A_c is the cross-sectional area of the cell, T_{cell} being the current cell temperature, T_{med} being the current media temperature, m_c being the mass of the cell, A_{sc} being the cell's surface area, and C_p being the specific heat of water. For the change in temperature of the media:

$$\frac{dT_{med}}{dt} = \frac{\alpha\, I_r\, A_m - h_m\, A_{sm}(T_{med} - T_{sur})}{m_{med}\, C_p}$$

Where A_m is the cross-sectional area of the media, h_m is the convective heat loss to the surrounding environment, T_{sur} is the environmental temperature, A_{sm} being the exposed surface area, and m_{med} being the mass of the media. Temperature values were in kelvin and mass in grams.

Table A-7: Parameters for the thermal simulations.

Parameter/Variable	Value/Initial Value	Reference
T_{cell}	300	
T_{med}	300	
T_{sur}	300	
α	0.04	A5
I_r	Varied	
A_c	1.5394×10^{-6}	
A_m	2.25	
h_c	0.026	A6
h_m	0.005	
A_{sc}	6.1575×10^{-6}	
A_{sm}	2.25	
m_c	1.44×10^{-9}	
m_{med}	2	
C_p	4.168	

Table A-7 references:

A5. Mason, M., Nicholls, P. and Cooper, C., 2014. Re-evaluation of the near infrared spectra of mitochondrial cytochrome c oxidase: Implications for non invasive in vivo monitoring of tissues. *Biochimica et Biophysica Acta (BBA) - Bioenergetics*, 1837(11), pp.1882-1891.

A6. Song, P., Gao, H., Zhang, M., Yang, F., Li, S., Kang, B., Xu, J. and Chen, H., 2019. Transient microscopy for measuring heat transfer in single cells. *ArVix.org*, [online] Available at: <https://arxiv.org/abs/1901.00141> [Accessed 13 August 2020].

Matlab Model Code:

```
%Input Parameters

    TS = 900000;                %Time Span (ms)
    T = 310;                    %Cell Temperature (K)
    Tm = 310;                   %Mitochondrial Temperature (K)
    glu =180;                   %glucose mg/dL
    Glu = glu/18;               %Glucose concentration (mM)

    PBMir = 0;                  %Irradiance (mW/cm2)
    EXP = 60;                   %Exposure duration at begining (s)
    AbsCCO = 0.06;              %Approximate for CCO @ 810 nm
    FAe = 0.6;                  %CCO fractional activity pre laser

    EFS = 1;                    %Field Strength (V/cm)
    Em = 0.3183;                %Coefficient for EFS (cm mV/V)
    Ae = (AbsCCO*PBMir*1E-6*(EXP*1E3));
    dFAe = 1+(1.6*Ae)-(0.9*Ae^2);
    DFAe = FAe*dFAe;
    IPCoe = 1;                  %IP3 Sensitivity Factor (manipulation)
    HKA = 1;                    %Glucokinase activity factor (manipulation)

    PoTRPV = 0;


%Universal Constants
    R = 8.314;                  %Gas constant (J/mol K)
    F = 96485;                  %Faraday's Constant (C/mol)
    zCa = 2;                    %Ionic charge Calcium
    zNaK = 1;                   %Ionic charge Na or K
    TV = (1000*R*T)/(F);        %Thermal Voltage (mV)
    TVm = (1000*R*Tm)/(F);      %Thermal Voltage mitochondria (mV)

%Cellular Parameters
    Ksg = 0.0001;               %Rate constant (1/ms)
    Vol = 0.764;                %Cytosolic Volume (pL)
    Ver = 0.280;                %ER Volume (pL)
    Vi = 0.53;                  %Relative cytoplasmic volume
    Vmit = 0.06;                %Relative mitochondrial volume
    Vmmit = 0.0144;             %Relative mitochondrial matrix volume
    Cm = 6158;                  %Membrane capacitance (fF)
    Cao = 2.6e3;                %Extracellular Calcium (uM)
    Nao = 140e3;                %Extracellular Sodium (uM)
    Ko = 8e3;                   %Extracellular Potassium (uM)
    fi = 0.01;                  %Fraction of free cytoplasmic calcium
    fer = 0.03;                 %Fraction of free ER calcium
    At = 4000;                  %Cellular total adenine concentration (uM)
    P = 4950;                   %Inorganic phosphate concentration (uM)
    KATPCa = 0.00005;           %Calcium dependent ATP consumption (uM/ms)
    KATP = 0.00005;             %Constant for ATP consumption (1/ms)

%IP3 Metabolism
    KIP = 0.0003;
    KdIP = 0.00004;
```

```
    KIPCa = 0.4;

%Insulin Dynamics
    Cb = 0.06;                  %Scale constant (uM)
    Co = 0.1;                   %Scale constant (uM)
    Smax = 0.000036;            %Maximum primed insulin (pmol)
    Ro = 1.2E-10;               %Scale constant (pmol/ms)
    Ar = 2;                     %Time constant (1/ms)
    INS = 0;                    %Total insulin secreted (pmol)

%Cellular Initial Conditions
    V = -60.9;                  %Membrane Voltage (mV)
    Cai = 0.085;                %Cytosolic Calcium (uM)
    Caer = 22.8;                %ER Calcium (uM)
    Nai = 9858;                 %Cytosolic Sodium (uM)
    Ki = 132.4e3;               %Cytosolic Potassium (uM)
    IP3i = 0.33;                %Cytosolic IP3 concentration (uM)
    ATPi = 932.1;               %Cytosolic ATP (uM)
    NADHc = 0.97;               %Cytosolic NADH (uM)
    ADPi = At - ATPi;           %ADP concentration (uM)
    MgADP = 0.055*ADPi;         %Sequestered ADP (uM)
    Vn = -14;
    Sn = 7;
    a = 65;
    b = 20;
    c = 20;
    n = 0.00123;
    Vtau = -75;
    Sr = Smax;                  %Primed insulin starting at full (pmol)
    It = 0.0222;                %Total insulin content (pmol)

%Membrane Channel Constants
    %Voltage Gated Calcium Channels (IVCa)
    GmVCa = 770;                %Conductance (pS)
    VCah = -19;                 %Half activated potential (mV)
    KCah = 9.5;                 %Slope at half max (mV)
    %Calcium Pumps (ICapump)
    PmCap = 2000;               %Maximum Current (fA)
    KCap = 0.1;                 %Half max pump (uM)
    %NaCa Exchanger (INaCa)
    GNaCa = 272;                %Conductance (pS)
    KNaCa = 0.75;               %Affinity Constant (uM)
    %Calcium release-activated nonselective cation current (ICran)
    GmCran = 0.7;               %Maximum Conductance (pS/mV)
    VCran = 0;                  %Reverse Potential (mV)
    KCar = 200;                 %Half-activation by ER calcium
    %Background Sodium Channels
    GmNa = 1200;                %Conductance (pS)
    %Voltage Gated Potassium Channels (IKDr)
    GmKDr = 3000;               %Conductance (pS)
    %Calcium Activated Potassium Channels (IKCa)
    GmKCa = 130;                %Conductance (pS)
    KKCa = 0.1;                 %Affinity constant (uM)
    %ATP sensitive Potassium Channels
    Kdd = 17;                   %Dissociation constant (uM)
    Ktd = 26;                   %Dissociation constant (uM)
```

```
    Ktt = 1;                    %Dissociation constant (uM)
    %ATP Sensitive Potassium Channels (IKATP)
    GmKATP = 24000;             %Conductance (pS)
    %Sodium Potassium exchanger
    f1 = 2.5e-10;               %Parameter (1/uM3 ms)
    f2 = 10;                    %Parameter (1/ms)
    f3 = 0.172;                 %Parameter (1/ms)
    f4 = 1.5e-8;                %Parameter (1/uM2 ms)
    ff5 = 0.002;                %Parameter (1/ms uM)
    f6 = 11.5;                  %Parameter (1/ms)
    b1 = 100;                   %Parameter (1/ms)
    b2 = 0.0001;                %Parameter (1/uM ms)
    b3 = 1.72e-17;              %Parameter (1/uM3 ms)
    b4 = 0.0002;                %Parameter (1/uM ms)
    bb5 = 0.03;                 %Parameter (1/ms)
    b6 = 6e-7;                  %Parameter (1/uM ms)
    PNaK = 600;                 %Coefficient with saturated ATP
    %TRPV1 Channels
    RTRP = 2.0E-3;
    GTRPVNa = 63;
    GTRPVK = 53;
    GTRPVCa = 15;
    DS = 0.47;
    DH = 150;
    FKC = 0.71;

%Endoplasmic Channel Constants
    %SERCA Pumps
    PCaER = 0.105;              %Concentration Pump Rate (uM/ms)
    KCarp = 0.5;                %Half Maximum (uM)
    %ER Calcium Leak
    Pleak = 0.0001;             %Flow rate (pL/ms)
    %IP3 Receptors
    PIP3 = 0.0012;              %Maximum flow rate (pL/ms)
    KRCa = 0.077;               %Affinity constant to Calcium (uM)
    KIP3 = 3.2;                 %Affinity constant to IP3 (uM)

%Mitochondrial Initial Conditions
    Psim = 94.7;                %Mitochondrial membrane voltage (mV)
    G3P = 2.79;                 %G3P concentration (uM)
    PYR = 8.62;                 %Pyruvate concentration (uM)
    NADHm = 57.2;               %Mitochondrial NADH (uM)
    Cam = 0.242;                %Mitochondrial calcium (uM)
    Nam = 5000;                 %Mitochondrial sodium (uM)
    Ntm = 2200;                 %Free pyridine in mitochondrial matrix (uM)
    Ntc = 2000;                 %Free pyridine in cytosol (uM)

%Mitochondrial Parameters
    fm = 0.0003;                %Fraction of free mitochondrial calcium
    Cmit = 1.812;               %Mitochondrial capacitance (uM/mV)
    Vmglu = 0.011;              %Maximum glucose consuption (uM/ms)
    KmATP = 500;                %Equation constant
    Kmgl = 7;                   %Half-max glucose concentration (mM)
    hgl = 1.7;                  %Glucose consumption hill coefficient
    VmGPD = 0.5;                %Maximum GAPDH activity (uM/ms)
    KmG3P = 200;                %Constant GAPDH (uM)
```

```
    KgNc = 0.09;                %NAD/NADH ratio for half-max glucose
flux/NADH production
    VmLDH = 1.2;                %Max LDH activity (uM/ms)
    KmLDH = 47.5;               %MM Constant for LDH (uM)
    KLNc = 1;                   %NADH/NAD ratio for half-max lactate/NAD
production
    VmPDH = 0.3;                %Max activity for PDH (uM/ms)
    Kmpyr = 47.5;               %Pyruvate MM constant (uM)
    KPNm = 81;                  %NAD/NADH ratio for half-max NADH production
    U1 = 1.5;                   %Fraction activation PDH (constant)
    U2 = 1.1;                   %Fraction activation PDH (constant)
    KCam = 0.05;                %Fraction activation PDH (constant)
    Vme = 22;                   %Optimal rate for ETC flux (uM/ms)
    KmNH = 3000;                %Complex I affinity for NADH (uM)
    KAT = -0.00492;             %FTe Constants (1/mV)
    KBT = -0.00443;             %FTe Constants (1/mV)
    Vmph = 8;                   %Optomal proton flux (uM/ms)
    KmADP = 20;                 %ATPase activation rate constatnt (uM)
    hph = 2;                    %Hill coefficient with Jph
    hp = 8;                     %Hill coefficient with Jph
    Kph = 131.4;                %Half-max mitochondrial membrane potentia ATP
production (mV)
    KPCam = 0.165;              %Calcium binding constant (uM)
    Plb = 0.0012;               %Basal proton leak coefficient (uM/ms)
    Plr = 0.0012;               %Regulated leak coefficient (uM/ms)
    Klp = 0.0305;               %Membrane potential coefficient (1/mV)
    TNADH = 0.05;               %Transport rate coefficient (uM/ms)
    KTNm = 16.78;               %Affinity coefficient mitochondria
    KTNc = 0.002;               %Affinity coefficient cytosol
    PCa = 0.004;                %Calcium activity factor for pyruvate
consumption
    am = 0.2;                   %Mitochondrial activity coefficient
    ai = 0.341;                 %Mitochondrial activity coefficient
    VmNC = 0.025;               %Max exchange velocity (uM/ms)
    KNaj = 8000;                %Binding coefficient for sodium (uM)
    KCaj = 8;                   %Binding coefficient for calcium (uM)
    Kgpd = 0.00001;             %G3P consumption in cytosol (1/ms)
    KNADHm = 0.0001;            %Consumption rate NADH in mitochondria (1/ms)
    KNADHc = 0.0001;            %Consumption rate NADH in cytosol (1/ms)
    NADm = Ntm + NADHm;         %NAD in mitochondria (uM)
    NADc = Ntc + NADHc;         %NAD in cytosol (uM)

%Measurments
    VM = zeros(TS,1);
    CaiM = zeros(TS,1);
    CaerM = zeros(TS,1);
    ATPiM = zeros(TS,1);
    ADPiM = zeros(TS,1);
    IP3iM = zeros(TS,1);
    CamM = zeros(TS,1);
    PsimM = zeros(TS,1);
    INaKM = zeros(TS,1);
    ICapumpM = zeros(TS,1);
    JerM = zeros(TS,1);
    INSRM = zeros(TS,1);
    RsM = zeros(TS,1);
    dSrM = zeros(TS,1);
```

```
    SrM = zeros(TS,1);
    INSM = zeros(TS,1);
    IVCaM = zeros(TS,1);
    ITRPVCaM = zeros(TS,1);
    RrM = zeros(TS,1);
    ItM = zeros(TS,1);
    DM = zeros(TS,1);
    JgluM = zeros(TS,1);
    JPYRM = zeros(TS,1);
    JLDHM = zeros(TS,1);
    PYRM = zeros(TS,1);
    NADHcM = zeros(TS,1);
    NADHmM = zeros(TS,1);
    JhresM = zeros(TS,1);
    JphM = zeros(TS,1);
    JhlM = zeros(TS,1);
    OinfM=zeros(TS,1);
    FAeM=zeros(TS,1);

%Cellular Model
for t=1:1:TS

%Nerst Potentials
        %Calcium
        VCa = (TV/zCa)*log(Cao/Cai);
        %Sodium
        VNa = (TV/zNaK)*log(Nao/Nai);
        %Potassium
        VK = (TV/zNaK)*log(Ko/Ki);
        %Sodium/Calcium
        VNaCa = (TV/zNaK)*(3*log(Nao/Nai)-log(Cao/Cai));
    %Calcium Currents
        %Voltage gated calcium channels
        PVCa = 1/(1+exp((VCah-V)/KCah));
        IVCa = GmVCa*PVCa*(V-VCa);
        %Calcium pumps
        ICapump = PmCap*((Cai^2)/((KCap^2)+(Cai^2)));
        %TRPV1 Calcium
        ITRPVCa = GTRPVCa*PoTRPV*(V-VCa);
    %Sodium Currents
        %Calcium release activated non selective cation current
        fCran = -GmCran/(1+exp((Caer-KCar)/3));
        pCran = (V-VCran);
        ICran = fCran*pCran*(V-VNa);
        %Background sodium channels
        pNa = 1/(1+exp((104+V)/8));
        INa = GmNa*pNa*(V-VNa);
        %TRPV1 Sodium
        ITRPVNa = GTRPVNa*PoTRPV*(V-VNa);
    %Potassium Currents
        %Voltage gated potassium channels
        IKDr = GmKDr*n*(V-VK);
        ninf = 1/(1+exp((Vn-V)/Sn));
        taun = c/(exp((V-Vtau)/a)+exp((Vtau-V)/b));
        %Calcium activated potassium channels
        funCa = (Cai^4)/((Cai^4)+(KKCa^4));
        IKCa = GmKCa*funCa*(V-VK);
```

```
    %ATP sensitive potassium channels
    OKATPnum = 0.08*(1+((0.33*ADPi)/Kdd))+0.89*(((0.165*ADPi)/Kdd)^2);
    OKATPden =
  ((1+(0.165*ADPi)/Kdd)^2)*(1+((0.135*ADPi)/Ktd)+((0.05*ATPi)/Ktt));
    OKATP = OKATPnum/OKATPden;
    IKATP = GmKATP*OKATP*(V-VK);
    %TRPV1 Potassium current
    ITRPVK = GTRPVK*PoTRPV*(V-VK);
 %Mixed Currents
    %NaCa Exchanger
    INaCa = GNaCa*((Cai^5)/((Cai^5)+(KNaCa^5)))*(V-VNaCa);
    %NaK Exchanger
    f5=ff5*exp(V/(2*TV));
    b5=bb5*exp(-V/(2*TV));
    F1=f1*(Nai^3);
    F4=f4*(Ko^2);
    F5=f5*ATPi;
    B2=b2*ADPi;
    B3=b3*(Nao^3);
    B4=b4*P;
    B6=b6*(Ki^2);
  D=(f2*f3*F4*F5*f6)+(b1*f3*F4*F5*f6)+(b1*B2*F4*F5*f6)+(b1*B2*B3*F5*f6)+(
  b1*B2*B3*B4*f6)+(b1*B2*B3*B4*b5);
    if (PNaK*((F1*f2*f3*F4*F5*f6)-(b1*B2*B3*B4*b5*B6))/D) > 4700
        INaK = 4700;
    else
    INaK = PNaK*((F1*f2*f3*F4*F5*f6)-(b1*B2*B3*B4*b5*B6))/D;
    end
%Endoplasmic Calcium Flux
    %SERCA flux into ER
    Jer = PCaER*((Cai^2)/((Cai^2)+(KCarp^2)));
    %ER leak and IP3R release
    Oinf = (Cai/((Cai)+(KRCa)))*((IP3i^3)/((IP3i^3)+(KIP3^3)));
    Jout = (Pleak + (PIP3*Oinf*IPCoe))*(Caer-Cai);
%Mitochondrial Metabolites
    %Glucokinase flux
    Jglu = HKA*(1+(dFAe-
  1)/14)*Vmglu*(ATPi/(ATPi+KmATP))*((Glu^hgl)/((Glu^hgl)+(Kmgl^hgl)));
    %Pyruvate consumption
    FPYR = (PYR/(Kmpyr+PYR));
    FPNAD = (NADm/NADHm)/(KPNm+(NADm/NADHm));
    FPCa = 1/(1+U2*(1+U1*((1+(Cam/KCam))^-2)));
    JPYR = VmLDH*FPYR*FPNAD*FPCa;
    %Flux through ETC
    FRA = (AbsCCO*(PBMir*1E-6)*t);
    FDe = (NADHm/(KmNH + NADHm));
    FTe = (KAT*Psim+1)/(KBT*Psim+1);
    Jhres = Vme*FDe*DFAe*FTe;
    %Proton flux through ATPase
    AD = (MgADP^hph)/((KmADP^hph)+(MgADP^hph));
    AT = (Psim^hp)/((Kph^hp)+(Psim^hp));
    ACa = 1-(1/(exp(Cam/KPCam)));
    Jph = Vmph*AD*AT*ACa;
    %Oxygen consuption by ETC flux
    JO2 = 0.1*Jhres;
 %Mitochondrial Mediators
    %GAPDH flux
```

```
    Jgpd = VmGPD*(G3P/(KmG3P+G3P))*((NADc/NADHc)/(KgNc+(NADc/NADHc)));
    %LDH flux
    JLDH = VmLDH*(PYR/(KmLDH+PYR))*((NADHc/NADc)/(KLNc+(NADHc/NADc)));
    %Proton leak flux
    Jhl = (Plb+Plr)*exp(Klp*Psim);
    %Flux via NADH
    JTNADH =
  TNADH*((NADHc/NADc)/(KTNc+(NADHc/NADc)))*((NADm/NADHm)/(KTNm+(NADm/NADH
  m)));
%Mitochondrial Ionic Currents
    %Calcium flux via mitochondrial uniporter
    Juni = PCa*(zCa*Psim/TVm)*((am*Cam*exp(-zCa*Psim/TVm)-
  (ai*Cai))/(exp(-zCa*Psim/TVm)-1));
    %Mitochondrial sodium calcium exchanger
    alpha1 = (((Nai^3)*(Cam))/((KNaj^3)*(KCaj)));
    alpha2 = (((Nam^3)*(Cai))/((KNaj^3)*(KCaj)));
    JNCa = (VmNC*(exp(0.5*Psim*alpha1/TVm)-exp(-
  0.5*Psim*alpha2/TVm)))/(1+alpha1+alpha2+((Nai^3)/(KNaj^3))+((Cam)/(KCaj
  ))+((Nam^3)/(KNaj^3))+((Cai)/(KCaj)));
%Insulin dynamics
    Chat = (Cai-Cb)/Co;
    if Ar*(Smax-Sr) >= (1.4E-6*It) && t <= 300000
       Rr = (1.4E-6*It);
    elseif Ar*(Smax-Sr) >= (5E-7*It) && t >300000
       Rr = (5E-7*It);
    else
       Rr = Ar*(Smax-Sr);
    end

    if It <= 0
       Rs = 0; It=0;
    elseif Sr == 0
       Rs = Rr;
    else
       Rs = Ro*(Chat^4)*(Sr/Smax);     %Insulin Secretion rate (pmol/ms)
    end

%Defferential Equations
    %Mitochondria
    dG3Pdt = ((2*Jglu-Jgpd)/Vi)-(Kgpd*G3P);
    dPYRdt = ((Jgpd-JPYR-JLDH)/(Vi+Vmmit));
    dNADHmdt = ((4.6*JPYR+JTNADH-0.1*Jhres)/(Vmmit))-(KNADHm*NADHm);
    dNADHcdt = ((Jgpd-JTNADH-JLDH)/(Vi))-(KNADHc*NADHc);
    dPsimdt = (Jhres-Jph-Jhl-JNCa-(2*Juni))/(Cmit);
    dCamdt = -(fm*(Juni-JNCa))/(Vmmit);

    %Cellular
    dVdt =
  ((IVCa+ICapump+INaCa+ICran+INa+INaK+IKDr+IKCa+IKATP+ITRPVCa+ITRPVNa+ITR
  PVK)/(-Cm));
    dCadt = fi*((((-IVCa-ITRPVCa+(2*INaCa)-(2*ICapump))/(2*F*Vi))-
  Jer)+(Jout/Vi)-dCamdt)-(Ksg*Cai);
    dCaerdt = (fer/Ver)*((Jer*Vi)-Jout);
    dNadt = (-1*((3*INaCa)+(3*INaK)+(INa)+(ICran)+(ITRPVNa)))/(Vi*F);
    dIP3dt = KIP*((Cai^2)/((Cai^2)+(KIPCa^2)))-(KdIP*IP3i);
```

```
    dATPdt = ((2*Jglu+0.231*Jph)/(Vi))-(Jer/2)-((INaK+ICapump)/(Vi*F))-
  (((KATPCa*Cai)+KATP)*ATPi);
    dndt = (ninf-n)/taun;

    %Insulin Dynamics
    dSrdt = Rr-Rs;
    dItdt = -Rs;

%Parameter Updates
    %Mitochondria
    G3P = G3P + dG3Pdt;
    PYR = PYR + dPYRdt;
    NADHm = NADHm + dNADHmdt;
    NADHc = NADHc + dNADHcdt;
    Psim = Psim + dPsimdt;
    Cam = Cam - dCamdt;
    NADm = Ntm + NADHm;
    NADc = Ntc + NADHc;
    ADPi = At - ATPi;
    MgADP = 0.055*ADPi;

    %Cellular
    Cai = Cai + dCadt;
    Caer = Caer + dCaerdt;
    Nai = Nai + dNadt;
    IP3i = IP3i + dIP3dt;
    ATPi = ATPi + dATPdt;
    V = V + dVdt + (Em*EFS);
    n = n + dndt;
    %Insulin Dynamics
    if (Sr + dSrdt) < 0             %RRVP cannot be less than 0
        Sr = 0;
    elseif (Sr + dSrdt) > Smax      %RRVP cannot be more than its maximum
        Sr = Smax;
    else
        Sr = Sr + dSrdt;            %RRVP content (pmol)
    end
    INS = INS + Rs;                 %Total insulin secretion (pmol)
    It = It + dItdt;                %Total insulin (pmol)
%Measurments
    VM(t) = V;
    CaiM(t) = Cai;
    CaerM(t) = Caer;
    ATPiM(t) = ATPi;
    ADPiM(t) = ADPi;
    IP3iM(t) = IP3i;
    CamM(t) = Cam;
    PsimM(t) = Psim;
    JphM(t) = Jph;
    INaKM(t) = INaK;
    ICapumpM(t) = ICapump;
    JerM(t) = Jer;
    INSRM(t) = Rs;
    RsM(t) = Rs;
    dSrM(t) = dSrdt;
    SrM(t) = Sr;
```

```
        INSM(t) = INS;
        IVCaM(t) = IVCa;
        ITRPVCaM(t) = ITRPVCa;
        RrM(t) = Rr;
        ItM(t) = It;
        DM(t) = D;
        JgluM(t) = Jglu;
        JPYRM(t) = JPYR;
        JLDHM(t) = JLDH;
        PYRM(t) = PYR;
        NADHcM(t) = NADHc;
        JhresM(t) = Jhres;
        JphM(t) = Jph;
        JhlM(t) = Jhl;
        OinfM(t)=Oinf;
        FAeM(t)=FAe;
        NADHmM(t)=NADHm;
end
```

Matlab Frequency Measurement Code:

```
CaiM = downsample(CaiM,5000);
dsp = 0;
spikes = 0;
Ts = (TS/5000);
IO=zeros(Ts+1,1);

for i=1:1:Ts
    if CaiM(i) > mean(CaiM)
        IO(i)=1;
    else
        IO(i)=0;
    end
end
for i=1:1:(Ts-1)
    if IO(i) + IO (i+1) == 1
        dsp = dsp + 1;
    else
    end
end

FRQ = (dsp/2)/(Ts*5/60); %Spikes per min
```

Matlab Thermal Simulation Code:

```
%Input Parameters
Irr = 0.3;              %Irradiance (W/cm2)
To = 300;                %Surrounding temp (K)
TS = 60000;             %Total time (ms)
Exp = 60000;             %Exposure time (ms)

%Water Heating Parameters
```

```
Wm = 2;                 %Mass of water (g)
Axw = 2.25;             %Cross section of laser with water (cm2)
hw = 0.005;             %Water Convection loss (W/cm2 K)
Tw = 300;               %Initial water temp (K)
absw = 0.04;            %Water 808nm absorbance
Cw = 4.168;             %Water specific heat (J/g K)

%Membrane Heating Parameters
Mc = 1.44E-9;           %Mass of cell (g)
Axc = 1.5394E-6;        %Cell cross-sectional area (cm2)
hc = 0.026;             %Cell convective loss to water (W/cm2 K)
Tc = 300;               %Cell temperature
Asc = 6.1575E-6;        %Cell surface area (cm2)

%Measurment Arrays
dTwM=zeros(TS+1,1);
dTcM=zeros(TS+1,1);
dTcwM=zeros(TS+1,1);

for t=1:1:TS+1
%Transfer Equations
if t<=Exp
    Qinw = Irr*absw*Axw*1E-3;         %Input power from laser on water (J/ms)
    Qinc = Irr*absw*Axc*1E-3;         %Input power from laser on membrane
(J/ms)
else
    Qinw=0;
    Qinc=0;
end
Qoutw = Axw*hw*(Tw-To)*1E-3;          %Heat loss to convection (J/ms)
Qoutc = Asc*hc*(Tc-Tw)*1E-3;          %Heat loss to water from membrane

%Differential Equations
dTwdt = (Qinw-Qoutw)/(Wm*Cw);
dTcdt = (Qinc-Qoutc)/(Mc*Cw);

%Parameter Updates
Tw = Tw + dTwdt;
Tc = Tc + dTcdt;

%Measurments
dTwM(t)=(Tw-To);
dTcM(t)=(Tc-To);
dTcwM(t)=Tc-Tw;
end
```